

Molecular processes in expanding plasmas : a laser spectroscopic study

Citation for published version (APA):

Meulenbroeks, R. F. G. (1996). *Molecular processes in expanding plasmas : a laser spectroscopic study*. [Phd Thesis 1 (Research TU/e / Graduation TU/e), Applied Physics and Science Education]. Technische Universiteit Eindhoven. <https://doi.org/10.6100/IR452097>

DOI:

[10.6100/IR452097](https://doi.org/10.6100/IR452097)

Document status and date:

Published: 01/01/1996

Document Version:

Publisher's PDF, also known as Version of Record (includes final page, issue and volume numbers)

Please check the document version of this publication:

- A submitted manuscript is the version of the article upon submission and before peer-review. There can be important differences between the submitted version and the official published version of record. People interested in the research are advised to contact the author for the final version of the publication, or visit the DOI to the publisher's website.
- The final author version and the galley proof are versions of the publication after peer review.
- The final published version features the final layout of the paper including the volume, issue and page numbers.

[Link to publication](#)

General rights

Copyright and moral rights for the publications made accessible in the public portal are retained by the authors and/or other copyright owners and it is a condition of accessing publications that users recognise and abide by the legal requirements associated with these rights.

- Users may download and print one copy of any publication from the public portal for the purpose of private study or research.
- You may not further distribute the material or use it for any profit-making activity or commercial gain
- You may freely distribute the URL identifying the publication in the public portal.

If the publication is distributed under the terms of Article 25fa of the Dutch Copyright Act, indicated by the "Taverne" license above, please follow below link for the End User Agreement:

www.tue.nl/taverne

Take down policy

If you believe that this document breaches copyright please contact us at:

openaccess@tue.nl

providing details and we will investigate your claim.



MOLECULAR PROCESSES IN EXPANDING PLASMAS

A laser spectroscopic study

Ralph Meulenbroeks

MOLECULAR PROCESSES IN EXPANDING PLASMAS

A laser spectroscopic study



Druk: Boek- en Offsetdrukkerij Letru, Helmond, (0492) 53 77 97

CIP-DATA KONINKLIJKE BIBLIOTHEEK, DEN HAAG

Meulenbroeks, Radulfus Franciscus Godfried

Molecular processes in expanding plasmas : a laser spectroscopic study / Radulfus Franciscus Godfried Meulenbroeks. - Eindhoven : Eindhoven University of Technology

Thesis Technische Universiteit Eindhoven. - With summary in Dutch.

ISBN 90-386-0187-5

Subject headings: plasma physics / laser spectroscopy / hydrogen kinetics

Part of this work has been supported by the Netherlands Technology Foundation (STW)

MOLECULAR PROCESSES IN EXPANDING PLASMAS

A laser spectroscopic study

PROEFSCHRIFT

ter verkrijging van de graad van doctor aan de Technische
Universiteit Eindhoven, op gezag van de Rector Magnificus,
prof.dr. J.H. van Lint, voor een commissie aangewezen door
het Kollege van Dekanen in het openbaar te verdedigen
op dinsdag 23 januari 1996 om 16.00 uur

door

Radulfus Franciscus Godfried Meulenbroeks

geboren te Eersel

Dit proefschrift is goedgekeurd door de promotoren:

prof.dr.ir. D.C. Schram

en

prof.dr. J. Uhlenbusch

en de copromotor:

dr. J.A.M. van der Mullen

...It is terrifying, and paralyzing, as the strands of sounds desintegrate. We hold on to them, hovering between hope and submission. And one by one, these spidery strands connecting us to life melt away, vanish from our fingers even as we hold them. We cling to them as they dematerialize; we are holding two - then one. One, and suddenly none. For a petrifying moment there is only silence. Then again, a strand, a broken strand, two strands, one...none. We are *half in love with easeful death...now more than ever seems it rich to die, to cease upon the midnight with no pain...* And in ceasing, we lost it all. But in letting go, we have gained everything.

Leonard Bernstein -
The Unanswered Question

Voor pa, ma en David

Table of Contents

General Introduction	3
Chapter 1: Fabry-Pérot Line Shape Analysis on an Expanding Cascaded Arc Plasma in Argon, <i>J. Appl. Phys.</i> 75 , 2775 (1994)	5
Chapter 2: Four Ways to Determine the Electron Density in Low-Temperature Plasmas, <i>Phys. Rev. E</i> 49 , 2272 (1994)	11
Chapter 3: Argon-Hydrogen Plasma Jet Investigated by Active and Passive Spectroscopic Means, <i>Phys. Rev. E</i> 49 , 4397 (1994)	15
Chapter 4: The Argon-Hydrogen Expanding Plasma: Model and Experiments <i>Plasma Sources Sci. Technol.</i> 4 , 74 (1995)	25
Chapter 5: Influence of Molecular Processes on the Hydrogen Atomic System in an Expanding Argon-Hydrogen Plasma, <i>Phys. Plasmas</i> 2 , 1002 (1995)	37
Chapter 6: Depolarization Rayleigh Scattering as a Means of Molecular Concentration Determination in Plasmas, <i>Phys. Rev. Lett.</i> 69 , 1379 (1992)	45
Chapter 7: CARS on Expanding Thermal Arc Plasmas, <i>submitted to Phys. Rev. E</i> (1995)	49
Chapter 8: Wall Association and Recirculation in Expanding thermal Arc Plasmas, <i>submitted to Phys. Rev.</i> (1995)	61
General Conclusions	67
Summary	71
Samenvatting	72
Dankwoord	73
Curriculum Vitae	74

General Introduction

R.F.G. Meulenbroeks

*Eindhoven University of Technology, Department of Physics,
P.O. Box 513, 5600 MB Eindhoven, The Netherlands*

This work deals mainly with hydrogen-related kinetics in plasmas, a field linked to many areas of research, including plasma surface modification (e.g., etching and deposition), diamond film production, and even astrophysics. In many practical cases, hydrogen kinetics play a dominant role in the description and understanding of plasma chemical processes [1]-[6]. The main content of the work is presented in the form of eight articles, six of which have already been published in refereed journals at the moment this thesis is printed. They do not appear in chronological order, but are arranged to fit a general trend departing from pure argon plasmas via argon-hydrogen mixtures to arrive at full hydrogen plasmas. This introduction aims to be a guideline along the forthcoming separate "chapters".

The work described can be classified as "fundamental" research, but it is by no means without practical impact. The field of plasma surface modification is gaining more and more importance for the creation of small structures in semiconductor materials. Plasma particle sources (in particular those creating H and H⁻ particles) are being used in neutral beam injectors for the next generation of fusion reactors and for the cleaning of archeological artefacts, to name but two examples. The expanding thermal arc plasma investigated in this work is used both for the deposition of thin films of different materials (ranging from amorphous hydrogenated silicon to diamond, see e.g., [7, 8]) and for the realization of particle sources [9]. Within the Eindhoven University of Technology, four expanding thermal arc experiments are devoted to this research: one for the deposition of carbon-containing films, another for silicon-containing films, a third for research on hydrogen sources, and the large fundamental experiment of which the latest results lie before you. In this last set up, several active and passive diagnostics are combined in order to gain a more profound understanding of the basic processes that govern this type of plasma. Ultimately, this understanding should lead to optimization of the above applications.

All four expanding thermal arc experiments have a similar construction: a plasma source (a thermal, wall-stabilized DC cascaded arc) connected to or suspended in a large vacuum vessel (e.g., Fig. 1 in chapter 1). The subatmospheric thermal arc plasma expands into the heavily pumped vessel through a nozzle, creating an expanding plasma jet with a typical length of about 0.5 m. The diameter increases with the downstream distance from 4 mm to several tenths of a meter, depending on the background pressure, which can vary between 5 and 5000 Pa. During deposition work, monomers (CH₄, C₂H₂, SiH₄,...) are injected into a pure argon or argon-hydrogen plasma beam and deposition takes place at a downstream substrate [10, 11]. When used as a hydrogen particle source, the

arc is operated on hydrogen [12].

The present thesis research on expanding plasma jets is a natural follow-up to the work of Van de Sanden [13], which focused on the study of a pure argon plasma jet. Using Thomson-Rayleigh scattering (TRS) and Optical Emission Spectroscopy (OES) as diagnostics, the argon jet has been thoroughly investigated. This pure argon expanding plasma jet behaves to a large extent as a normal gasdynamical expansion. The influence of the charged particles is mainly seen in the temperature behaviour. This work inevitably left some questions unanswered, and one of the most important ones concerned the heavy particle temperatures in the jet. In chapter 1 of this work, therefore, results of measurements on a pure argon plasma beam using a pressure-scanned Fabry-Pérot interferometer are discussed. A unexpected spin-off of these measurements are the observation of asymmetric argon (4p')-(4s) line profiles, showing self absorption and yielding information on metastable densities in the periphery of the plasma. Another long-standing problem, encountered in the thesis work of De Graaf, Meeusen, and others [10, 12, 13, 14] concerns the reliability of different methods to determine the electron density in low-temperature plasmas. As the fundamental set up offers the possibility to combine several diagnostics (especially because the plasma is moveable inside the vacuum vessel [15]), it constitutes the ideal opportunity for the comparison of different electron density diagnostics: probes, TRS, OES, and continuum analysis. The results are presented in a *Physical Review* article, chapter 2.

In order to obtain a better understanding of a molecule-rich deposition plasma, understanding of a purely atomic argon jet is clearly insufficient. A line of study has been chosen to approach the deposition plasma environment by inserting varying amounts of H₂ gas to the argon plasma. A very pronounced influence on the behaviour of the jet is observed, when small amounts of hydrogen are admixed to the argon flow before it enters the arc. Small amounts of hydrogen (i.e., ≤ 5 %) were chosen so as not to change the transport properties of the plasma too much. The gasdynamical expansion is supposed to stay governed by the large (relatively heavy) majority of argon. These argon-hydrogen jets have been studied very extensively using TRS, OES, and modeling. Ion-molecule reactions appear to be of major importance in these mixtures. Their influence is noticed very clearly in the ion densities, but also in the excited state populations of both H and Ar. Chapters 3 to 5 reflect this study, describing TRS and OES results (chapter 3), TRS, OES, and a quasi one-dimensional model (chapter 4), and some peculiar OES results (chapter 5).

Eventually, one arrives at the study of 50% H₂ in argon mixtures (which are totally dominated by the hydrogen kinet-

ics) and pure hydrogen plasmas. As these plasmas exhibit an extremely fast recombination, almost no light is emitted, and the electron density drops to very low values, eliminating both OES and TRS as diagnostic options. Therefore, other diagnostics have to be implemented: a novel technique has been developed to measure molecular concentrations in plasmas of simple composition (i.e., with one dominant molecular component): *Depolarization Rayleigh Scattering*, presented in a 1992 *Physical Review Letters* paper, chapter 6. To measure *in situ* the rovibrational distribution of $H_2^{(v,J)}$ molecules in hydrogen and argon-hydrogen plasmas, a Coherent anti-Stokes Raman scattering (CARS) set up has been used. This difficult option has been chosen to answer another long-standing question concerning possible wall-association of H atoms to rovibrationally excited H_2 molecules when using hydrogen-containing plasmas. Chapter 7 deals with the construction of this very sensitive diagnostic and the experiments performed on 50% H_2 in argon and full hydrogen plasmas. The main body of the thesis is concluded by chapter 8, describing the formation of stable molecules (in this case, HD) in plasmas containing both H_2 and D_2 . Here, both HD and H_2 are measured by CARS in order to gain understanding on the formation of HD.

As the journal articles represent a period of over 4 years, it is to be expected that some of the early conclusions have to be modified (or abandoned) later on, as new experimental and theoretical facts arise. CARS, for example, brought a great surprise in showing that vibrationally highly excited H_2 molecules are not present in significant amounts, as was earlier assumed. To tie up some of the loose ends, chapter 9, giving the "history of recirculation" presents the present view of the matters discussed in this thesis. It will undoubtedly be altered or refined further and further during future research.

References

- [1] W. Luft and Y. Simon Tsuo, *Hydrogenated Amorphous Silicon Alloy Deposition Processes*, Marcel Dekker, New York (1993).
- [2] R.E. Clausing, J.C. Angus, L.L. Horton, and P. Koidl (eds.), *Diamond and Diamond-like Films and Coatings*, NATO ASI Series, Series B: Physics Vol. 266, Plenum, New York (1991).
- [3] J.A. Mucha, D.L. Flamm, and D.E. Ibbotson, *J. Appl. Phys.* **65**, 3448 (1989).
- [4] L. St-Onge and M. Moisan, *Plasma Chem. Plasma Proc.*, **14**, 87 (1994).
- [5] B. Jackson and M. Persson, *J. Chem. Phys.*, **96**, 2378 (1992).
- [6] M.C.M. van de Sanden, R.J. Severens, R.F.G. Meulenbroeks, M.J. de Graaf, Z. Qing, D.K. Otorbaev, R. Engeln, J.W.A.M. Gielen, J.A.M. van der Mullen, and D.C. Schram, *Surface and Coatings Technology* **74-75**, 1 (1995).
- [7] A.J.M. Buuron, G.J. Meeusen, J.J. Beulens, M.C.M. van de Sanden, and D.C. Schram, *J. Nucl. Mater.* **200**, 430 (1993).
- [8] A.T.M. Wilbers, G.J. Meeusen, M. Haverlag, G.M.W. Kroesen, and D.C. Schram, *Thin Solid Films* **204**, 59 (1991); R.J. Severens, G.J.H. Brussaard, M.C.M. van de Sanden, and D.C. Schram, *Appl. Phys. Lett.* **67** (4), 491 (1995).
- [9] M.J. de Graaf, R. Severens, R.P. Dahiya, M.C.M. van de Sanden, and D.C. Schram, *Phys. Rev. E* **48** (3), 2098 (1993).
- [10] G.J. Meeusen, Ph.D. Thesis Eindhoven University of Technology (1994).
- [11] A.J.M. Buuron, Ph.D. Thesis Eindhoven University of Technology (1993).
- [12] M.J. de Graaf, Ph.D. Thesis Eindhoven University of Technology (1994).
- [13] M.C.M. van de Sanden, Ph.D. Thesis Eindhoven University of Technology (1991).
- [14] G.J. Meeusen, E.A. Ershov-Pavlov, R.F.G. Meulenbroeks, M.C.M. van de Sanden, and D.C. Schram, *J. Appl. Phys.* **71** (9), 4156 (1992).
- [15] M.C.M. van de Sanden, J.M. de Regt, G.M. Janssen, J.A.M. van der Mullen, D.C. Schram, and B. van der Sijde, *Rev. Sci. Instrum.* **63** 3369 (1992).

Fabry-Pérot Line Shape Analysis On An Expanding Cascaded Arc Plasma in Argon

R.F.G. Meulenbroeks P.A.A. van der Heijden M.C.M. van de Sanden
D.C. Schram

*Eindhoven University of Technology, Department of Physics,
P.O. Box 513, 5600 MB Eindhoven, The Netherlands*

Abstract. Fabry-Pérot line profile measurements have been used to obtain heavy particle temperatures and electron densities for an expanding cascaded arc plasma in argon. This was done for the argon 415.9 nm and 696.5 nm neutral lines as a function of the distance from the onset of the expansion. Temperatures in the range of 2,000-12,000 K were obtained. The electron density in the beginning of the expansion appeared to be $5.6 \times 10^{21} \text{ m}^{-3}$. The 696.5 nm line profiles appeared to be asymmetric because of selfabsorption by cool metastables around the plasma. The density and temperature of these metastables could be determined by fitting the measurements to a theoretical model, and appeared to be around 10^{17} m^{-3} and around 3,000 K, respectively.

I. INTRODUCTION: THE CASCADED ARC SET UP

Expanding cascaded arc plasmas are used for fast deposition of thin films of various kinds. Materials deposited thus far include amorphous hydrogenated carbon, graphite, diamond [1, 2], as well as amorphous hydrogenated silicon [3, 4]. Deposition rates, obtained using this method, are far larger (i.e., on the order of 0.1 $\mu\text{m/s}$) than the ones obtained using conventional deposition techniques, such as Plasma Enhanced Chemical Vapour Deposition (PECVD).

To achieve a thorough understanding of the plasma deposition process, knowledge of the particle densities in the expanding plasma beam is essential [5]. It is the aim of the present study to analyze the characteristics of the expanding plasma, sketched in figure 1. It consists of a cascaded arc plasma source [6], creating a thermal plasma (electron temperature $T_e \approx 12,000 \text{ K}$), connected to a heavily pumped vacuum vessel (background pressure 40 Pa). The arc channel has a length of 80 mm and a diameter of 4 mm. The arc plasma expands supersonically into the vessel, creating a supersonic expansion, ending in a stationary shock and followed by a subsonic relaxation region. The diagnostics to study this plasma jet are the following:

Thomson-Rayleigh scattering: accurate and local values for the electron density n_e , the electron temperature T_e , as well as the neutral particle density n_0 can be obtained as a function of axial and radial position. These measurements clearly reveal the structure of the expanding plasma jet [7].

Optical emission spectroscopy: information about the excited level population can be obtained by means of line intensity measurements.

Fabry-Pérot interferometry: the set of plasma parameters n_e , T_e , and n_0 can be completed by measuring the neutral particles temperature T_0 by means of line shape analysis.

In this paper, the results of the Fabry-Pérot experiment are presented and discussed. Fabry-Pérot line shape analysis provides the opportunity to measure several important plasma parameters. To begin with, the temperature of the neutral particles in the jet can be obtained by measuring the *Doppler* broadening of spectral lines; it constitutes an important param-

eter for computer models describing the plasma jet [8]. Furthermore, a measurement of the *Stark* broadening yields the electron density: this is an independent check of the Thomson scattering data.

A third parameter, one which is more difficult to obtain, is the density of the metastable (4s) levels in, as well as around, the plasma jet. The metastable density is important for deposition experiments, as metastables may cause Penning-like ionization [4]. Fabry-Pérot analysis of the asymmetric line profile of the self-absorbed argon 696.5 nm line gives information about both the density and the temperature of the metastables *around* the plasma. These data are difficult to obtain by any other (especially passive) means.

II. EXPERIMENT

A. Fabry-Pérot interferometry

The experimental set up for line shape analysis is depicted in figure 2. The plasma is imaged onto a monochromator entrance slit by an optical system, consisting of several lenses and mirrors. The monochromator (Bentham M300) is used as a rough wavelength selector and is set for a flat transmission bandwidth of about 0.24 nm in order to separate the line to be studied from the rest of the spectrum. After this rough selection, a parallel beam is created (lenses L_5 , $f = 150 \text{ mm}$ and L_6 , $f = 200 \text{ mm}$), in which the Fabry-Pérot interferometer is placed. The interferometer mirrors are flattened to $\lambda/200$ for the 420-500 nm wavelength region, and to $\lambda/100$ for the 650-720 nm region. Reflectivities for both wavelength regions are around 98%. Lens L_6 images the light on a 0.5 mm pinhole, after which it falls on a photomultiplier tube (RCA 31034). The photomultiplier is placed in a cooled housing: the working temperature is -20 °C. The total (theoretical) finesse of the system is around 60 for both wavelength intervals. The Free Spectral Ranges are $2.978 \times 10^{-2} \text{ nm}$ for the red (using a mirror spacer of 8.15 mm) and $5.65 \times 10^{-2} \text{ nm}$ for the blue. Apparatus profiles are measured using a low pressure argon lamp; a correction is made for the temperature of the lamp, which is known to be approximately 600 K.

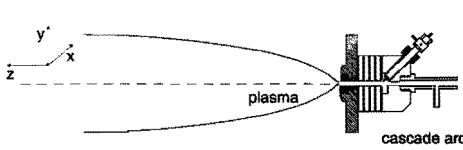


Figure 1: *The cascaded arc experiment: a thermal plasma at atmospheric pressure is created in a continuously operated D.C. arc, consisting of three cathodes, three electrically isolated copper plates, and an anode plate. All parts are water cooled. The plasma expands into a low-pressure region, creating a supersonically expanding plasma jet.*

The Fabry-Pérot is a pressure-scanned type: a wavelength scan is made by varying the pressure of the gas inside the mirror cavity (in our case: neon), thus altering the refractive index of the medium between the mirrors and, hence, the wavelength which is transmitted through the system. The pressure in the Fabry-Pérot is monitored by the same software that controls the photon counting system. The software runs on a (M68000) modular laboratory computer system. A measured line profile can be processed by a least-mean-squares fit with either a Lorentzian, a Gaussian, or a Voigt profile (convoluted with the measured apparatus profile).

B. Measurements

The working plasma conditions for all measurements are: $I_{arc} = 45$ A, $V_{arc} = 140$ V, argon flow = 3.5 standard liters per minute, vessel background pressure $p_{back} = 40$ Pa. Line profiles of the 415.9 nm Ar(I) line are measured up to a distance of 28 mm from the nozzle. After $z=28$ mm, the intensity of this line has dropped too far to give accurate results. For larger distances from the nozzle, therefore, the much stronger 696.5 nm line is used, which is measured up to $z=300$ mm. The profiles are all measured at the axis of the plasma jet, i.e., at $x=y=0$. The axial scanning is performed by moving the cascaded arc source *itself*, leaving the diagnostics fixed.

III. RESULTS

A. Heavy particle temperatures and electron densities

The 415.9 nm line profiles all proved to be symmetric, whereas the 696.5 nm profiles showed a persistent asymmetry for measurements close to the arc (where n_e and T_e values are high). The apparatus profile, however, was always symmetric. Furthermore, the asymmetry of the 696.5 nm emission line profile disappeared for larger z -values, as well as at the edges of the plasma (measured by varying the x and y -positions). The explanation for this effect will be given later on. After $z=30$ mm, the 696.5 nm profiles proved to be essentially Gaussian.

As mentioned before, one of the contributions to the line broadening is due to random motion of the atoms in the plasma, giving a Gaussian broadening in the case of a Maxwellian

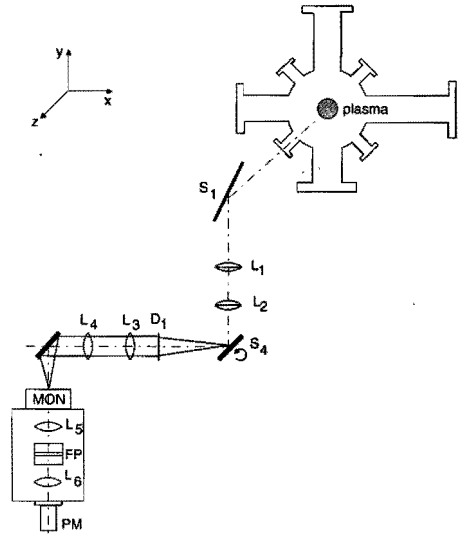


Figure 2: *The Fabry-Pérot diagnostic. Plasma radiation is transmitted through an optical system consisting of lenses (L_1 - L_6) and mirrors. A Cherny-Turner monochromator (MON) selects the spectral line. The interferometer (FP) is placed in the equidistant beam part created between L_5 and L_6 . L_6 focuses the light on a inhole, after which a photomultiplier is detects the signal. The Fabry-Pérot interferometer is placed in a thermally controlled chamber.*

velocity distribution. For the half one-over-e ($\Lambda_{\frac{1}{2}}$, in nm) width of the Gaussian contribution, the well-known formula:

$$\Lambda_{\frac{1}{2}} = \lambda_0 \sqrt{\frac{2kT_0}{m_0c^2}} \quad (1)$$

holds, where λ_0 is the wavelength of the line (in nm), k is Boltzmann's constant, T_0 is the temperature of the neutral particles (degrees K), m_0 is the mass of the neutrals (in kg), and c is the speed of light (in m/s).

A Lorentzian contribution to the line profile is due to the Stark effect: a broadening and shift of spectral lines, caused by the random electric field of the electrons in the plasma [10]. For most atoms (with the important exception of hydrogen) this effect is linear in the electron density. The Full Width at Half Maximum (FWHM) γ_L (in nm) of the Lorentzian contribution is given by:

$$\gamma_L = \frac{n_e}{10^{22}} C_S, \quad (2)$$

where n_e is the electron density in m^{-3} . The constants C_S are listed by Griem [10, 11] for a large number of atomic transitions. The Stark *shift* of the line is proportional to the Stark width γ_L ; the proportionality constants are also listed by Griem [10, 11].

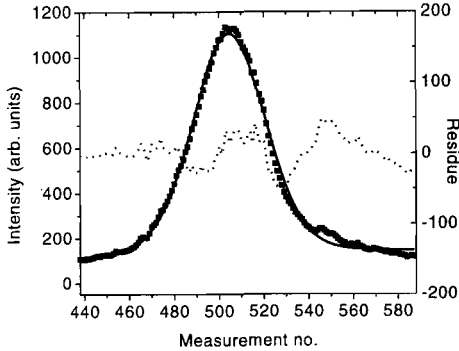


Figure 3: An example of a measurement (\blacksquare) of the argon 451.9 nm line and its least-mean-squares Voigt fit (with residue). The horizontal axis gives only the measurement number, the interval between two neighbouring points corresponds to a wavelength interval of 1.69×10^{-4} nm.

In a plasma of the kind studied here, both effects are important, whereas other effects (natural broadening etc.) can be neglected. So the total line profile will be a convolution of a Lorentzian, a Gaussian and an apparatus profile. A Voigt-fit (convoluted with the apparatus profile) gives the values of Δ_L and γ_L for a given measurement. The Stark effect, however, is only noticeable in the line profile for relatively large electron densities, i.e., in the beginning of the expansion: further from the arc, the measured 415.9 nm profiles become essentially Gaussian. Figure 3 gives an example of a measured line profile (415.9 nm, $z = 2$ mm) and its least-mean-squares Voigt fit.

Figure 4 gives the results of the Doppler broadening analysis of the spectral lines as a function of axial position z . In the axial profile, composed of the results of both lines, the shock structure can clearly be seen after the initial sharp decrease of the heavy particle temperature: a temperature increase around $z = 40$ mm, followed by a slow decrease. The temperature in the beginning of the expansion is in good agreement with the temperature at the end of the cascaded arc [12]: around 12,000 K. The temperature further in the expansion approaches a value of about 2,000 K, which is equal to the electron temperature further in the expansion [7]. The shock position is coincident with the position of the shock in the electron (and neutral) density, as measured by Thomson-Rayleigh scattering.

The electron density, as determined from the width of the Lorentzian component of a measured profile, can only be accurately obtained from the 415.9 nm line profiles close to the nozzle. These line profiles show a prominent Voigt shape, and the electron densities obtained are $5.6 \times 10^{21} \text{ m}^{-3}$ and $1.5 \times 10^{21} \text{ m}^{-3}$, for $z = 2$ mm and $z = 4$ mm, respectively. These values are higher than the ones obtained by Thomson scattering. However, Thomson scattering measurements close to the arc ($z=2-8$ mm) suffer from a large amount of stray light

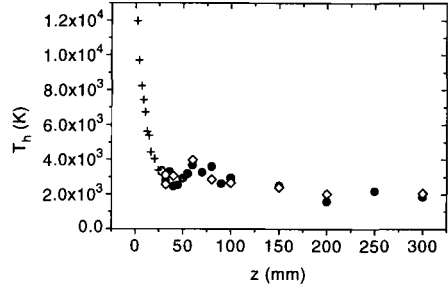


Figure 4: The heavy particle temperature of the neutrals in the plasma jet vs. the distance from the onset of the expansion (z): \bullet , \circ , \diamond : measurements of the 696.5 nm line and reproducibility measurements; $+$: measurements of the 451.9 nm line.

[7] and are significantly less accurate than measurements with the same technique further in the expansion (for $z > 8$ mm, the accuracy for n_e is very high: about 3-5%). Figure 5 shows the electron density measurements using both methods as a function of axial position. The solid line represents the adiabatic model by Ashkenas and Sherman [8, 13]; this model describes the supersonic expansion of a neutral gas through a nozzle. The values measured by Fabry-Pérot interferometry provide additional information for n_e in a region where Thomson scattering becomes less accurate due to stray light. Good agreement with the adiabatic model is found.

B. Metastable densities

Until now, we have not considered the asymmetric 696.5 nm ($4p'[\frac{1}{2}]-4s[\frac{3}{2}]^0$) line profiles. This asymmetry of the 696.5 nm line was persistent after several new alignments, where, in each case, the apparatus profiles proved to be perfectly symmetric. Furthermore, the 415.9 nm line profile shows no asymmetry whatsoever. Together with the fact that the 696.5 nm profiles become symmetric at larger z -values ($z > 28$ mm) and at the edges of the plasma, we conclude that the asymmetry is a *real*, physical effect (see figure 6).

The following simple model gives an explanation for the observed phenomenon. We envisage the expanding plasma as consisting of two parts (see figure 7): a hot, fully homogeneous, central part with known n_e , T_e , $4p'$ level density, and T_0 . This region is surrounded by a relatively cool argon gas, containing a lot of metastables. In this peripheral region, the electron density and $4p'$ level density are assumed to be negligible (Figure 8). Both the temperature of the gas surrounding the plasma as well as the density of the $4s$ level are unknown. The distances a and b in figure 8 are determined from lateral emission scans (giving the value of a) and the geometry of the vessel, respectively.

Because the 696.5 nm line has a relatively large transition probability ($0.067 \times 10^8 \text{ s}^{-1}$) and ends in a metastable $4s$ level, self absorption is to be expected. In the plasma, the self ab-

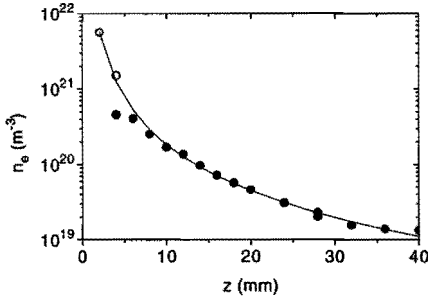


Figure 5: Electron density measurements vs. axial position. Open circles denote data obtained from the Stark broadening of the argon (I) 451.9 nm spectral line, measured with the Fabry-Pérot interferometer. Dots denote electron density measurements by Thomson scattering. The drawn line represents the adiabatic model by Ashkenas and Sherman (ref. [13]) for a supersonic expansion of a neutral gas through a nozzle.

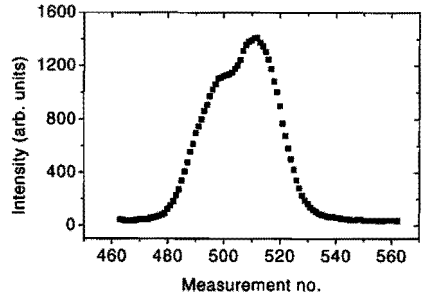


Figure 6: An example of an asymmetric line profile, as measured at $z = 12$ mm. The interval between two neighbouring points corresponds to a wavelength interval of 2.98×10^{-4} nm.

sorption profile is the same as the emission profile: a Voigt, shifted to the red due to the Stark effect. Absorption in the cold gas surrounding the plasma, however, takes place at the unshifted wavelength, because the electron density is negligible. So the absorption profile in the periphery of the jet is a Gaussian (Doppler broadening) with its center at the unshifted wavelength.

The total intensity profile I_λ is given by:

$$I_\lambda = C(1 - \exp(-\kappa_p, \lambda a)) \exp(-\kappa_g, \lambda b), \quad (3)$$

where $\kappa_{p,\lambda}$ and $\kappa_{g,\lambda}$ are the absorption coefficients, embedding the $4p'$ and $4s$ densities [14] for the plasma and the gas, respectively. The λ -dependence has the form of a Stark-shifted Voigt profile for the plasma, and the form of a Gaussian profile centered around the unshifted wavelength for the gas. C is a constant.

In order to fit the measured line profiles with a least-mean squares program containing Eq. (3), one has to use data from other sources: the electron density (Thomson-Rayleigh scattering), the heavy particle temperature in the plasma (415.9 nm line profile analysis), the lengths a and b , and the $4p'[\frac{3}{2}]$ level density (optical emission spectroscopy). By measuring the latter [8, 9], one has to in principle account for the fact that self absorption is important (as indicated by the asymmetric 696.5 nm line profiles!). In practice, however, this is not very important, as the absorption coefficients in Eq. (3) are proportional to $[(n/g)_{4s} - (n/g)_{4p'}]$ (where g is the statistical weight of the level concerned). Within and outside the plasma, the $4s$ density is much larger (about a factor 100) than the $4p'$ density, whereas the statistical weights of the two levels involved are of the same order of magnitude. So, the influence of errors in $(n/g)_{4p'}$ on the line profile is small. The free parameters for the fits, then, are the $4s[\frac{3}{2}]^0$ level density and the temperature of the metastable gas T_{4s} .

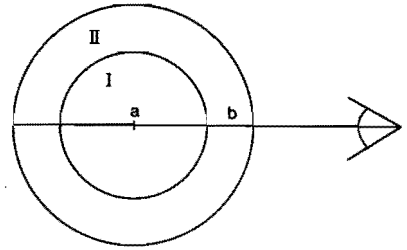


Figure 7: A schematic view of the model used to explain the asymmetric line profiles. The plasma cross section is envisaged as consisting of two parts: I, the (hot) plasma itself, and II, the cool gas surrounding the plasma. a and b are the dimensions of the two regions.

Figure 9 shows a line profile (at $z = 14$ mm, at the axis of the plasma jet) with its best fit. The simple model is capable of reproducing the line profiles very well. The fits thus give results for the metastable density and metastable temperature, as all the other parameters are known. The values are accurate within 30 %, in view of the errors in a and b and the simplification by considering only two (homogeneous) zones in the vessel. In figure 10, the metastable temperature in the periphery is compared to the heavy particle temperature of the plasma jet. An increase of the temperature of the periphery with increasing z , to the temperature of the central plasma, is clearly visible. This means that the total jet is becoming more and more isothermal. This is also indicated by Thomson-Rayleigh scattering measurements [7]. The metastable densities as a function of z are given in figure 11. Note, that these reflect the $4s[\frac{3}{2}]^0$ level densities in the periphery of the plasma (Figs. 7 and 8).

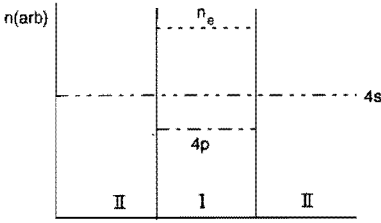


Figure 8: A sketch of the species concentrations as assumed in the model: The plasma has a finite electron density and a finite ($4p'$) level density, whereas the ($4s$) metastable density is supposed to be finite and constant both inside and around the plasma.

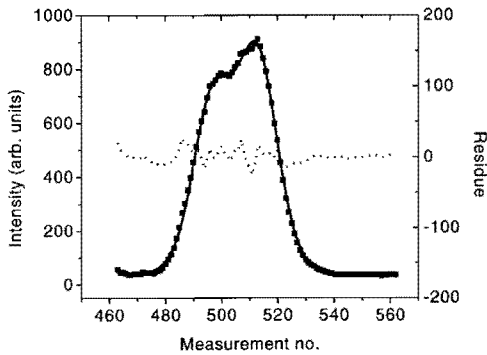


Figure 9: An example of a measured asymmetric line profile (at $z = 14$ mm) with its least-mean-squares fit and residue.

IV. DISCUSSION AND CONCLUSIONS

Fabry-Pérot measurements can extend the set of known plasma parameters (n_e , T_e , and n_0 , Thomson-Rayleigh scattering) by adding the heavy particle temperature T_0 . The information, however, is not spatially resolved, but always reflects a certain line of sight. This blurs some of the features so distinct in spatially resolved measurements, such as the internal structure of the (Barrel-type) shock [8, 7].

The accuracy of the Fabry-Pérot measurements is estimated to be within 30% for T_0 . This estimate was established by performing reproducibility checks on different days and by the margins of error as indicated by the fitting procedure.

The measured heavy particle temperatures are consistent with other measurements, as they fit to the heavy particle temperature at the end of the arc as well as to the electron temperature further in the vessel. Furthermore, the background pressure in the vessel gives an extra indication of the accuracy of the measurements. If pressure equilibrium is assumed further in the vessel, the background pressure is equal to the

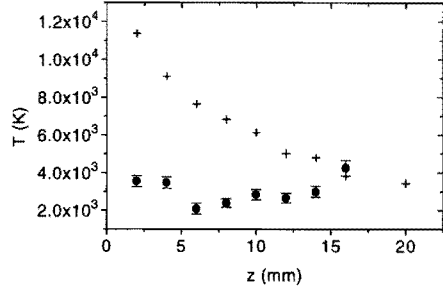


Figure 10: Heavy particle temperatures inside and around the plasma jet vs. axial position; (+) argon neutral temperature (compare Fig. 4); (•) temperature of the argon neutrals around the plasma, as derived from the fits of the asymmetric line profiles.

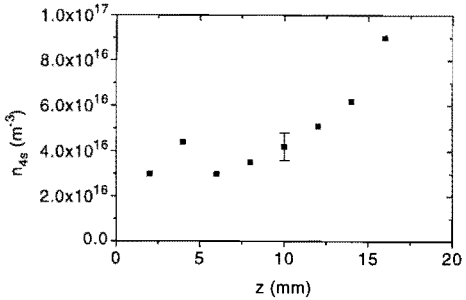


Figure 11: The $4s[3/2]^0$ metastable density around the plasma vs. the axial position.

sum of the gas pressure (which is equal to nkT and is, hence, largely determined by the heavy particles in these plasmas with a low ionization degree (3-4%)) and the stagnation pressure, which depends on the velocity of the particles [8]. If we insert an estimated value for this speed (600 m/s after the shock) and the measured values of T_e and T_0 further in the vessel, the sum of stagnation and gas pressures indeed matches the background pressure within 5%.

Electron density measurements using Stark broadening analysis appear to give additional information to Thomson scattering data, as the latter suffer from stray light close to the arc. The values obtained from Stark broadening of the lines are accurate within 30%, and show a good agreement with the adiabatic expansion model by Ashkenas and Sherman [13]. This strongly supports the view that the supersonic part of the expansion very closely resembles an adiabatic expansion [7].

The asymmetric line profiles give a wealth of information. In order to obtain the metastable densities and temperatures, we inserted all other known variables (such as the electron densities) into the fit. In principle, however, one may also use

this asymmetry to determine electron densities, as the asymmetry essentially proves to be a Stark shift effect. In this case, the fitting procedure uses more free parameters. The simple model of a two-region plasma jet is capable of reproducing the asymmetric line profiles very well. The accuracies of $T_{e,s}$ and $n_{e,s}$ are around 30% and 50%, respectively. These margins of error are indicated by reproduceability checks and the errors given by the fitting procedure, as well as by uncertainties in the emission and absorption lengths a and b (Figs. 7 and 8).

The fitting procedures were also performed with a slightly different model, in which the metastable densities (see Fig. 8) are assumed to be constant as well, but *different* in regions I and II. This, however, did not significantly change the metastable densities or temperatures in the periphery.

The measured metastable densities around the plasma are substantial (10^{17} m^{-3}). After a few centimeters in the expansion, these metastables are probably produced by the capture of resonant radiation from the plasma center. The temperature of the metastables around the plasma is a unique result from the line shape analysis. The metastable temperatures indicate that the plasma jet is becoming more and more isothermal, which is also indicated by Thomson scattering measurements [7].

ACKNOWLEDGMENT

We would like to thank H.M.M. de Jong and M.J.F. van de Sande for their skilful technical assistance during the measurements and M.C.K. Gruijters for drawing some of the figures.

References

- [1] J.J. Beulens, G.M.W. Kroesen, D.C. Schram, P.K. Bachman, H. Lydtin, and D.U. Wiechert, *Surf. Mod. Techn.* **III**, 69 (1989).
- [2] J.J. Beulens, A.J.M. Buuron, L.A. Bisschops, A.B.M. Hüsken, G.M.W. Kroesen, G.J. Meeusen, C.J. Timmermans, A.T.M. Wilbers, and D.C. Schram, *J. Phys. (Paris), Colloq.* **51**, C5-361 (1990).
- [3] A.T.M. Wilbers, G.J. Meeusen, M. Haverlag, G.M.W. Kroesen, and D.C. Schram, *Thin Solid Films* **204**, 59 (1991).
- [4] G.J. Meeusen, E.A. Ershov-Pavlov, R.F.G. Meulenbroeks, M.C.M. van de Sanden, and D.C. Schram, *J. Appl. Phys.* **71**, (may 1992).
- [5] R.F.G. Meulenbroeks, D.C. Schram, L.J.M. Jaegers, and M.C.M. van de Sanden, *Phys. Rev. Lett.* **69** (9), 1379 (1992).
- [6] G.M.W. Kroesen, D.C. Schram, and J.C.M. de Haas, *Plasma Chem. Plasma Proc.* **10**, 531 (1990).
- [7] M.C.M. van de Sanden, J.M. de Regt, G.M. Jansen, J.A.M. van der Mullen, D.C. Schram, and B. van der Sijde, *Rev. Scient. Instrum.* **63** (6), 3369 (1992).
- [8] M.C.M. van de Sanden, Ph.D. Thesis Eindhoven University of Technology (1991).
- [9] D.A. Benoy, J.A.M. van der Mullen, M.C.M. van de Sanden, B. van der Sijde, and D.C. Schram, *J. Quant. Spectrosc. Radiat. Transfer* **49** (2), 129 (1992).
- [10] H.R. Griem, *Spectral Line Broadening by Plasmas*, Academic Press, New York (1974).
- [11] H.R. Griem, *Plasma Spectroscopy*, McGraw-Hill, New York (1964).
- [12] J.J. Beulens, D. Milojevic, D.C. Schram, and P.M. Vallinga, *Phys. Fluids B* **3**, 2548 (1991).
- [13] H. Ashkenas and F.S. Sherman, *Proceedings of Rarefied Gasdynamics* **4**, ed. J.H. de Leeuw, Academic Press, New York (1966).
- [14] J.A.M. van der Mullen, Ph. D. Thesis Eindhoven University of Technology (1986).

Four Ways to Determine the Electron Density in Low-Temperature Plasmas

R.F.G. Meulenbroeks M.F.M. Steenbakkers Z. Qing
M.C.M. van de Sanden D.C. Schram

*Eindhoven University of Technology, Department of Physics,
P.O. Box 513, 5600 MB Eindhoven, The Netherlands*

Abstract. Four ways to measure the electron density in low-temperature plasmas are presented: Thomson scattering, Langmuir probe, optical emission spectroscopy, and continuum radiation analysis. The results of the four methods are compared to each other and discussed. For the electron density range of $10^{19} - 10^{21} \text{ m}^{-3}$, Thomson scattering proved to give the most accurate results (within a few percent); the Langmuir probe measurements also proved accurate (15%). A collisional radiative model fit through excited level populations and continuum analysis yield results in good agreement with Thomson scattering data, although with larger margins of error (around 40%). A simple Saha-fit proved to be inadequate.

I. INTRODUCTION

In a sense, the study of plasmas begins with measuring n_e , the electron density. It constitutes one of the most fundamental parameters for plasmas, as for many plasma types n_e varies a great deal more than, e.g., the electron temperature T_e . However, it is often difficult to determine accurately n_e (say, within 10%). In the present study, we present four methods to determine n_e in low-temperature (electron temperature below 0.5 eV) plasmas.

Probably the most accurate, local, and unambiguous way to determine n_e (i.e., for our experiment: $n_e > 10^{18} \text{ m}^{-3}$) is Thomson scattering [1]. Accuracies of 3% can be achieved using this diagnostic; the tradeoffs are price and complexity [2]. In the present study we compare other (cheaper and more simple) methods, i.e. Langmuir double probe, optical emission spectroscopy (OES), and continuum analysis, to Thomson scattering. The measurements are carried out on a low-pressure recombining plasma jet, which has been used successfully for deposition of carbon and silicon materials [3, 4] and looks promising for source applications (H^+ , H^-) [5] as well (Fig. 1). With its greatly varying n_e [2, 6] and recombining character, it also proved very suitable as a subject for this investigation.

II. EXPERIMENT AND DIAGNOSTICS

A continuously operated D.C. arc creates an argon plasma at subatmospheric pressures (0.6-0.2 bar, diameter plasma channel 4 mm) which expands into a heavily pumped vacuum vessel, creating a supersonic expansion, ending in a stationary shock and followed by a subsonic relaxation. The plasma source can be moved within the vacuum vessel (in the x , y , and z directions). The vacuum vessel has a length of 3 m and a diameter of 0.36 m; the plasma jet has a length of about 0.7 m and a diameter increasing from 4 mm to about 15 cm. The plasma condition is kept constant: arc current: 45 A, arc voltage: 100 V, background pressure: 40 Pa, argon flow: 3.5 standard liters per minute. Details can be found in [2, 7]. Before turning to the results, we will discuss very shortly the

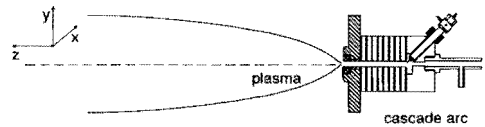


Figure 1: *The cascaded arc experiment. A thermal plasma at subatmospheric pressure is created in a continuously operated D.C. arc, consisting of three cathodes, three electrically isolated copper plates, and an anode plate. All the parts are water cooled. The plasma expands through the nozzle into a low-pressure (40 Pa) vessel, creating a supersonically expanding plasma jet.*

principles and diagnostic characteristics of the different methods, as they are well known from literature.

Thomson scattering is the scattering of electromagnetic radiation off free electrons in a plasma. In the classical view, the electron is forced to oscillate with the incident field, after which it becomes a dipole oscillator itself. This dipole radiation can be detected (during Thomson scattering, the wavelength remains unchanged save for Doppler effects, which give T_e information) and is proportional to the number of electrons in the detection volume. For Thomson scattering, Nd:YAG (yttrium aluminum garnet) frequency-doubled laser radiation (532 nm) is focused on the plasma by a $f = 0.5$ m lens, resulting in a beam waist in the focal plane of $100 \mu\text{m}$. The 90° scattered radiation is transmitted through an optical system, dispersed by a hollow concave grating, and detected by an image-intensified photo diode array. The total Thomson scattered radiation (which can be distinguished from the Rayleigh scattering off bound electrons) is directly proportional to n_e . Calibration is performed at a known amount of pure argon gas. The apparatus has been used very successfully to determine electron densities and temperatures as well as neutral particle densities in recombining plasma jets [2, 7].

Table 1. A comparison of four methods to determine n_e in recombining plasmas: T.S.: Thomson Scattering, CRM: Collisional Radiative Model, Saha: Saha fit through uppermost levels, Cont.: Continuum measurements averaged for blue and red part of the spectrum, Probe: double Langmuir probe. In the third main column, n_e^* represents n_e values calculated using T_e obtained from Thomson scattering measurements.

z (mm)	n_e (10^{19}m^{-3})			Δn_e (%)			n_e^* (10^{19}m^{-3})		
	20	40	70	20	40	70	20	40	70
T.S.	6.5	1.8	4.6	15	7.5	8			
CRM	5.0	1.7	8.4	50	50	50	5.0	2.0	4.5
Saha	3.7	4.2	9.8	60	60	60	3.5	2.8	4.5
Cont.	5.3	2.2	3.8	30	30	30			
Probe	6.0	5.4	4.5	15	15	15			

The dynamic range for n_e is 10^{18} - 10^{22}m^{-3} , the accuracy around 3-5%.

The double Langmuir probe is an intrusive method, i.e. it does not leave the plasma undisturbed, as the other techniques described here. By inserting two electrodes (length 7 mm, diameter 0.4 mm) in the plasma, the ion saturation current is measured, from which n_e can be determined [8, 9]. I-V-characteristics are obtained using a function generator and a personal computer. The PC also determines n_e and T_e from the shape of the characteristics. The Langmuir probe is a local method with a large dynamic range (n_e detection limit around 10^{16}m^{-3}).

Optical Emission Spectroscopy (OES): The atomic state distribution function (ASDF) for an excitation system (e.g. argon I) reflects the (non-) equilibrium state of a plasma [10]. For the determination of n_e , the procedure is as follows: using line intensity measurements, an n_p/g_p vs. I_p (Boltzmann-) plot is constructed, with n_p/g_p the absolute level population per statistical weight and I_p the ionization potential of the level designated p . By assuming the uppermost levels in an atomic system to be in Saha-equilibrium with the adjacent ion ground state, n_e can be determined as well [10, 11]. Fitting a straight line through the uppermost levels in a Boltzmann plot gives the electron density (and temperature). A second, more sophisticated method introduces a collisional-radiative (CR) model to describe the level population of all the measured levels. In our recombining case, we used a simple model by Biberman *et al* [12], which assumes that the deexcitation from level p downward is equal to the deexcitation ending on level p . The model was slightly adjusted to incorporate highly excited states [13]:

$$\frac{n_p}{g_p} = \left(\left(\frac{I_p}{kT_e} \right)^{\frac{1}{2}} + 1 \right) \left(\frac{n_e^2 h^3}{g_i g_e (2\pi m_e k T_e)^{\frac{3}{2}}} \right). \quad (1)$$

In (1), k is Boltzmann's constant, T_e is the electron temperature, h is Planck's constant, g_i and g_e are the statistical weights of the ion ground state and the free electron, respectively, and m_e is the electron rest mass. This model is valid for $I_p \gg kT_e$, whereas for $I_p \leq kT_e$ Saha equilibrium is assumed. A model fit yields n_e and T_e . A similar model can be applied to ionizing plasmas [12].

In the OES system, plasma light is transmitted through

an optical system, analyzed by a monochromator (Jerryl-Ash 0.5 m, resolution 0.16 nm), and detected by a cooled (-20°C) photomultiplier (RCA 31034) [7, 14]. A number of lines in the argon system are used: 811.5, 763.4, 750.4, 703.0, 696.5, 693.8, 591.2, 588.9, 531.8, 518.8, 505.0, and 420.1 nm. Data on these transitions can be found in [14, 15]. The optical system is calibrated in an absolute way using a tungsten ribbon lamp (accuracy $< 10\%$). Lateral plasma scans are taken using a stepper motor driven rotating mirror. Abel-inversion is used to convert the lateral scans into radial n_p/g_p profiles [11, 16, 17].

The continuum radiation of this type of plasma is dominated by the electron-ion free-bound radiation. The total continuum emissivity ϵ ($\text{Wm}^{-3}\text{sr}^{-1}\text{m}^{-1}$) can be written as [18, 19]:

$$\epsilon = C \frac{(n_e)^2}{\lambda^2 \sqrt{T_e}} \xi_{tot}, \quad (2)$$

with λ the wavelength (in m), $C = 1.63 \cdot 10^{-43} \text{Wm}^4\text{K}^{\frac{1}{2}}\text{sr}^{-1}$, and $\xi_{tot} = 1.7 \pm 0.2$ is the total Biberman factor [18, 19]. If T_e can be estimated (e.g. from a simple Saha fit in a Boltzmann plot, the T_e dependence is very weak), n_e can be determined.

The continuum part of the spectrum is measured using the OES diagnostic. Continuum radiation was measured in the red ($\lambda = 633.5$ nm) and in the blue ($\lambda = 468.8$ nm) part of the spectrum. Also in this case, lateral scans are taken and Abel-inverted into radial emissivity data.

The fact that the plasma can be moved inside the vessel without changing significantly facilitates the application of different diagnostic techniques to the same plasma. Great care is taken to make sure that all of the above diagnostics are applied at exactly the same z position (i.e. $\Delta z \approx 0.5$ mm). With the OES system, measurements are taken at $z = 20, 40,$ and 70 mm ($z = 0$ representing the onset of the expansion, the exit nozzle of the arc). With the Thomson scattering apparatus and the Langmuir probe, data are taken at smaller intervals, covering the entire plasma jet from $z = 0$ to 500 mm. A comparison between all four methods will be made at $z = 20, 40,$ and 70 mm.

III. RESULTS AND DISCUSSION

Table 1 gives a compilation of the results. The Thomson scattering data are taken as a standard, as this diagnostic requires

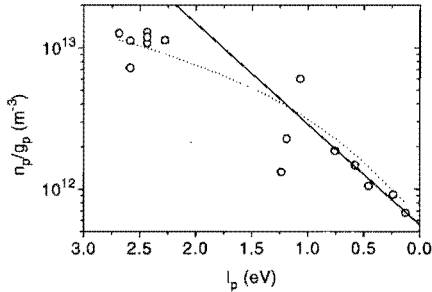


Figure 2: An example of a Boltzmann plot: n_p/g_p vs. I_p , constructed using the OES measurements. The data are taken at $z = 70$ mm. The dotted line represents a fit with a collisional radiative model, whereas the drawn line is a simple straight line fit through the uppermost levels, assuming these to be in Saha-equilibrium with the adjacent continuum.

no assumptions on plasma equilibrium etc.. The margins of error are established by adding the relative errors in the measurement and data acquisition procedure (5% [2]) to those introduced by plasma reproducibility. Thomson scattering is the only diagnostic which is intrinsically accurate enough to render these day-to-day plasma changes observable.

Figure 2 gives an example of a Boltzmann plot at $z=70$ mm, with both a CRM fit and a simple Saha fit. The margins of error indicated in Table 1 are a result of: (a) plasma reproducibility errors (10%), (b) errors in the calibration (<10%), (c) errors in the transition probabilities (25-50%, [15]), the Poisson statistics (usually <10%), and (d) errors in the Abel-inversion procedure (a few %).

The margins of error for the results calculated from the continuum emissivity are due to: (a) plasma reproducibility errors (10%), (b) calibration errors (<10%), (c) errors in the Abel-version procedure (a few %), and (d) the Poisson statistics (around 30%, as the signal is very weak).

The double probe measurements need some additional explanation. Even though the statistical errors (indicated in Table 1) are rather small, a large difference with the Thomson data is observed at $z = 40$ mm, where the stationary shock front is situated [2]. This may be caused by the disturbance of the flow pattern by the probe insertion, which is most drastic within the shock, where gradients are large. Furthermore, the probe area (2×7 mm²) may be too large to fully resolve the shock features, introducing systematic errors. The values outside the shock region are in rather good agreement (within the stochastic errors) with the Thomson scattering data. This is clear in Fig. 3, which shows a comparison of Thomson scattering and probe data for a range of axial positions. The systematic deviation downward for $z > 150$ mm is a consequence of a poorly determined T_e , resulting in a low n_e value. When the Thomson scattering T_e [2] is used to correct for these errors, an agreement within 10% is reached for $z > 150$ mm. The discrepancy at the shock position, however, is not solved in this manner [20].

The Thomson scattering values for T_e can also be used to

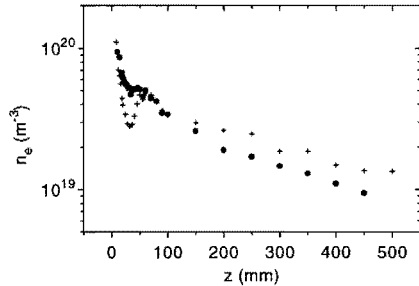


Figure 3: A comparison between Thomson scattering and Langmuir probe data; the electron density on the axis of the plasma jet vs. the distance from the onset of the expansion. The general agreement is good (i.e. within 15%), whereas in the shock region (around $z = 40$ mm) a deviation is observed: insertion of the probe evidently disturbs the flow pattern significantly at these axial positions.

correct the n_e values as determined from the OES measurements, thus eliminating one of the major drawbacks of the OES method. The T_e values are 0.17, 0.24, and 0.26 eV at $z = 20, 40,$ and 70 mm, respectively [14]. The results are given in the last column of table 1. The n_e values, thus obtained with the Saha-method, show a much better agreement with Thomson scattering data. For the CR model, the value at $z = 70$ mm is brought in line with Thomson data. This shows that, particularly when determining n_e using Saha, the error in T_e is a dominant factor. The continuum measurements show no significant difference when Thomson scattering T_e values are used.

In conclusion we can state that there are some good alternatives to Thomson scattering for the determination of n_e , if accuracies around 30% are permissible. Probe measurements are an alternative, especially since the detection limit is low: around 10^{16} m⁻³. A drawback may be the fact, that flow patterns are disturbed when the probe is inserted. Both the continuum results and the CRM fits yield results in good agreement with Thomson scattering data. A simple Saha fit proved to be adequate only to give an indication for the order of magnitude of n_e (i.e. within a factor of 2-3).

ACKNOWLEDGEMENT

The authors would like to thank A. Griguoli, H.M.M. de Jong, and M.J.F. van de Sande for their skillful assistance during the measurements.

References

- [1] J. Sheffield, *Plasma Scattering of Electromagnetic radiation*, Academic Press, New York (1975).
- [2] M.C.M. van de Sanden, J.M. de Regt, G.M. Janssen, J.A.M. van der Mullen, D.C. Schram, and B. van der Sijde, *Rev. Scient. Instr.* **63** (6), 3369 (1992).

- [3] J.J. Beulens, G.M.W. Kroesen, D.C. Schram, P.K. Bachman, H. Lydtin, and D.U. Wiechert, *Surf. Mod. Techn.* **III**, 69 (1989).
- [4] A.T.M. Wilbers, G.J. Meeusen, M. Haverlag, G.M.W. Kroesen, and D.C. Schram, *Thin Solid Films* **204**, 59 (1991).
- [5] R.F.G. Meulenbroeks, D.C. Schram, L.J.M. Jaegers, and M.C.M. van de Sanden, *Phys. Rev. Lett.* **69** (9), 1379 (1992).
- [6] M.C.M. van de Sanden, J.H. de Regt, and D.C. Schram, *Phys. Rev. E* **47** (4), 2792 (1993).
- [7] M.C.M. van de Sanden, Ph.D. Thesis Eindhoven University of Technology (1991).
- [8] L. Schott in *Plasma Diagnostics* (ed. W. Lochte-Holtgreven), North Holland, Amsterdam (1968).
- [9] M.J. de Graaf, R. Severens, R.P. Dahiya, M.C.M. van de Sanden, and D.C. Schram, *Phys. Rev. E* **48**, 2098 (1993).
- [10] J.A.M. van der Mullen, *Phys. Rep.* **191** (2,3), 109 (1990).
- [11] G.J. Meeusen, E.A. Ershov-Pavlov, R.F.G. Meulenbroeks, M.C.M. van de Sanden, and D.C. Schram, *J. Appl. Phys.* **71** (9), 4156 (1992).
- [12] L.M. Biberman, V.S. Vorob'ev, and I.T. Yakubov, *Kinetics of Non-equilibrium Low Temperature Plasmas*, Plenum New York (1987).
- [13] D.A. Benoy, J.A.M. van der Mullen, M.C.M. van de Sanden, B. van der Sijde, and D.C. Schram, *J. Quantit. Spectrosc. Radiat. Transfer* **49**, 129 (1993).
- [14] R.F.G. Meulenbroeks, A.J. van Beek, A.J.G. van Helvoort, M.C.M. van de Sanden, and D.C. Schram, *Phys. Rev. E* **49**, 4397 (1994).
- [15] W.L. Wiese, M.W. Smith, and B.M. Miles, *Atomic Transition Probabilities*, Reprt No. NSRDS-NBS22, Nat. Bur. Std., Washington, D.C. (1969).
- [16] S.R. Deans, *The Radon Transform and Some of its Applications*, Wiley Interscience, New York (1983).
- [17] C.A. Kak and M. Slaney, *Principles of Computerized Tomographic Imaging*, IEEE press, New York (1988).
- [18] V.M. Lelevkin, D.K. Otorbaev, and D.C. Schram, *Physics of Non-Equilibrium Plasmas*, chapter 8, North-Holland, Amsterdam (1992).
- [19] A.T.M. Wilbers, G.M.W. Kroesen, C.J. Timmermans, and D.C. Schram, *J. Quantit. Spectrosc. Radiat. Transfer* **45**, 1 (1991).
- [20] Z. Qing, M.J. de Graaf, D.K. Otorbaev, M.C.M. van de Sanden, and D.C. Schram (unpublished).

Argon-Hydrogen Plasma Jet Investigated by Active and Passive Spectroscopic Means

R.F.G. Meulenbroeks

A.J. van Beek

A.J.G. van Helvoort

M.C.M. van de Sanden

D.C. Schram

Eindhoven University of Technology, Department of Physics,

P.O. Box 513, 5600 MB Eindhoven, The Netherlands

Abstract. A supersonically expanding argon cascaded arc plasma, with different amounts of hydrogen added (0, 0.7, and 1.4 vol. % H_2), was studied using Thomson-Rayleigh scattering and optical emission spectroscopy. With hydrogen added, the electron density profile as a function of the distance from the onset of the expansion shows a large extra ionization loss (compared to the pure argon case), especially after the stationary shock front. This anomalous loss of ionization is attributed to molecular processes, such as associative charge transfer between Ar^+ and H_2 and dissociative recombination of the resulting ArH^+ molecular ion. Spatially resolved emission spectroscopy shows, that in the expansion the radial hydrogen emission profiles are broader than the argon profiles. The addition of hydrogen appears to change the characteristic shock behaviour of pure argon. For both the argon and the hydrogen system it is shown, that the uppermost levels are in Saha equilibrium with their adjacent continuum. The measurements are in agreement with the view, that association of hydrogen atoms at the vessel walls, results in a re-entry flow of hydrogen molecules in the plasma beam.

I. INTRODUCTION

The fundamental study of plasmas, expanding out of a cascaded arc thermal plasma source, is important in view of the use of these plasmas for ultra fast deposition of a:Si-H, a:C-H, graphite, and diamond thin films [1]-[3]. In the past, pure argon expanding plasmas have been studied extensively, especially the stationary shock front, occurring a few centimeters after the onset of the supersonic expansion. This research has resulted in a good understanding of expanding plasmas in pure argon [4]-[6]. The next step towards deposition plasmas is the study of argon plasmas with small amounts of simple molecules added, e.g. H_2 . The research on argon-hydrogen plasmas is important for another reason: these plasmas may be used as hydrogen atom and hydrogen negative or positive ion sources. In the following, an experimental study of argon/hydrogen plasma jets is presented.

II. EXPERIMENT

A. The cascaded arc experiment

In Fig. 1, the experiment is sketched [5]. The cascaded arc plasma source consists of three cathodes, three electrically isolated copper plates, and an end anode plate. All the parts are water cooled [7]. The arc channel has a diameter of 4 mm. The arc produces a thermal plasma at subatmospheric pressure, characterized by a relatively high heavy particle temperature ($T_h \approx T_e \approx 1$ eV) and high electron densities (10^{22} - 10^{23} m^{-3}).

This plasma is allowed to expand onto a low pressure background, creating a supersonically expanding jet, ending in a stationary shock. The low pressure region consists of a heavily pumped (max. 700 litres per second) stainless-steel vessel. After the shock, axial velocities are subsonic (i.e., around 600 m/s). The experimental conditions for all the following experiments are: $I_{arc} = 45$ A, $V_{arc} = 105$ V, background pres-

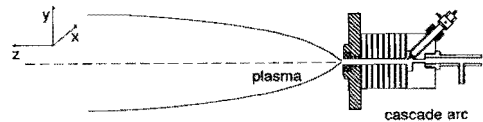


Figure 1: *The cascaded arc experiment: a thermal plasma at atmospheric pressure is created in a continuously operated D.C. arc, consisting of three cathodes, three electrically isolated copper plates, and an anode plate. All these parts are water cooled. The plasma expands into a low-pressure region, creating a supersonically expanding plasma jet.*

sure $p_{back} = 40$ Pa, argon gas flow = 3.5 SLM (standard liter per minute).

Hydrogen can be added in small amounts to the flow *before* it enters the cascaded arc. In the experiments the hydrogen flows chosen were 25 sccm (standard cubic centimeters per minute) and 50 sccm, resulting in H_2 fractions of 0.7 vol. % and 1.4 vol. % entering the arc.

B. Diagnostics

B1. Thomson-Rayleigh scattering

Figure 2 shows the combined Thomson-Rayleigh diagnostic, which is described in detail elsewhere [5]. The frequency doubled Nd:YAG (yttrium aluminum garnet) laser (Quanta Ray DCR 11) radiation at 532 nm is focused onto the plasma. The scattered radiation is observed under a 90° angle and analyzed by a polychromator and an image intensified photo diode array. The stray light level is reduced substantially by placing the laser dump far away, outside the vessel. The analysis of the

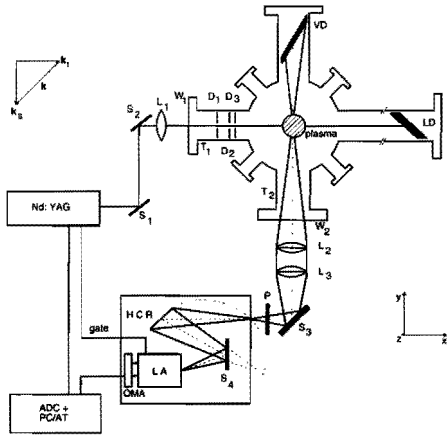


Figure 2: The Thomson-Rayleigh diagnostic. Frequency doubled Nd:YAG radiation is focused onto the plasma by a system of two dichroic mirrors (S_1 and S_2) and a lens L_1 . The stray light level is reduced by placing the laser dump (LD) far away (i.e., 2 m), and installing several diaphragms D_1 - D_3 . The scattered radiation is transmitted through a system consisting of lenses L_2 and L_3 and a mirror S_3 . Detected radiation is dispersed by a hollow concave grating (HCR), amplified by a gated light amplifier (LA), and detected by an optical multichannel analyzer (OMA). The data are processed by a personal computer (PC/AT), using an analog-to-digital converter (ADC).

scattered signal gives accurate and spatially resolved (scattering volume $\approx 0.25\text{mm}^3$) information about the electron density, electron temperature, and the neutral particle density in the plasma. The plasma source can be moved along the z -axis without significantly changing the plasma, making axial scans possible while keeping the diagnostics fixed.

B2. Optical emission spectroscopy (OES)

Plasma radiation is measured with an optical emission spectroscopy experiment (Fig. 3, [4]). A Czerny-Turner type monochromator (Jarrell-Ash 0.5 m) is used in combination with a Peltier-cooled photomultiplier tube (RCA 31034) to analyze the plasma radiation. Entrance and exit slits of $25\ \mu\text{m}$ and $100\ \mu\text{m}$, respectively, are used and result in a spectral resolution of $0.16\ \text{nm}$. The output of the photomultiplier is amplified and analyzed by a photon counting system. Lateral plasma scans are possible by moving a step motor-driven rotating mirror in the system. The photon-counting data processing and step motor control are implemented in a modular, M68000 processor based, laboratory computer system. A low wavelength cut off filter was used for wavelengths above $500\ \text{nm}$ to eliminate second-order radiation. The OES system was calibrated in an absolute way using a tungsten ribbon lamp placed at the plasma location in the vessel.

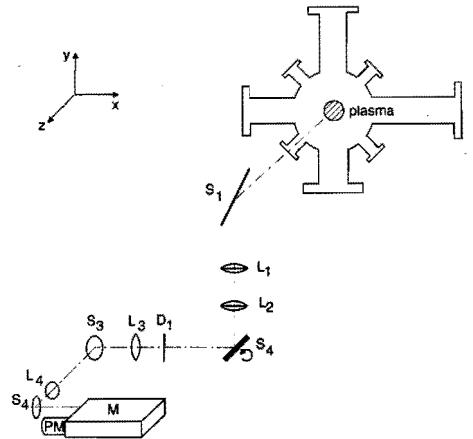


Figure 3: The optical emission spectrometer. Plasma radiation is transmitted through a system of mirrors (S_1 - S_4) and glass lenses (L_1 - L_4). Mirror S_2 can be rotated in order to perform lateral plasma scans. A second order filter can be inserted in front of lens L_4 (for wavelengths above $500\ \text{nm}$). A Czerny-Turner monochromator (M) analyzes the radiation with a resolution of $0.16\ \text{nm}$. A cooled photomultiplier (PM) detects the transmitted photons.

C. Measurements

C1. Thomson-Rayleigh scattering

Spatially resolved measurements of the electron density, electron temperature, and neutral particle density are carried out at different distances from the expansion nozzle, at the plasma jet axis. Because of an effective stray light reduction and an accurate fit procedure, relative errors in these measured quantities are low: about 5%, 15%, and 20%, respectively [5]. The neutral particle density, determined from the Rayleigh scattered signal, is about equal to the argon heavy particle concentration, as the hydrogen seed-in flow is very small. The measurements are performed for 0.7 and 1.4 vol. % H_2 admixed in argon.

C2. Optical emission spectroscopy

Lateral scans of the plasma are performed for 13 argon neutral lines and the first four hydrogen Balmer lines. Usually, every lateral scan consists of 80 measurements, covering a lateral range of $100\ \text{mm}$. These lateral measurements are converted to radial profiles by a fast Abel-inversion procedure using filtered back projection [8]. After correction for the efficiency of the system (using the ribbon lamp calibration), these radial profiles can be converted into radial profiles of the absolute level population per statistical weight. The lines, selected for the light emission measurements, with relevant data [9], are presented in table 1.

Table 1. The argon and hydrogen lines selected for the OES measurements. E_p (in eV) is the energy measured from the ground state, I_p (in eV) is the ionization energy of the level $E_i - E_p$, λ gives the wavelength of the transition in nm, g_p is the degeneracy of the upper level, A_{pq} is the transition probability (in 10^8 s^{-1}). The accuracies are the relative errors in the A_{pq} 's.

transition	λ	E_p	I_p	g_p	A_{pq}	accuracy
<i>argon</i>						
4p \rightarrow 4s	811.5	13.07	2.69	7	0.366	25%
4p \rightarrow 4s	763.5	13.17	2.59	5	0.274	25%
4p' \rightarrow 4s	696.5	13.32	2.44	3	0.067	25%
4p' \rightarrow 4s'	750.4	13.48	2.275	1	0.472	25%
5p \rightarrow 4s	416.4	14.52	1.239	3	0.00295	25%
5p \rightarrow 4p	420.1	14.57	1.185	7	0.0103	25%
4d \rightarrow 4p	693.8	14.69	1.065	1	0.0321	25%
6s \rightarrow 4p	703.0	14.84	0.915	5	0.0278	25%
4d' \rightarrow 4p	591.2	15.00	0.755	3	0.0105	25%
7s \rightarrow 4p	588.9	15.18	0.575	5	0.0134	25%
5d' \rightarrow 4p	518.8	15.30	0.456	5	0.0138	25%
8s \rightarrow 4p	506.0	15.32	0.235	9	0.0039	50%
7d' \rightarrow 4p'	531.8	15.63	0.125	7	0.0027	50%
<i>hydrogen</i>						
3 \rightarrow 2	656.3	12.09	1.507	18	0.4410	1%
4 \rightarrow 2	486.1	12.75	0.847	32	0.0841	1%
5 \rightarrow 2	430.4	13.06	0.519	50	0.0253	1%
6 \rightarrow 2	410.2	13.22	0.378	72	0.0097	1%

The OES measurements are performed at three axial positions, at distances of 20, 40, and 70 mm from the nozzle, for the pure argon case and for the two hydrogen-argon mixtures. The accuracy of OES results is mainly determined by the inaccuracies in the transition probabilities (table 1), which amount up to 25-50% for argon. Furthermore, plasma reproducibility errors as well as calibration errors have to be taken into consideration: $\pm 20\%$ and 10% , respectively.

III. RESULTS

A. Thomson/Rayleigh scattering results

The results of the axial scans are presented in Fig. 4. The neutral density behaviour is equal (within the margin of error) for all three conditions. Adding a small amount of hydrogen, therefore, does not influence the general structure of the expansion, as expected for these low admixtures. The expansion consists of a supersonic part ($z \approx 0-40$ mm), a shock region ($z \approx 40-70$ mm), and a subsonic relaxation region (after $z=70$ mm).

The electron temperature is also nearly independent of the hydrogen admixture. The data scattering in this case, however, makes it difficult to draw conclusions about possible slight changes in temperature behaviour. The electron density is severely influenced by adding such a small amount of hydrogen, especially in the subsonic relaxation region. To make this more clear, Fig. 5 gives the electron density as normalized to that of the pure argon case. The data show a somewhat lower electron density right from the onset of the expansion. The ratio remains constant for the first 70 mm, but starts to decrease rapidly after the shock. This decrease turns out to be

about twice as fast when the amount of admixed hydrogen is doubled.

B. Optical emission spectroscopy results

As was pointed out above, proper calibration of the OES system makes possible the calculation of radial profiles of the absolute level population per statistical weight n_p/g_p . These profiles turned out to be quite congruent both for the different argon lines and for the different hydrogen lines. The differences between the two species, however, are substantial, so we concentrate on one argon and one hydrogen line (Ar I 696.5 nm; H I 656.3 nm).

Figure 6, then, shows these radial n_p/g_p -profiles for the 696.5 Ar I transition (4p' level, table 1), at three z -positions and for 0, 0.7, and 1.4 vol. % hydrogen added. Especially the behaviour at $z=40$ mm is interesting, as the characteristic shock-dip at $r=0$ seems to disappear when more hydrogen is added, a phenomenon observed for all argon lines measured. The hydrogen H α (p (principle quantum number) = 3) radial profiles are shown in Fig. 7 for the same two hydrogen admixture conditions. These hydrogen profiles prove to be substantially wider than the corresponding argon profiles. This is even more apparent in Fig. 8, where the n_p/g_p -profiles for argon and hydrogen have been normalized.

The n_p/g_p -profiles of highly excited levels can be used to obtain the ion concentration ratio n_{Ar^+}/n_{H^+} by a method utilized by Meeusen *et al* [10]. The argument starts by assuming a Saha-equilibrium between the uppermost excited levels and their adjacent continuum:

$$\frac{n_s + n_e}{(n/g)_{s,p}} = C u_s + T_e^{-3/2} \exp[-(E_i - E_p)/kT_e]. \quad (1)$$

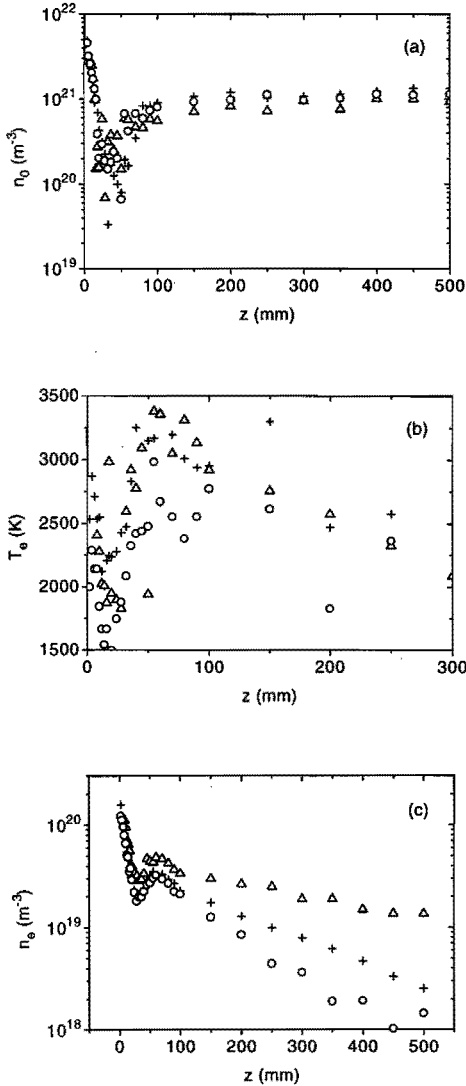


Figure 4: The results from the Thomson and Rayleigh scattering measurements for the three conditions mentioned in the text. (a) The neutral density n_0 vs. the axial position z ; (b) the electron temperature T_e vs. z ; (c) the electron density n_e vs. z . Δ : pure argon, +: 0.7 vol.% H_2 , \circ : 1.4 vol.% H_2 .

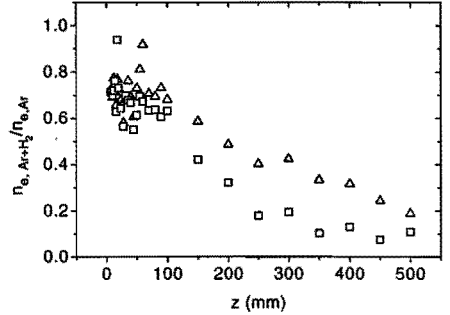


Figure 5: The normalized electron density $n_{e, Ar+H_2}/n_{e, Ar}$ vs. the axial position z . Triangles denote 0.7 vol.% H_2 , squares denote 1.4 vol.% H_2 .

The subscript s is used to indicate one of the species Ar or H, whereas a superscript "+" denotes the corresponding ionized species. The constant $C = (2\pi m_e k/h^2)^{3/2}$, u_{s+} is the ion partition function. The other symbols have their usual meaning: k - Boltzmann's constant; h - Planck's constant; m_e - the electron rest mass; T_e - the electron temperature; E_i - the ionization potential of the species concerned, and E_p - the excitation energy from the atom ground state of the level designated p . The lowering of the ionization potential due to the plasma environment is very small (0.01 eV) and is neglected [11].

If we write Eq. (1) for both the hydrogen and the argon system, an expression for the ion concentration ratio can be obtained:

$$\frac{n_{Ar+}}{n_{H+}} = \frac{(n_p/g_p)_{Ar} u_{Ar+}}{(n_q/g_q)_{H} u_{H+}} \times \left(\frac{(E_i - E_p)_{Ar} - (E_i - E_q)_H}{kT_e} \right), \quad (2)$$

where the hydrogen excited level is designated q . When applying Eq. (2), our main interest is to make sure, that the upper levels of the transitions chosen are in Saha-equilibrium with their respective continua, i.e., that their population is governed by (1). An estimate of this "Saha-region" for recombining plasmas can be obtained using [11, 12]. In our case, with $n_e \approx 3 \times 10^{19} m^{-3}$, and $T_e \approx 0.20$ eV, the region of Saha equilibrium extends to about 1.1 eV from the continuum. This leads us to use $H\delta$ ($E_i - E_q = 0.378$ eV) and Ar I 518.8 nm ($E_i - E_p = 0.456$ eV). The accuracy of n_{Ar+}/n_{H+} is mainly determined by the accuracy of n_p and n_q , as T_e is known within 20%.

Figure 9, then, gives the results of the calculations using Eq. (2): the n_{Ar+}/n_{H+} ratios for both conditions with hydrogen, for the three z -positions where measurements were taken. The corresponding absolute ion concentrations can be calculated using the principle of quasi-neutrality:

$$n_{Ar+} + n_{H+} = n_e, \quad (3)$$

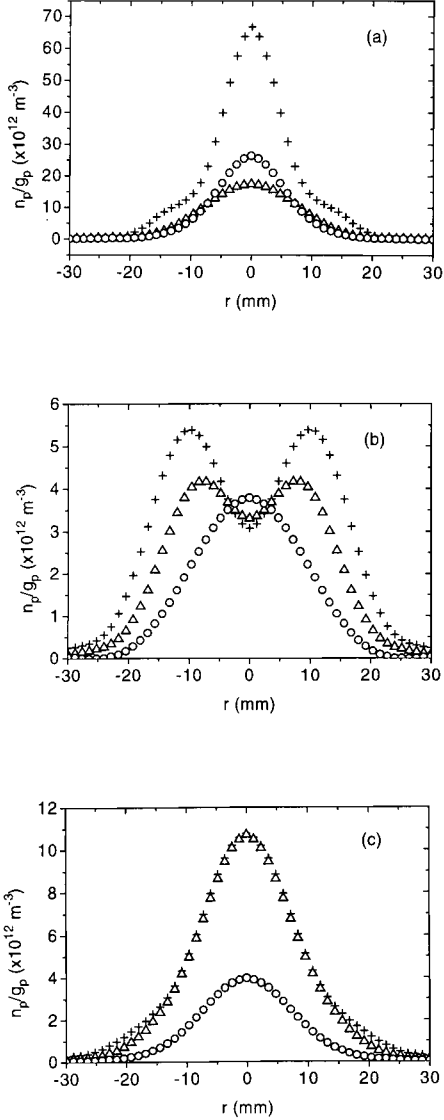


Figure 6: Optical emission spectroscopy results: Ar $4p'[\frac{1}{2}]$ density (per statistical weight) radial profiles, for different hydrogen admixtures, at three z -positions: (a) $z=20$ mm; (b) $z=40$ mm; (c) $z=70$ mm. +: pure argon, Δ : 0.7 vol.% H_2 , o: 1.4 vol.% H_2 .

where we neglect doubly ionized species as well as molecular and negative ions as a first approximation. As $n_{Ar^+} \gg n_{H^+}$, in particular at the plasma axis (Fig. 9), we can actually take $n_e \approx n_{Ar^+}$.

C. Combined results

We can look more closely at the presence of some kind of equilibrium between the different excited levels by combining the OES results with the Thomson-Rayleigh scattering data. To do so, we introduce the *population factor* b_p , which represents the absolute level population weighed against the level population according to Saha:

$$b_p = \frac{n_p}{n_{p,Saha}}, \quad (4)$$

where $n_{p,Saha}$ is calculated from (1) using the measured values of n_e and T_e (Fig. 4). In the region of Saha-equilibrium, of course, $b_p = 1$.

For the case of a *pure argon* plasma, b_p vs. $E_i - E_p$ plots for all levels measured are presented at three z -positions. As can clearly be seen, $b_p \approx 1$ holds for highly excited levels ($E_i - E_p \leq 0.5$ eV) at all z -positions. This constitutes a secure test for measurements and calibrations, as these plots combine theory ($b_p = 1$ for highly excited states in recombining plasmas), Thomson scattering results (n_e, T_e values to calculate $b_{p,Saha}$), and OES results (n_p measurements). The fact, that b_p approaches unity when $E_i - E_p$ approaches zero means, that the Thomson and OES measurements are in good agreement with each other within the experimental errors.

Finally, then, the b_p vs. $E_i - E_p$ plots for the *hydrogen-argon mixtures* are presented in Figs. 10 and 11 (all at $r = 0$). The hydrogen and argon systems can be presented in a single frame, as b_p is a universal quantity: the b_p values for hydrogen and argon can actually be compared at the same ($E_i - E_p$)-value (i.e., at the same energy distance from their respective continuum). For the calculation of the hydrogen b_p values, we used the data from Fig. 9, and Eq. (3) in order to obtain n_{H^+} . For argon, we simply used $n_{Ar^+} = n_e$ at the plasma axis.

IV. DISCUSSION

A. General

In the present section, a qualitative model for the argon-hydrogen expanding plasma jet will be developed, in order to understand the experimental findings. It is appropriate to start by presenting the general view, as supported by other measurements [4, 10, 13, 14, 15], for this type of plasma.

Starting inside a pure argon cascaded arc, it has been established, that n_e, T_e , and T_h (the heavy particle temperature) are around $10^{22} m^{-3}$, 1 eV, and 1 eV, respectively. The ionization degree is around 8 % [3, 7]. With hydrogen added to the argon before it enters the arc, we assume this ionization degree to remain unchanged, at least for very low H_2 seedings.

As a next step, we compare the dissociation energy of H_2 (4.4 eV), the ionization potential of H (13.6 eV), and the argon ionization potential (15.8 eV). As, in a pure argon arc, a substantial part of the particles is ionized, a comparison of the above potentials leads us to believe that with a small

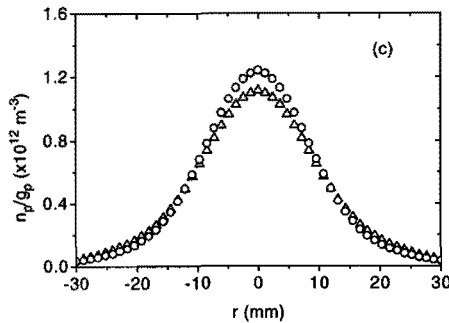
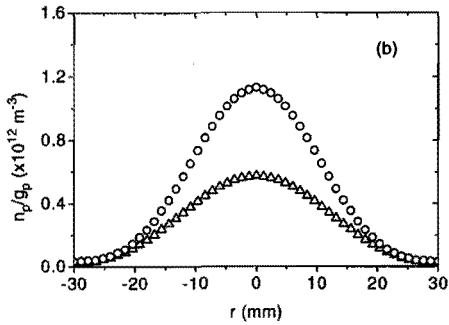
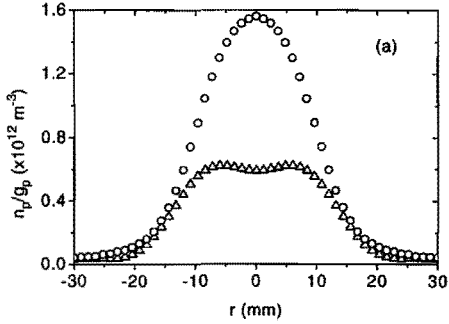


Figure 7: OES results: $H(p=3)$ density (per statistical weight) radial profiles for different hydrogen admixtures, at: (a) $z=20$ mm, (b) $z=40$ mm, and (c) $z=70$ mm. Δ : 0.7 vol.% H_2 , \circ : 1.4 vol.% H_2 .

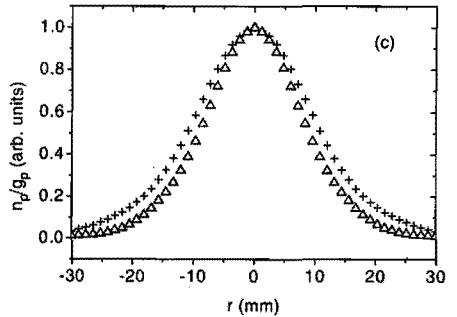
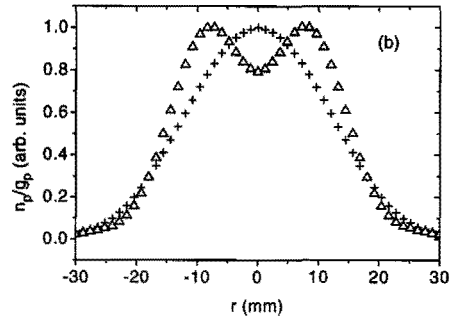
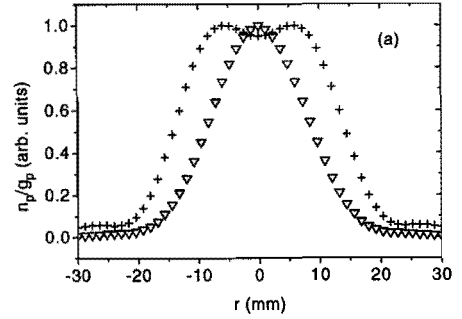


Figure 8: OES results: $Ar(4p')$ and $H(p=3)$ level density (per statistical weight) radial profiles, normalized to 1 at $r=0$, for 0.7 vol.% H_2 admixed, and at three z -positions: (a) $z=20$ mm; (b) $z=40$ mm; (c) $z=70$ mm. Δ : argon, +: hydrogen. The graphs for 1.4 vol.% are similar.

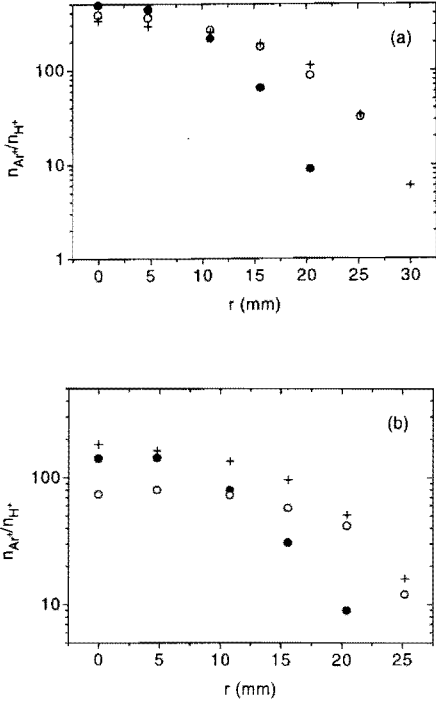


Figure 9: The calculated ion concentration ratios n_{Ar^+}/n_{H^+} vs. r , at different z -positions: (a) 0.7 vol. % H_2 ; (b) 1.4 vol. % H_2 . \bullet : $z = 20$ mm, \circ : $z = 40$ mm, $+$: $z = 70$ mm.

amount of hydrogen added the hydrogen will be completely dissociated. The Ar^+/H^+ ratio can be calculated using the Boltzmann equation:

$$\frac{Ar^+}{H^+} = \frac{Ar_{neutral} g_{Ar^+} g_H}{H_{neutral} g_{Ar} g_{H^+}} \exp\left(\frac{13.6 - 15.8}{T_e(eV)}\right) \quad (5)$$

For a 0.7 vol. % H_2 seed-in (i.e. 1.4% H particles) and $T_e = 1$ eV, Eq. (5) gives a Ar^+/H^+ ratio (inside the cascaded arc) of approximately $\frac{100}{1.4} \times 12 \times 0.11 \approx 10^2$. Thus, very little H^+ ions are produced in the arc, if we assume the ionization degree to be roughly the same as in the pure argon case.

With our assumption that only Ar^+ , Ar , H^+ , H and e^- particles leave the arc, the extremely enhanced recombination with hydrogen added (Fig. 4) is difficult to explain, as ordinary three-particle recombination is far too slow at the densities and temperatures present [4]. Therefore, we are forced to consider the influence of the stainless steel vacuum vessel in which the expansion takes place (length 3 m, diameter 0.36 m). It is a well-known fact, that stainless steel constitutes a perfect surface for association of hydrogen atoms. In our case (Fig. 12 gives a sketch), after recombination in the subsonic part of the expansion, hydrogen atoms will reach the walls: the ves-

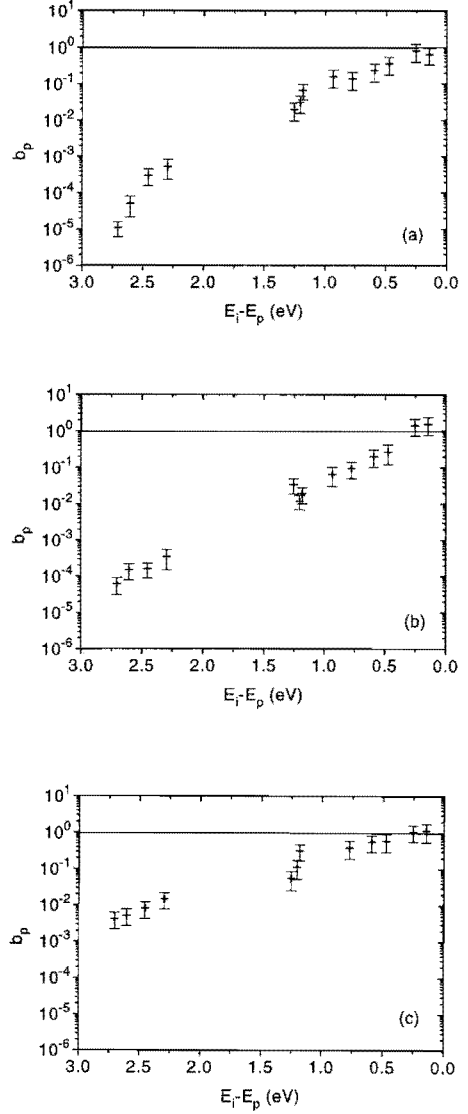


Figure 10: The population factor b_p vs. $E_i - E_p$ for the expanding plasma jet in pure argon: (a) $z = 20$ mm; (b) $z = 40$ mm; (c) $z = 70$ mm.

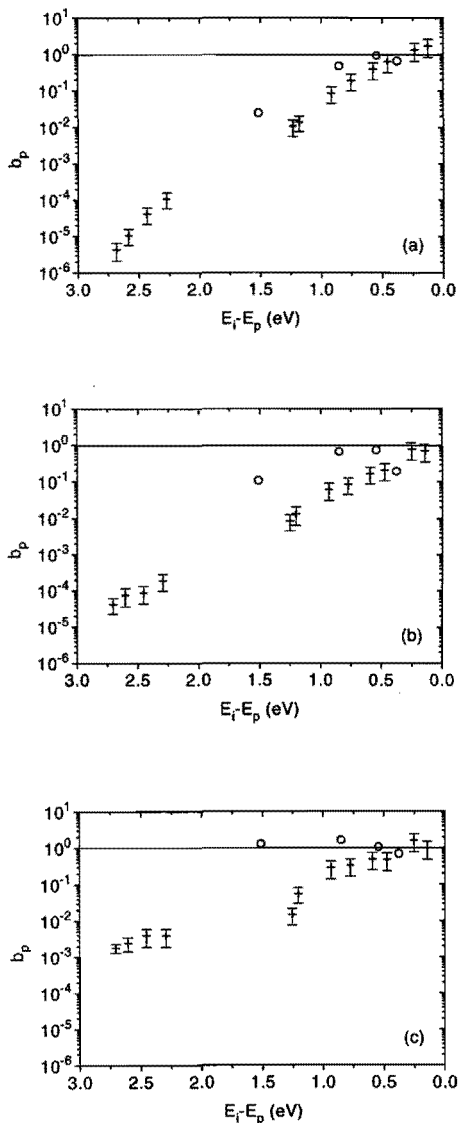


Figure 11: The population factor b_p vs. $E_i - E_p$ for 0.7 vol. % H_2 admixed: (a) $z=20$ mm; (b) $z=40$ mm; (c) $z=70$ mm. +: argon, o: hydrogen.

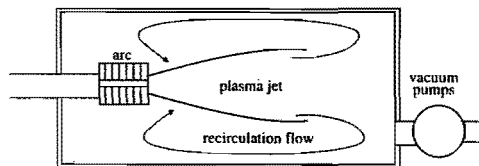


Figure 12: A sketch of the recirculation pattern within the vacuum vessel. The recirculation flow is responsible for the transport of the H_2 from the vessel walls into the plasma jet.

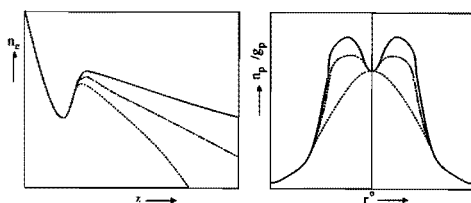
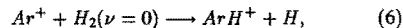


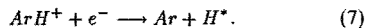
Figure 13: The disappearance of the shock ridges in the Ar I ($4p^1$) radial profiles (see Fig. 6) is the radial analogy of the electron density decrease in axial direction (see Fig. 4c), as a consequence of hydrogen molecules reentering the plasma jet.

sel walls may well be saturated with hydrogen. Association and subsequent desorption of hydrogen molecules could be responsible for a re-entry flow of hydrogen molecules (rotationally and vibrationally excited) into the expanding plasma, in combination with a recirculation pattern, which may be present within the vessel.

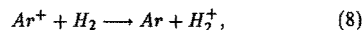
It is this re-entry flow of wall-associated hydrogen molecules that is thought to be responsible for the fast ionization loss in the expansion. The following is the proposed reaction mechanism [10, 14, 15]:



followed by:

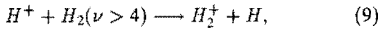


The second (dissociative recombination) step is known to be very fast (rate constant around $10^{-13} \text{ m}^3 \text{ s}^{-1}$), while the first step has a rate constant lower by a factor of about 10^2 at the present conditions ($K = 1.1 \times 10^{-15} \text{ m}^3 \text{ s}^{-1}$, [16]). In principle, Ar^+ can also react with H_2 to form H_2^+ :

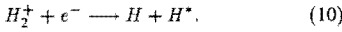


followed by formation of H_3^+ and subsequent dissociative recombination [14, 15]. This reaction, however, has been shown to be of little importance for energies below 0.5 eV [17]; at low energies, reaction (6) dominates.

Another reaction that may occur involves vibrationally excited hydrogen molecules and hydrogen ions:



followed by:



The reaction rates for (10) and (7) are about equal. The reaction rate for (9) is about $2.5 \times 10^{-15} \text{ m}^3 \text{ s}^{-1}$ [14]. Note, that both in (6) and (10), the formed hydrogen appear in an excited state, most probably $p = 2$ or 3.

B. Thomson-Rayleigh scattering

From the Thomson-Rayleigh measurements, we can actually make an estimate of the amount of (re-entrant) hydrogen molecules. To do so, we assume, that reactions (6 - 7) constitute the dominant process in the ionization loss as seen in Fig. 4c. We describe this dominant loss term in the electron mass balance as follows:

$$\left(\frac{\partial n_e}{\partial t} \right)_{E_{i,(6,7)}} = -n_{Ar^+} n_{H_2} K_{ArH^+}, \quad (11)$$

as the first step (6) determines the reaction speed. If we assume, for the moment, $n_{Ar^+} \approx n_e$, and n_{H_2} constant along the z -axis, (11) is integrated easily:

$$\ln \left(\frac{n_{e,t}}{n_{e,t=0}} \right) = -n_{H_2} K_{ArH^+} t. \quad (12)$$

In (12), $t=0$ corresponds to $z=70$ mm, whereas $t = t$ corresponds to $z=500$ mm (see Fig. 4). Thus, $t = \Delta z/v_z$, with v_z the axial velocity after the shock; $v_z \approx 600 \text{ m/s}$. We take $K_{ArH^+} = 1.1 \times 10^{-15} \text{ m}^3 \text{ s}^{-1}$. If we insert the measured quantities for a 0.7 vol. % seed fraction: $n_{e,t=0} = 3 \times 10^{19} \text{ m}^{-3}$, $n_{e,t=t} = 3 \times 10^{18} \text{ m}^{-3}$, $\Delta z \approx 0.430$ m, we obtain an estimate for n_{H_2} :

$$n_{H_2} \approx 3 \times 10^{18} \text{ m}^{-3}. \quad (13)$$

So far, we have neglected any influence of reactions (9-10), even though the rate of the slower of these two, (9), exceeds that of (6) by a factor of about 2. However, the H^+ concentration is smaller than the Ar^+ concentration by a factor of 10-500. Furthermore, a hydrogen molecule must be vibrationally excited in order to participate in reaction (9). Thus, even though the rate constant of (9) is large, the contribution of reactions (9-10) to the ionization loss can be neglected in our plasma.

C. Optical emission spectroscopy

The most crucial point in the discussion of the OES measurements, is the origin of a certain level's population. In principle, this population is a result of excitation from lower levels and/or recombination from higher ones. In cases where T_e is very low, i.e., in the 0.2-eV range, only three particle recombination is important (for atomic plasmas). In a pure argon expanding plasma jet the levels are populated by the destruction of Ar^+ ions [4]. From Eq. (1) it can be shown that this results in a level population roughly proportional to

n_2^2 . Thus, in a sense, we are "looking at" the Ar^+ population by examining the atomic state distribution function in the Ar I system.

In our case, where two ionic species (Ar^+ and H^+ , in a ratio of about 100:1) leave the arc, the situation is more complex. We shall confine ourselves to the view that Ar I excited states are populated mainly through three-particle recombination, i.e., we leave out processes such as excitation exchange for the moment. As three particle recombination is proportional to $T_e^{-\frac{3}{2}}$, higher line intensities are to be expected at $z=20$ mm, where T_e is low (Fig. 4b). This is reflected in the behaviour of the ($4p'$) levels, shown in Fig. 6.

The hydrogen excited level population may also arise from dielectronic recombination, but in this case an extra source term almost certainly comes in: the dissociative recombination in (7) and (10), ending in hydrogen excited states $p=2,3$. The H I 636.5 nm emission probably arises, then, due to a combination of the two processes: three-particle recombination mainly at the plasma axis, and dissociative recombination "wings" at the edges, where the re-entrant H_2 molecules are most abundant. This is reflected in the fact, that the $p = 3$ radial profiles are broader than the corresponding $Ar_{4p'}$ profiles (Fig. 8), especially at $z = 20$ mm.

One can attempt to explain the changing of the shock behaviour as reflected in the Ar ($4p'$) emission (Fig. 6b) at $z = 40$ mm within the qualitative model. At the plasma axis, the ($4p'$) density is roughly constant for different hydrogen admixtures, but the characteristic ridges at $r \approx \pm 20$ mm (in pure argon) are smoothened and eventually disappear. This can be viewed analogous to the electron density decrease in axial direction, as seen in Fig. 4b. If we still assume that Ar I emission represents the Ar^+ population, as stated above, the disappearance of the shock ridges may be due to reactions (6) and (7) under the influence of radially entering H_2 molecules. Fig. 13 gives a sketch of the hypothetical analogy: the Ar I emission at the edges of the beam decreases due to the loss of argon ions.

The fact, that the hydrogen system has an extra input can also be seen in Figs. 10 and 11: all H levels have higher to much higher b_p values (up to a factor 10^2) compared to argon (at a certain $E_i - E_p$). Note the fact that even $p = 3$ has $b_p \approx 1$ at $z = 70$ mm, for $E_i - E_p = 1.511$ eV. The overpopulation of $p = 2, 3$ states due to dissociative recombination could well be smoothened over the other levels by electron collisions at $T_e \approx 0.2$ eV.

At $z=70$ mm, the plasma is almost homogeneous, as illustrated by Fig. 8c: the hydrogen and argon profiles are almost equally wide - a substantial difference with $z=20$ mm, indeed. This may point to the reentrant hydrogen molecules being absorbed by the beam before the stationary shock front at $z \approx 40-70$ mm. As can be seen from Figs. 10 and 11, the atomic level distribution function is closest to Saha equilibrium at $z=70$ mm, because T_e is higher than at the other two z -positions considered here (Fig. 4b). The Ar^+/H^+ ratio turns out to be of the right order of magnitude (compare the outcome of Eq. (5) to Fig. 9 for a 0.7 vol. % seed fraction). However, it is higher by a factor of about 5. Some extra H^+ loss can be explained through gasdynamical reasoning, based on the fact that hydrogen ions are lighter than argon ions by a factor of 40.

This should be reflected in a much faster radial and axial expansion (factor $\sqrt{40} \approx 6$), within the limits of quasineutrality. This results in a larger Ar^+/H^+ ratio (factor 6).

D. Conclusions

The n_0 vs. z profile shows that the gasdynamical expansion in axial direction is not heavily influenced by adding a small amount of hydrogen to the plasma.

The n_0 axial profile, however, is severely changed by the addition of hydrogen, most probably because of a reentry flow of hydrogen molecules. These molecules are formed at the vessel walls and could trigger a very effective recombination channel (6-7).

The broad hydrogen emission profiles, especially at $z=20$ mm can be explained by the occurrence of this reaction at the edges of the plasma. A different expansion behaviour of hydrogen may also induce broader radial profiles.

The smoothening of the shock ridges in the argon ($4p'$) profiles could be caused by reactions (6-7) occurring at the edges of the plasma: the ($4p'$) level density at the plasma axis is almost unaffected.

The Ar^+/H^+ concentration ratios are larger than expected (following the basic arc picture) by a factor of about 5. This can be explained by the fact that hydrogen ions are much lighter than their argon counterparts.

The fact, that highly excited levels in the Ar I system approach $b_p = 1$ (in all three conditions) is a solid test for both Thomson-Rayleigh and OES measurements.

ACKNOWLEDGMENT

We would like to thank M.J.F. van de Sande and H.M.M. de Jong for their skillful technical assistance during the measurements.

References

- [1] A.T.M. Wilbers, G.J. Meeusen, M. Haverlag, G.M.W. Kroesen, and D.C. Schram, *Thin Solid Films* **204**, 59 (1991).
- [2] J.J. Beulens, A.J.M. Buuron, L.A. Bisschops, A.B.M. Hüsken, G.M.W. Kroesen, G.J. Meeusen, C.J. Timmermans, A.T.M. Wilbers, and D.C. Schram, *J. Phys. (Paris), Colloq.* **51**, C5-361 (1990).
- [3] P.K. Bachmann, J.J. Beulens, G.M.W. Kroesen, H. Lydtin, D.C. Schram, and D.U. Wiechert, *Surf. Modif. Technol.* **III**, 69 (1989).
- [4] M.C.M. van de Sanden, Ph. D. Thesis Eindhoven University of Technology (1991).
- [5] M.C.M. van de Sanden, J.M. de regt, G.M. Jansen, J.A.M. van der Mullen, D.C. Schram, and B. van der Sijde *Rev. Scient. Instr.* **63** (6), 3369 (1992).
- [6] R.F.G. Meulenbroeks, P.A.A. van der Heijden, M.C.M. van der Sanden, and D.C. Schram, accepted for publication in *J. Appl. Phys.* (March 1994).
- [7] G.M.W. Kroesen, D.C. Schram, and J.C.M. de Haas, *Plasma Chem. Plasma Process.* **10**, 531 (1990).
- [8] C.A. Kak and M. Slaney, *Principles of Computerized Tomographic Imaging*, IEEE press, New York (1988).
- [9] W.L. Wiese, M.W. Smith, and B.M. Miles, *Atomic Transition Probabilities* (NSRDS-NBS22), U.S. GPO, Washington D.C. (1969).
- [10] G.J. Meeusen, E.A. Ershov-Pavlov, R.F.G. Meulenbroeks, M.C.M. van de Sanden, and D.C. Schram, *J. Appl. Phys.* **51** (9), 4156 (1992).
- [11] L.M. Biberman, V.S. Vorob'ev, and I.T. Yakubov, *Kinetics of Non-equilibrium Low-Temperature Plasmas* Plenum, New York (1987).
- [12] J.A.M. van der Mullen, *Phys. Rep.* **191**, 161 (1989).
- [13] R.F.G. Meulenbroeks, D.C. Schram, L.J.M. Jaegers, M.C.M. van de Sanden, *Phys. Rev. Lett.* **69** (9), 1379 (1992).
- [14] M.J. de Graaf, R.P. Dahiya, J.L. Jauberteau, F.J. de Hoog, M.J.F. van de Sande, and D.C. Schram, *J. Phys. (Paris), Colloq.* **51** C5-387 (1990).
- [15] M.J. de Graaf, R. Severens, R.P. Dahiya, M.C.M. van de Sanden, and D.C. Schram, *Phys. Rev. E* **48** (3), 2098 (1993).
- [16] K.M. Ervin and P.B. Armentrout, *J. Chem. Phys.* **83** (1), 166 (1895).
- [17] Eric A. Gislason and Gérard Parlant, *J. Chem. Phys.* **94** (10), 6598 (1991).

The Argon-Hydrogen Expanding Plasma: Model and Experiments

R.F.G. Meulenbroeks R.A.H. Engeln M.N.A. Beurskens R.M.J. Paffen
M.C.M. van de Sanden J.A.M. van der Mullen
D.C. Schram

*Eindhoven University of Technology, Dept. of Physics
P.O.Box 513 5600 MB Eindhoven, The Netherlands*

Abstract. An argon expanding cascaded arc plasma, with small amounts (0-10 vol.%) of hydrogen added to the flow, is investigated by means of Thomson-Rayleigh scattering and optical emission spectroscopy. The results, especially the electron density behaviour as a function of the distance from the onset of the expansion, are interpreted by comparison with results of a quasi one-dimensional model. The associative charge exchange reaction between Ar^+ ions and H_2 molecules plays a dominant role in the model. Assuming that H_2 molecules from the wall enter the plasma in the shock region, the large ionization loss can be explained. Good agreement between model and experiment is found for the electron and neutral density and the electron temperature behaviour. This makes plausible the existence of a recirculation flow inside the vacuum vessel, which transports wall-associated hydrogen molecules towards the plasma.

I. INTRODUCTION

In a previous paper [1] we reported on the study of a supersonically expanding cascaded arc plasma in argon with small amounts of hydrogen added to the flow. In the present work we shall extend this study by comparing new measurements to a quasi one-dimensional model. We will especially elaborate on the speculation that wall-associated hydrogen molecules play an important role in the large ionization loss in argon plasmas with low hydrogen seed fractions. A re-entry flow of hydrogen molecules into the plasma beam is thought to be caused by wall-associated molecules transported towards the plasma by a strong recirculation flow inside the vessel, as was hypothesized by the authors in [1] as well as by De Graaf *et al.* [2].

The study of plasmas of this type is important in view of the applications: deposition of thin films and particle sources ([2]-[6]).

II. THE QUASI ONE-DIMENSIONAL MODEL

Modeling of a pure argon plasma, expanding out of a cascaded arc source has proved to give good insight in the transport phenomena and the plasma kinetics [7, 8]. This relatively easy approach will therefore be extended to describe the expansion of an argon-hydrogen plasma. The hydrogen is added to the flow before it enters the cascaded arc.

The experiment is shown in Fig. 1 and described in detail elsewhere [1, 3].

A. Basic assumptions

Before fully writing out the equations that govern the expansion, the basic assumptions will be discussed.

- The plasma is assumed to be ideal, i.e., the velocity distributions for all particles are assumed to be Maxwellian in this type of plasma and the number of electrons within

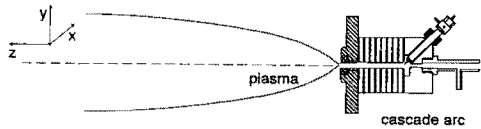


Figure 1: The expanding plasma jet. A subatmospheric plasma (pressure 0.2-0.6 bar) is created inside the cascaded arc, consisting of three cathodes, three electrically isolated copper plates, and an anode plate. The formed plasma expands into a vacuum vessel, creating a supersonically expanding jet.

a Debye sphere is assumed to be large. The actual minimum value is around 10-20 electrons per Debye sphere.

- The effects of turbulence and viscosity are neglected.
- The assumption is made that hydrogen is totally dissociated for low hydrogen seed fractions (i.e. up to 2 vol%) in the cascaded arc (T_e , the electron temperature, around 1 eV). Thus, the heavy particles leaving the arc are: Ar, Ar^+ , H, and H^+ . Most of the molecular hydrogen in the expanding jet is assumed to originate from the vessel walls [1, 2]. The presence of molecular and negative ions (H_2^+ , H_3^+ , H^-) is neglected. The presence of ArH^+ , however, is considered, as this ion is an important intermediate in molecular reactions.
- All heavy particle temperatures are assumed to be equal.
- The charge exchange reaction $\text{Ar}^+ + \text{H}_2 \rightarrow \text{Ar} + \text{H}_2^+$ is neglected in favor of the associative charge exchange reaction $\text{Ar}^+ + \text{H}_2 \rightarrow \text{ArH}^+ + \text{H}$. This is justified at the

temperatures in the expansion, which are all well below 0.5 eV [9].

- The energy loss due to line and continuum radiation is neglected compared to other energy losses [3].
- Ohmic dissipation due to pressure induced currents will be neglected, despite its known influence on the electron temperature in argon plasma jets [8, 10].
- In the supersonic part of the expansion, axial velocities are assumed to be large compared to the radial velocities.

B. The axial velocities of the different particles

One important matter has to be settled: to which extent are the axial velocities of the plasma particles identical when hydrogen as a light "heavy particle" is added to the plasma? The case of pure argon has been extensively discussed by Van de Sanden *et al.* [8].

We start by comparing the relaxation times τ_{xy} and mean free paths λ_{xy} for momentum exchange (for particles x in species y) in the expansion as given by [11, 12, 13] for the densities close to the stationary shock front and a 2 vol% H_2 seed fraction: $n_{Ar} = 10^{20} m^{-3}$, $n_H \approx n_{H^+} \approx 10^{18} m^{-3}$, $n_{Ar^+} \approx n_e \approx 10^{19} m^{-3}$. We shall only give the values for the mean free paths, as the relation between τ and λ is well known:

$$\tau_{xy} = \frac{1}{n_y \langle \sigma_{xy} \cdot v_{xy} \rangle}, \quad (1)$$

and:

$$\lambda_{xy} = \frac{v_x}{n_y \langle \sigma_{xy} \cdot v_{xy} \rangle}, \quad (2)$$

where v_{xy} is the relative speed of the particles, σ_{xy} is the cross-section, and τ_{xy} denotes the time constant for momentum exchange from species x to y .

Figure 2 gives the mean free paths for momentum exchange between the different particles. If we examine the mean free paths for the temperature range $T = 2000$ -3000 K and compare them to typical gradient lengths in the plasma $L \approx 10^{-2}$ - 10^{-3} m we can conclude, that: (a) all charged particles are coupled; (b) the electron-argon and argon-argon ion mean free paths are small enough; (c) the neutral-neutral coupling could be a problem. Especially the hydrogen atoms appear to be quite free in the argon neutral gas.

For the moment, however, we shall assume all axial velocities to be equal to the plasma velocity designated u .

C. The system of equations

The expanding plasma can be described by a two gas model - electrons and heavy particles. This method (as well as the quasi one-dimensional approach) is well described by Kroesen *et al.* and Van de Sanden *et al.* [7, 8, 14] and we shall only give a brief outline.

We start by writing the number balances for the different plasma species. For the electron gas, we neglect two particle recombination, as this process is much less efficient than three particle recombination at the present conditions [15].

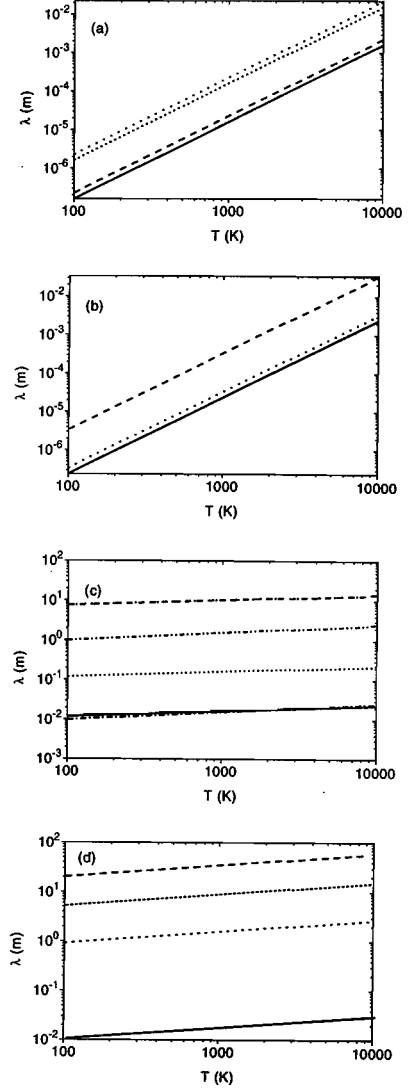


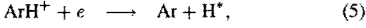
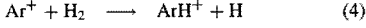
Figure 2: Mean free paths at the stationary shock front (2 vol% H_2 seed fraction): $n_{Ar} = 10^{20} m^{-3}$, $n_H \approx n_{H^+} \approx 10^{18} m^{-3}$, $n_{Ar^+} \approx n_e \approx 10^{19} m^{-3}$. (a) ion-ion interactions (---: $Ar^+ - Ar^+$, - - -: $H^+ - H^+$, - · - : $Ar^+ - H^+$) (b) electron-ion (... : $Ar^+ - e$, - - - : $H^+ - e$) and electron-electron (-) interactions, (c) electron-neutral (- · - : $e - Ar$, - - - - : $e - H$) and ion-neutral (- : $Ar^+ - Ar$, - - - : $Ar - Ar^+$, - - - : $H^+ - H$, ...: $H - H^+$) interactions, and (d) neutral-neutral (- : $Ar - Ar$, - - - : $H - H$, - · - : $Ar - H$, ... : $H - Ar$) interactions.

The value of the rate constant for three particle recombination $K_{rec,3}$ is taken from Van de Sanden [15]:

$$K_{rec,3} = 3.3 \cdot 10^{-21} \cdot T_e^{-9/2}, \quad (3)$$

in units $m^6 s^{-1}$, with T_e the electron temperature in K. This rate is assumed to be the same for recombination of argon and hydrogen ions, because the recombination of an argon ion usually ends in a highly excited state, where the system is essentially hydrogen-like.

Furthermore, we assume the following associative charge exchange/dissociative recombination reactions to be responsible for ionization loss:



where the hydrogen molecules are assumed to mainly originate from the vessel walls. An excited hydrogen atom is formed in the second step. For the above reactions, the first step limits the reaction speed, with a rate constant $K_{ArH^+} = 1.1 \cdot 10^{-15} m^3 s^{-1}$ [16]. This reaction is virtually independent of T_e . The second (dissociative recombination) step is faster by a factor of about 100, depending on n_e .

Thus, we can write the electron number balance as follows:

$$\nabla(n_e \mathbf{u}) = -K_{rec,3} n_e^2 (n_{Ar^+} + n_{H^+}) - K_{ArH^+} n_{Ar^+} n_{H_2}, \quad (6)$$

where n denotes a species density (in m^{-3}) and \mathbf{u} is the plasma velocity. The right hand side of Eq. (6) will be referred to as B_e from now on.

The number balances for the heavy particles can be written as:

$$\nabla(n_H \mathbf{u}) = K_{rec,3} n_e^2 n_{H^+} + 2K_{ArH^+} n_{Ar^+} n_{H_2} \stackrel{\text{def}}{=} B_H, \quad (7)$$

$$\nabla(n_{H_2} \mathbf{u}) = -K_{ArH^+} n_{Ar^+} n_{H_2} + \frac{\phi_{H_2}}{\pi r^2 l} \stackrel{\text{def}}{=} B_{H_2}, \quad (8)$$

$$\nabla(n_{H^+} \mathbf{u}) = -K_{rec,3} n_e^2 n_{H^+} \stackrel{\text{def}}{=} B_{H^+}, \quad (9)$$

$$\nabla(n_{Ar} \mathbf{u}) = K_{rec,3} n_e^2 n_{Ar^+} + K_{ArH^+} n_{Ar^+} n_{H_2} \stackrel{\text{def}}{=} B_{Ar}, \quad (10)$$

$$\nabla(n_{Ar^+} \mathbf{u}) = -K_{rec,3} n_e^2 n_{Ar^+} - K_{ArH^+} n_{Ar^+} n_{H_2} \stackrel{\text{def}}{=} B_{Ar^+}, \quad (11)$$

where B_H etc. are short-hand notations for the respective right hand sides. In the calculations an extra input is added to B_{H_2} (second term r.h.s. in (8)) in order to simulate a re-entry flow of wall associated hydrogen molecules to the plasma beam. In Eq. (8), ϕ_{H_2} denotes the total radial influx (in s^{-1}), r denotes the plasma radius, and l represents the length of the absorbing part of the beam, i.e., the distance over which H_2 molecules enter the plasma. This distance does not include the length of the shock region, which is treated separately and analytically (see next section).

The total balance for the mass density ρ reads:

$$\nabla(\rho \mathbf{u}) = 0. \quad (12)$$

The equation for the total momentum balance (without viscosity and the Lorentz force) is written as:

$$\rho(\mathbf{u} \cdot \nabla) \cdot \mathbf{u} + \nabla p = 0, \quad (13)$$

where $p = k(n_e T_e + n_h T_h)$ is the total pressure. T_h is the heavy particle temperature and k is Boltzmann's constant. In principle $\rho = \sum_x m_x n_x$ includes all plasma species x with masses m_x . In our case with small hydrogen seed fractions ($< 2\%$), however, we can simplify this expression using the fact that electrons, H^+ , H , and H_2 particles are all much lighter than argon atoms or ions. With a very small error ($< 0.1\%$) we can therefore simply write:

$$\rho \approx m_{Ar}(n_{Ar} + n_{Ar^+}) = m_{Ar}(n_{Ar} + n_e). \quad (14)$$

Finally, we need the two energy balances for the electrons and the heavy particles (without viscosity term):

$$\begin{aligned} \nabla \left(\frac{3}{2} n_h k T_h \mathbf{u} \right) + n_h k T_h (\nabla \cdot \mathbf{u}) \\ + \nabla \cdot \mathbf{q}_h = Q_h, \end{aligned} \quad (15)$$

$$\begin{aligned} \nabla \left(\frac{3}{2} n_e k T_e \mathbf{u} \right) + n_e k T_e (\nabla \cdot \mathbf{u}) \\ + \nabla \cdot \mathbf{q}_e = Q_e, \end{aligned} \quad (16)$$

with \mathbf{q}_x the particle heat flux ($\mathbf{q}_x = -\kappa_x \nabla T_x$, with κ_x the thermal conductivity for species x and T_x the corresponding temperature) and $Q_{h,e}$ the energy source terms for the respective particles. The particle heat flux is taken into consideration in a simplified form, following Van de Sanden [8]: only the radial heat flux is considered, as a loss term. With argon as the dominant species, the heavy particle energy source term can be written as:

$$Q_h = Q_{ch} + Q_{diss.rec.} - Q_q, \quad (17)$$

with:

$$\begin{aligned} Q_{ch} = 3 \frac{m_e}{m_{Ar}} n_e \left(\frac{1}{\tau_{e,Ar^+}} + \frac{1}{\tau_{e,Ar}} \right) \\ \times k(T_e - T_h); \end{aligned} \quad (18)$$

$$Q_{diss.rec.} = K_{ArH^+} n_{Ar^+} n_{H_2} \frac{3}{2} k T_e; \quad (19)$$

$$Q_q = \frac{\kappa_h T_h}{r^2}, \quad (20)$$

where Q_q represents the radial heat conduction in a simplified form, as an energy loss term: κ_h is taken from Braginskii [11] and r denotes the plasma radius. This is a simplified form valid if the temperature profile is taken to be a Gaussian [8]. The values for the relaxation times for momentum transfer τ_{e,Ar^+} and $\tau_{e,Ar}$ are taken from Braginskii and Timmermans [11, 13]. For the energy transfer between electrons and heavy particles due to reactions (4,5) we assume, that a thermal electron is lost, i.e. the electron temperature is not very much effected. This is justified by the fact, that the temperature dependence of K_{ArH^+} is not very strong in the temperature range considered here [16]. The heavy particle, however, gains the energy of the lost electron, which equals $\frac{3}{2} k T_e$. The heavy particles could gain more from the dissociative recombination, but this is not taken into account.

The electron energy source term can be written as:

$$Q_e = Q_{rec,3} - Q_{ch} - Q_q, \quad (21)$$

with the three particle recombination source term:

$$Q_{rec,3} = K_{rec,3} n_e^2 (n_{Ar} + \Delta E_{Ar} + n_{H} + \Delta E_H), \quad (22)$$

and the "loss" by heat conduction:

$$Q_q = \frac{\kappa_e T_e}{r^2}. \quad (23)$$

The amount of energy gained by the second electron in the reaction $A^+ + e + e \rightarrow A^* + e$ is approximately equal to 0.15 times the ionization energy of the species concerned, depending on n_e (Van de Sanden *et al* [15]). This determines the values of ΔE_H and ΔE_{Ar} in Eq. (22).

It is convenient to introduce dimensionless parameters $\alpha, \beta, \delta, \epsilon$ and ρ instead of the particle densities:

$$n_e = \frac{\alpha \rho}{m_{Ar}}, \quad (24)$$

$$n_{Ar} = \frac{\beta \rho}{m_{Ar}}, \quad (25)$$

$$n_H = \frac{\delta \rho}{m_{Ar}}, \quad (26)$$

$$n_{H^+} = \frac{\epsilon \rho}{m_{Ar}}. \quad (27)$$

The equations discussed so far can be rewritten to form a system of eight first order differential equations with eight variables: $\alpha, \beta, \delta, \epsilon, T_e, T_h, \rho$, and u [7, 10], where u is a scalar: the axial expansion speed.

We can now combine the above equations to a complete set:

$$\frac{du}{dz} = -\frac{u}{(1-M^2)} \left(\frac{1}{A} \frac{dA}{dz} \right) + \frac{2}{5} \frac{Q_e + Q_h}{\mathcal{R} \rho T_p (1-M^2)}, \quad (28)$$

$$\frac{d\rho}{dz} = \frac{\rho M^2}{(1-M^2)} \left(\frac{1}{A} \frac{dA}{dz} \right) - \frac{2}{5} \frac{Q_e + Q_h}{\mathcal{R} \rho T_p (1-M^2)}, \quad (29)$$

$$\frac{dT_h}{dz} = \frac{2}{3} \frac{T_h M^2}{(1-M^2)} \left(\frac{1}{A} \frac{dA}{dz} \right) + \frac{2}{3} \frac{Q_h}{\rho u \mathcal{R}} - \frac{4}{15} \frac{T_h}{T_p} \frac{Q_e + Q_h}{\mathcal{R} \rho u (1-M^2)}, \quad (30)$$

$$\frac{dT_e}{dz} = \frac{2}{3} \frac{T_e M^2}{(1-M^2)} \left(\frac{1}{A} \frac{dA}{dz} \right) + \frac{2}{3} \frac{Q_e}{\alpha \rho u \mathcal{R}} - \frac{4}{15} \frac{T_e}{T_p} \frac{Q_e + Q_h}{\mathcal{R} \rho u (1-M^2)} - \frac{m_{Ar} T_e B_e}{\alpha \rho u}, \quad (31)$$

$$\frac{d\alpha}{dz} = \frac{m_{Ar} B_e}{\rho u}; \quad (32)$$

$$\frac{d\beta}{dz} = \frac{m_{Ar} B_{Ar}}{\rho u}; \quad (33)$$

$$\frac{d\delta}{dz} = \frac{m_{Ar} B_H}{\rho u}; \quad (34)$$

$$\frac{d\epsilon}{dz} = \frac{m_{Ar} B_{H^+}}{\rho u}. \quad (35)$$

Eqn. (28) is obtained by combining the momentum and energy balances ((13),(15), and (16)); Eq. (29) by using (28) and the

mass balance (12); Eqns. (32- 35) by using the mass balances (12) and (6- 9). Finally, Eqns. (30-31) are derived using (28),(29), and (32).

In the above equation set, M denotes the plasma Mach number, defined by:

$$M^2 = \frac{3u^2 m_{Ar}}{5kT_p}, \quad (36)$$

with $T_p = T_h + \alpha T_e$ the plasma temperature. The gas constant \mathcal{R} is given by:

$$\mathcal{R} = \frac{k}{m_{Ar}}. \quad (37)$$

Note, that in Eqs. (36,37) argon is assumed to be the main species. In the quasi one dimensional case, A corresponds to the surface over which the plasma parameters are averaged to make the problem one dimensional. For A , the following equation:

$$\frac{1}{A} \frac{dA}{dz} = \frac{2 \tan \phi}{r}, \quad (38)$$

holds, where ϕ is half the angle of expansion and r is the radius of the plasma at a certain axial position z [7].

It may be noted, that the equation set (28-35) basically represents the pure argon model as treated by Van de Sanden *et al.* [8] with a perturbation due to the presence of hydrogen. The gas dynamical behaviour of the plasma is equal to the pure argon case (we shall return to this later when we discuss the neutral particle density measurements). The hydrogen, however, appears to play a decisive role in the plasma kinetics. This will become clear when the electron density behaviour is discussed. This approach with hydrogen as a perturbation is allowed for low hydrogen seed fractions, as the masses of all hydrogen atoms, molecules, and ions are all much lower than the masses of the argon atoms and ions.

Eqns. (28-35) form a complete set and will be solved numerically by Runge-Kutta integration to cover the first (supersonic) part of the expansion. The stationary shock front will be treated analytically in the next section.

D. The stationary shock front

To describe a discontinuity in flow variables, one could in principle use the Rankine-Hugoniot relations, as was done by Kroesen *et al* [7]. A better approximation is obtained with the method developed by Mott-Smith [8, 10, 17, 18, 19]. In order to get an impression of the shape of the shock, we assume the shock to be identical for all particles. In the shock region ($z = 40-70$ mm) the numerical integration is taken over by an analytical approach, in which T_h , u , and ρ are transformed according to the Mott-Smith relations (for a ratio of specific heats $\gamma = 5/3$):

$$\frac{\rho(z)}{\rho(0)} = \frac{4M_0^2 + (M_0^2 + 3) \exp\left(\frac{-4(z-z_0)}{L_0}\right)}{(M_0^2 + 3) \left(1 + \exp\left(\frac{-4(z-z_0)}{L_0}\right)\right)}, \quad (39)$$

$$\frac{u(z)}{u(0)} = \frac{\rho(0)}{\rho(z)}, \quad (40)$$

$$\frac{T_h(z)}{T_h(0)} = \frac{1}{4} \left(\frac{14}{5} \left(\frac{\rho(0)}{\rho(z)} - \frac{1}{4} \right)^{-1} - 1 \right) \frac{\rho(0)}{\rho(z)}. \quad (41)$$

In the above set of equations, L_0 represents the shock thickness. In our first approximation λ_{00} , the neutral particle mean free path (argon in argon) is taken as a measure for L_0 . Following Van de Sanden *et al* [8], we take $L_0 \approx 4 \lambda_{00}$ for high Mach numbers M_0 (around 10) before the shock. The Mott-Smith relations are taken relative to the center of the shock region: z_0 denotes the middle of the shock region. $\rho(0)$, $u(0)$, and $T_h(0)$ denote the values of the flow variables before the shock.

In the shock, all densities are transformed like the mass density ρ . The H_2 density, however, can be changed at each position to account for a re-entry flow of hydrogen molecules into the jet. This extra input of hydrogen molecules constitutes the major fitting parameter when comparing the model to the experiments, as the existence of a re-entry flow has only been hypothesized so far.

The electrons themselves do not experience a shock, since their motion never becomes supersonic (because of their low mass: Eq. (36)): it is the ion shock that dictates the electron density in the shock region (quasi-neutrality). As a consequence, the electron temperature is not transformed in a way similar to the heavy particle temperature. Adiabatic compression is assumed in order to calculate the electron temperature at each axial position in the shock. For a ratio of specific heats $\gamma = 5/3$, this relation reads:

$$\frac{T_e(z)}{T_e(0)} = \left(\frac{n_e(z)}{n_e(0)} \right)^{\frac{2}{3}}. \quad (42)$$

The actual position of the shock front is obtained by equation the stagnation pressure p_{stag} to the vessel background pressure p_{back} at each point in the expansion. When the former exceeds the latter, the shock position z_{shock} is found. The program then uses Eqs. (39-42) to calculate ρ , u , T_h , and T_e for the range ($z_{shock} - L_0$) to z_{shock} . The middle of the shock region (z_0) is situated at $z_{shock} - \frac{1}{2}L_0$. After the shock (in the subsonic region) numerical integration starts again, using the values obtained from the analytical expressions as starting values. The analytical shock calculation causes a small discontinuity in the calculated profiles around $z_{shock} - L_0$.

E. The subsonic relaxation region

In the region after the shock, axial gradients are no longer large compared to the radial gradients. This means, that the radial expansion of the beam is mainly diffusion determined [7]. The model uses Eqs. (28-35) again to calculate the values of the parameter set. The difference with the supersonic expansion part is, that the angle of expansion ϕ is now given by:

$$\tan \phi = \mathcal{F} \frac{D}{ru}, \quad (43)$$

where r is the plasma radius, \mathcal{F} is a constant depending on the actual shape of the plasma radial profile, and D is a diffusion coefficient. The value of \mathcal{F} is around 2 for any reasonable plasma profile (e.g., a Gaussian or a parabolic) [7]. D is assumed to be equal to the ambipolar diffusion coefficient for a pure argon plasma [7, 13]:

$$D = \frac{5.52 \times 10^{18}}{n_0 + n_e} T_e T_i^{-0.36}. \quad (44)$$

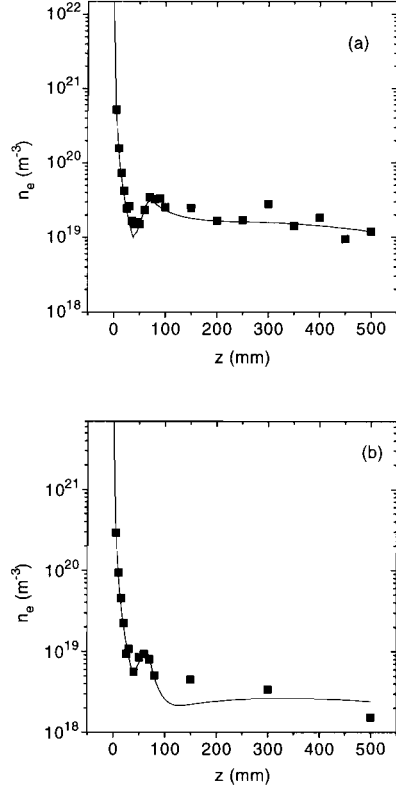


Figure 3: The electron density vs. the axial position (distance from the onset of the expansion) (a) for a pure argon flow entering the arc and (b) for a 2 vol.% hydrogen admixture. The drawn lines present the results of the model as described in the main text.

When applying Eq. (44), $T_i \approx T_h$ is assumed; n_0 denotes the neutral particle density.

This concludes the discussion of the model.

III. EXPERIMENTS

A. Thomson-Rayleigh scattering measurements

A1. Axial scans

As in the previous paper [1], the expanding argon-hydrogen plasma jet is investigated both by active and passive spectroscopic means. The Thomson-Rayleigh diagnostic has been described extensively by Van de Sanden [3] and we will not repeat the description here. In very short summary: frequency doubled Nd:YAG radiation is focused into the plasma and the scattered photons (under a 90° angle) are dispersed by a polychromator and detected by an image intensified photo diode array. The only difference with the previous set up [1] is the

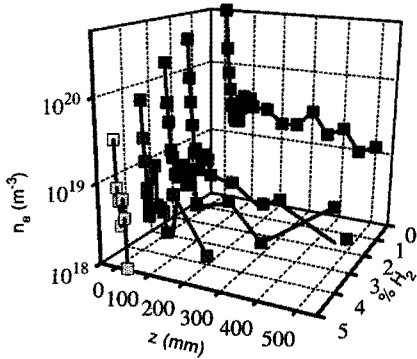


Figure 4: The electron density vs. the axial position (z) for higher admixtures.

fact, that the Nd:YAG laser has been replaced by a more powerful type (Quanta Ray GCR-190, 250 mJ/pulse @ 532 nm, 50 Hz). This results in shorter measurement times.

The parameters, determined by Thomson-Rayleigh scattering are n_e , T_e , and n_0 , with accuracies of about 10%, 25%, and 15%, respectively. Due to the small Rayleigh scattering cross sections for H and H₂ and the small densities of these species compared to the argon neutral density the measured neutral densities are equal to the argon neutral densities. The parameters are determined locally (detection volume about 0.25 mm³). The measurements are performed on the plasma in Fig. 1 under the following conditions: arc current $I_{arc} = 45$ A, arc voltage $V_{arc} = 100$ V, background pressure $p_{back} = 40$ Pa, total flow (argon and hydrogen): 3.5 standard litres per minute, hydrogen flow 0-10 vol.%. The hydrogen is admixed to the argon before it enters the cascaded arc. For seed fractions of 0, 2, 3, 4, 5, and 10 vol.%, axial scans are performed. Radial scans are performed for 0 and 2 vol.% seed fractions. As the cascaded arc can be moved inside the vessel without significantly changing the plasma, axial and radial scans can be made with great ease - without moving the laser system.

The experiments for a "pure" argon plasma (i.e., with the possible pollution of hydrogen molecules originating from the vessel walls [1, 2]) and for a 2 vol.% hydrogen seed fraction are compared to the model. The reason for leaving out the higher percentages lies in the fact, that the behaviour of the arc itself changes severely when more than, say, 3 vol.% hydrogen is admixed. This is reflected in the fact that with a 5 or 10 vol.% seed fraction, the electron density just after the arc exit drops to very low values (a few times 10^{18} m⁻³).

In Fig. 3, the axial electron density profiles are presented. The observed agreement between model and experiments is very good. In the case of 2 vol.% hydrogen, a total H₂ inflow from the vessel walls into the plasma of about 4×10^{18} particles/s is implemented in the model. The extra input has to take place before and in the shock region, i.e. between $z=0$ and $z=70$ mm. The input is assumed to be constant over this region. If an input in the subsonic region is assumed,

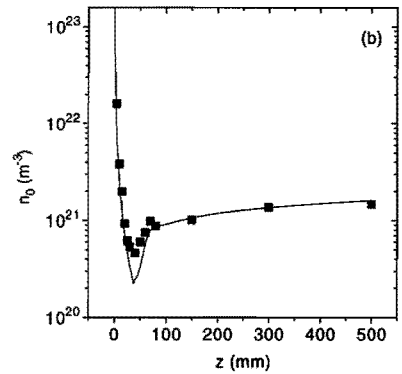
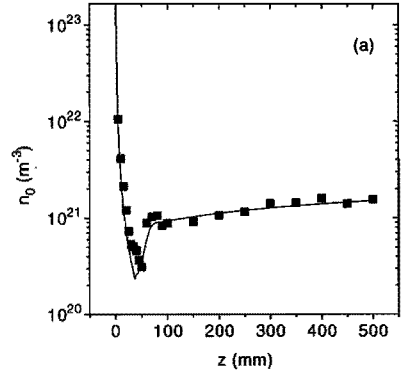


Figure 5: The neutral density vs. the axial position (z), for (a) pure argon and (b) a 2 vol.% hydrogen admixture. The drawn lines present the results of the model.

the agreement between model and experiments is significantly poorer. This is in agreement with our earlier hypothesis [1]. The value of 4×10^{18} s⁻¹ depends largely on the re-entrance flow pattern. In our case, where a constant radial inflow is assumed, the actual value is very sensitive to changes in the magnitude of the external hydrogen input. The total flux of re-entering hydrogen molecules has to be compared to the total quantity of molecules entering the arc: 2 vol.% hydrogen corresponds to approximately 2.5×10^{19} s⁻¹.

In the "pure" argon case, a 2.4×10^{17} s⁻¹ re-entry flow has to be assumed. This is to be expected, as the saturation of the vessel walls with hydrogen during hydrogen experiments will still cause a (smaller) re-entry flow of hydrogen molecules when returning to a pure argon plasma. The emission spectroscopy work (to be discussed later on) confirms this, as the hydrogen Balmer series are still observed when the arc is burning on pure argon. Also in this case, the model is very sensitive to the magnitude of the re-entry flow. The extra input has to take place before and in the shock: addition of extra hydrogen in the subsonic region causes the model values to strongly devi-

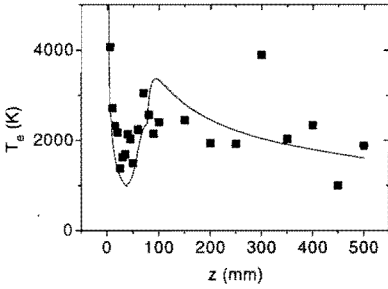


Figure 6: The electron temperature vs. the axial position (z) for pure argon. The drawn line represents the model. The 2 vol.% data show too much scatter to make a comparison with the model useful.

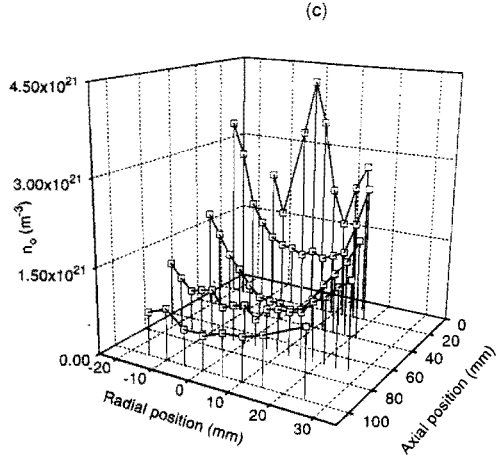


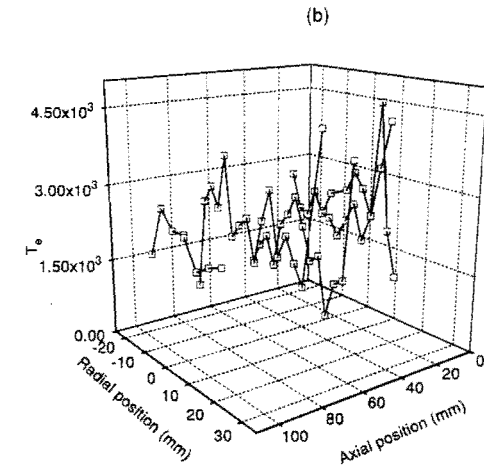
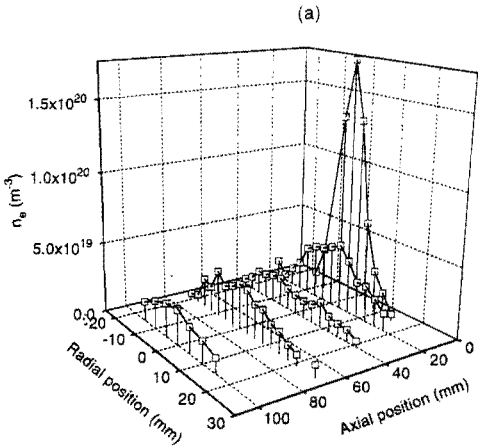
Figure 7: Radial profiles for the electron density n_e (a), the electron temperature T_e (b), and the neutral density n_0 (c): pure argon.

ate after $z = 100$ mm. It should be stressed that an external input of hydrogen molecules is absolutely necessary to obtain a good agreement between model and experiments.

The axial scans for higher admixtures of hydrogen (Fig. 4) are not compared to the model, because it is almost certain that the behaviour of the arc itself changes severely when, e.g., 10 vol.% H_2 is added. This aspect needs further research. For a 10 vol.% seed fraction, the ion flux from the arc has decreased significantly, as the electron density at $z=5$ mm has dropped to a low value (around $10^{18} m^{-3}$, compare Fig. 3).

Fig. 5 gives the neutral densities versus the axial position. Here also, the model describes the experiments very well. The neutral density behaviour appears to be independent of hydrogen seed fraction. So our initial assumption [1] that we could study the plasma beam kinetics without disturbing the basic transport phenomena remains justified (at least up to 5 vol.% H_2 seed fractions). So, as was mentioned before, we can consider hydrogen to be a small perturbation on the argon expanding jet, as far as transport phenomena are concerned.

The electron temperature behaviour is difficult to describe, as was pointed out by Van de Sanden [8]. Especially in the shock region, current generation appears to be of importance, causing the electron temperature to rise before the actual shock position. As our model does not include current generation, the agreement between model and experiments is not expected to be very good. Nevertheless, the general trends are clear in Fig. 6. The data for hydrogen admixture show too much scatter to make a comparison with the model useful. Further research is needed to get more insight in the electron temperature behaviour when hydrogen is admixed to the flow.



A2. Radial scans

For 0 and 2 vol.% hydrogen seed fractions, radial scans have been performed at 5 axial positions: $z=10, 20, 40, 70$, and 100 mm. The results for the electron density and temperature as well as the neutral density are given in Figs. 7 and 8. Especially the electron density profiles support the view, that hydrogen molecules enter the plasma beam from the periphery. This becomes clear in Fig 9. Here, we have used the adiabatic model by Ashkenas *et al* [20] to fit the radial profiles at $z=10$ and 20 mm. For the “pure” argon case, the fits appear to be quite good, especially at $z=10$. This is an extra conformation of the view [3] that the supersonic part of the pure argon jet closely resembles an adiabatic expansion.

For the 2 vol.% case, we simply used the fits for the pure argon case and normalized them to the maximum value (at $r=0$ mm) of the 2 vol.% radial scans. The results are also shown in Fig. 9. It can clearly be seen that the adiabatic expansion model no longer coincides with the measurements: the measurements tend to be much lower than they would have been in the case of an adiabatic expansion. The simple transfer of the pure argon fits to the 2 vol.% data is justified because the adiabatic model only depends on the specific size and form of the expansion hole and the pressure ratio inside and outside the expansion chamber [20]. In our view, this is a clear hint that reactions (4,5) take place at the edges of the plasma, and that a radial re-entry flow of hydrogen molecules is needed to make this possible. The effect on the central electron density could have two reasons: arc effects or the occurrence of the same reactions. This latter process is not expected to have much influence, however, before $z=30-40$ mm.

B. Optical emission spectroscopy

Even though line and continuum radiation are not taken into account in the discussed model, optical emission spectroscopy (OES) results can give extra insight in the plasma beam kinetics. The OES measurements have proved to be especially effective in combination with the Thomson-Rayleigh scattering results. The OES diagnostic has been extensively discussed elsewhere [1, 10] and we will only give the results here.

OES measurements have been performed on the same set of Ar(I) and H(I) lines as reported our previous paper [1], at three axial positions: $z=20, 40$ and 70 mm and for the same hydrogen seed fractions as mentioned above. The OES system was calibrated using a tungsten ribbon lamp in order to obtain absolute level densities per statistical weight. We choose to present the data in the form of *population factors* b_p . In this representation, the absolute level density per statistical weight (n_p/g_p) is related to the density as calculated with the Saha-equation ($n_{p,Saha}/g_p$) [1, 21]:

$$b_p \stackrel{\text{def}}{=} \frac{n_p}{n_{p,Saha}}, \quad (45)$$

where the Saha density $n_{p,Saha}$ is calculated using the n_e and T_e values obtained by Thomson scattering. To calculate the H^+ Saha density, the H^+ density is needed. It is calculated using intensity ratios of highly excited hydrogen and argon levels, as discussed previously [1].

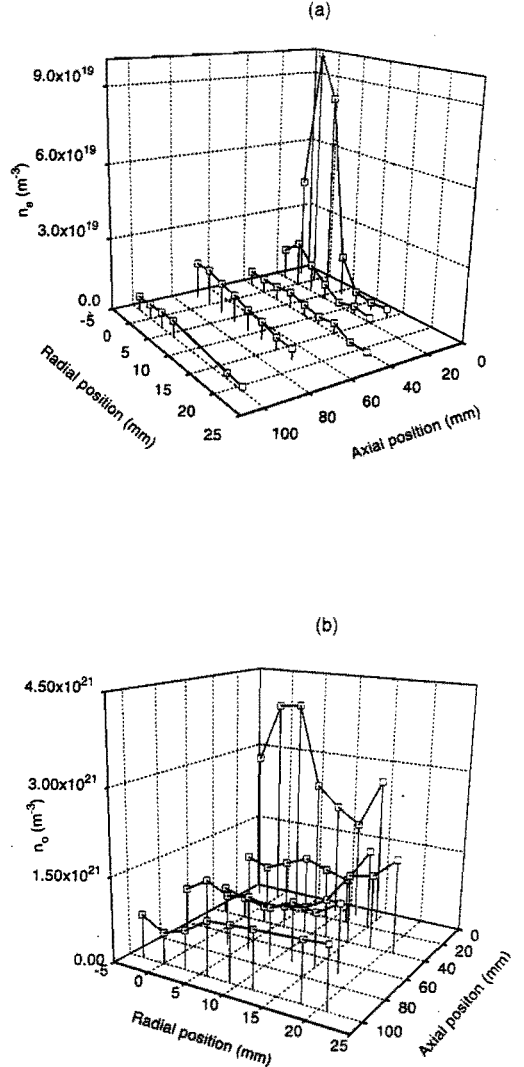


Figure 8: Radial profiles for the electron density n_e (a) and the neutral density n_0 (b) for a 2 vol.% hydrogen admixture.

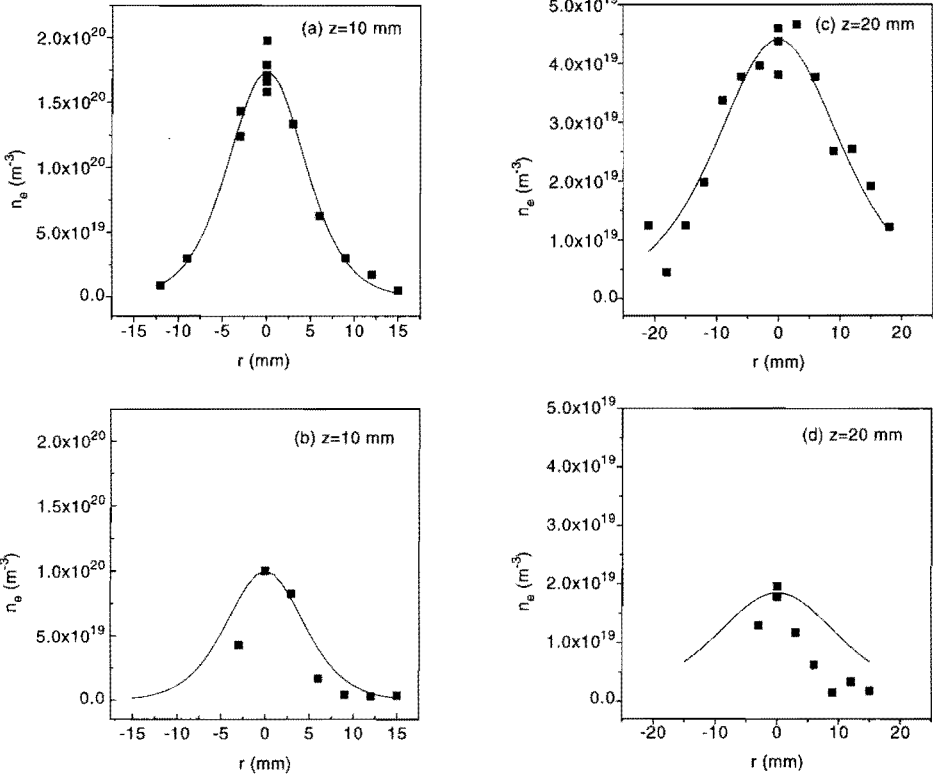


Figure 9. Radial scans for $z=10$ mm ((a): pure argon, (b) 2 vol.% hydrogen) and $z=20$ mm ((c): pure argon, (d) 2 vol.% hydrogen). The drawn lines represent the Ashkenas adiabatic model for a supersonically expanding jet. The 2 vol.% data cannot be described with the adiabatic model.

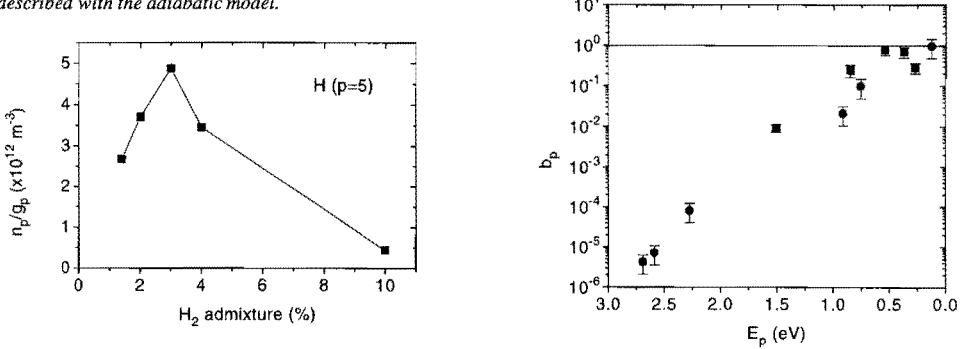


Figure 10. (left) The hydrogen $p=5$ level population per statistical weight vs. the hydrogen seed fraction at $z=20$ mm.

Figure 11. (right) Population factors b_p for hydrogen and argon vs. E_p , the ionization energy of the level concerned ($z=40$ mm, 3 vol.% hydrogen). Squares denote hydrogen levels, whereas circles represent argon levels.

In general, a strong decrease in intensity of the argon lines is observed if hydrogen is admixed, we reported before. As the excitation in the argon system results from three-particle recombination [15], this must be a consequence of the disappearance of argon ions. Two processes can be responsible for this loss: (a) the occurrence of reactions (4-5), and (b), the arc ionization changing from argon to hydrogen, as the ionization potential of hydrogen is smaller by about two eV [1]. For seed fractions above 4 vol.% hydrogen even the strongest argon lines disappear.

The behaviour of the hydrogen line intensities is more complicated. The intensity rises with the hydrogen admixture until 3 vol.%, after which it drops (Fig. 10). The effect can be explained by assuming that the excitation in the hydrogen system is a result not only of three particle recombination, but also of the occurrence of reactions (4-5). We assume for the moment that the total arc ionization degree remains more or less constant until 3 vol.% hydrogen is admixed, above which the ionization degree must drop dramatically to explain the low n_e value measured by Thomson scattering. The increase in hydrogen line intensities can, then, be explained by (a) the fact that more and more hydrogen molecules enter the plasma beam to participate in reaction (4) and (b) the fact that more and more hydrogen ions are coming out of the arc. The former effect could, however, be balanced by the decrease in the amount of argon ions leaving the arc. The decrease for higher seed fractions (> 3 vol.%) must be a consequence of the arc becoming less efficient in producing (predominantly hydrogen) ions - as indicated by the Thomson scattering data.

It is also observed that the hydrogen $H\alpha$ line is clearly visible when *no* hydrogen is added to the flow. This has been observed by Meeusen *et al* in a similar situation [23]. The $H\alpha$ emission appeared to decrease slowly (on an hour time scale). In our view this can only be explained by a recirculation flow inside the vessel in combination with a stainless steel vessel wall saturated with hydrogen [1].

The population factors for the argon and hydrogen systems are depicted in Fig. 11. The general shape of the Ar(I) and H(I) distributions is similar to the ones reported before [1], so only one example is given. As can be seen, the Ar(I) b_p factors close to the continuum approach the value 1, indicating the presence of a Saha equilibrium, as expected for this type of recombining plasmas. This constitutes a test for both the Thomson data and the OES calibration [1, 21].

More remarkable is the "bulge" in the hydrogen b_p factors around p (principal quantum number) = 5-7. It has been verified, that this effect can *not* be attributed to Stark broadening, an effect which could boost the width of the hydrogen Balmer lines above the width of the apparatus profile of the monochromator, thus causing a systematical error (as higher excited levels are Stark broadened more strongly). This can be thoroughly tested by recording wavelength scans of the different Balmer lines: for all lines, the line profile appears to be equal to the monochromator apparatus profile. If Stark broadening would be of any influence, the line profiles of higher excited levels would be broader. We can, thus, safely assume that all hydrogen Balmer line profiles are smaller than the apparatus profile (which equals 0.16 nm).

Another physical process must therefore be responsible for

this bulge, and the most likely candidate is, once more, the occurrence of reactions (4- 5), resulting in an extra input of hydrogen excited states. The fact that the maximum of the bulge is not fixed, but can be found around $p=5-7$ makes a excitation exchange process (e.g. between Ar ($4p'$) and the H(I) system) unlikely, as this would be a very state-selective process. No evidence for excitation exchange processes between argon and hydrogen has been found using laser induced fluorescence experiments [22]. If vibrationally excited hydrogen molecules participate in reaction (4), however, the hydrogen produced in the dissociative recombination reaction (5) could appear in a highly excited state, thus explaining the bulge. The exact location of the maximum would then depend on the amount of vibrational (and rotational) excitation of the hydrogen molecules.

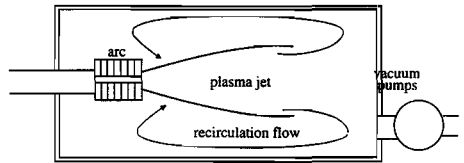


Figure 12. A sketch of the envisaged recirculation pattern in the vacuum vessel. This recirculation flow is thought to transport wall-associated hydrogen molecules towards the plasma, especially around the shock region.

IV. CONCLUSIONS

The transport phenomena of the expanding cascaded arc plasma remain unaffected for small hydrogen seed fractions: the neutral density behaviour is virtually unaffected by the addition of hydrogen, and well described by a quasi one-dimensional model, where the plasma parameters are averaged over a surface at right angles with the expansion axis.

The electron density is strongly affected by the addition of hydrogen: a strong decrease of the electron density is observed. This effect can be modeled using the quasi one-dimensional approximation, assuming that a certain amount of hydrogen molecules form at the vessel walls and re-enter the plasma before and in the shock region. With this extra input from the periphery, a very good agreement between model and experiments is obtained.

A recirculation pattern within the vacuum vessel (Fig. 12) is thought to be responsible for the re-entry flow of hydrogen molecules into the jet. The largest fraction of this re-entering molecules must reach the beam before or in the shock region.

The electron temperature behaviour is reasonably well described by the model. However, since current generation has not been taken into account, the observed rise of the electron temperature before the actual shock position ([8]) can not be modeled.

The behaviour of the cascaded arc itself changes dramatically when the hydrogen seed fraction exceeds 3 vol.%. This is shown by the fact that the electron density drops to levels below the detection limit of the Thomson-Rayleigh scattering set up, even just outside the nozzle exit (for a 10 vol.% seed fraction).

The Ar(I) excited level population is determined by three particle recombination: therefore the Ar(I) line intensities drop when hydrogen is added to the flow, resulting in a net loss of argon ions. The hydrogen excited level population arises due to three particle recombination and dissociative recombination (5). The hydrogen Balmer emission decreases for higher seed fractions, most probably due to the reduced arc efficiency.

The "bulge" in the hydrogen excited level distribution (b_p vs. E_p) can be attributed to the dissociative recombination of the ArH⁺ molecular ion. If rovibrational excitation of the hydrogen molecules is present, the formed hydrogen atom could end up in a highly excited state.

ACKNOWLEDGEMENT

The authors gratefully acknowledge H.M.M. de Jong, M.J.F. van de Sande, and A.B.M. Hüsken for their skillful technical assistance. This work is supported by the Netherlands Technological Foundation (STW). The work of M.C.M. van de Sanden is supported by the Royal Netherlands Academy of Arts and Sciences (KNAW).

References

- [1] R.F.G. Meulenbroeks, A.J. van Beek, A.J.G. van Helvoort, M.C.M. van de Sanden, and D.C. Schram, *Phys. Rev. E* **49** (5), 4397 (1994).
- [2] M.J. de Graaf, R. Severens, R.P. Dahiya, M.C.M. van de Sanden, D.C. Schram, *Phys. Rev. E* **48** (3), 2098 (1993).
- [3] M.C.M. van de Sanden, J.M. de Regt, G.M. Janssen, J.A.M. van der Mullen, D.C. Schram, and B. van der Sijde, *Rev. Scient. Instr.* **63** (6), 3369 (1992).
- [4] A.J.M. Buuron, G.J. Meeusen, J.J. Beulens, M.C.M. van de Sanden, and D.C. Schram, *J. Nucl. Mat.* **200**, 430 (1993).
- [5] A.T.M. Wilbers, G.J. Meeusen, M. Haverlag, G.M.W. Kroesen, and D.C. Schram, *Thin Solid Films* **204**, 59 (1991).
- [6] R.F.G. Meulenbroeks, D.C. Schram, L.J.M. Jaegers, and M.C.M. van de Sanden, *Phys. Rev. Lett.* **69** (9), 1379 (1992).
- [7] G.M.W. Kroesen, D.C. Schram, A.T.M. Wilbers, and G.J. Meeusen, *Contrib. Plasma Phys.* **31** (1), 27 (1991).
- [8] M.C.M. van de Sanden, R. van den Bercken, and D.C. Schram, submitted to *Plasma Sources Science Techn.* (1994).
- [9] Eric A. Gislason and Gérard Parlant, *J. Chem. Phys.* **94** (10), 6598 (1991).
- [10] M.C.M. van de Sanden, Ph.D. Thesis Eindhoven University of Technology (1991).
- [11] S.I. Braginskii in *Reviews of Plasma Physics*, ed. M.A. Leontovich, Plenum N.Y. (1965).
- [12] H. Venugopalan *Reactions under Plasma Conditions*, Wiley Interscience, London (1971).
- [13] C.J. Timmermans, Ph.D. Thesis Eindhoven University of Technology (1984)
- [14] G.M.W. Kroesen, Ph.D. Thesis Eindhoven University of Technology (1988).
- [15] M.C.M. van de Sanden, J.M. de Regt, and D.C. Schram, *Phys. Rev. E* **47** (4), 2792 (1993).
- [16] K.M. Ervin and P.B. Armentrout, *J. Chem. Phys.* **83** (1), 166 (1985).
- [17] H.M. Mott-Smith, *Phys. Rev.* **82**, 885 (1951).
- [18] C. Muckenfuss, *Phys. Fluids* **3**, 320 (1960).
- [19] P Glansdorff, *Phys. Fluids* **5**, 371 (1962).
- [20] H. Ashkenas and F.S. Sherman, *Proc. Rarefied Gas Dynamics* **4**, ed. J.H. de Leeuw, Academic Press N.Y. (1966).
- [21] J.A.M. van der Mullen, *Phys. Rep.* **191**, 109 (1989).
- [22] R.A.H. Engeln, R.F.G. Meulenbroeks, A.J. Snoeijer, J.A.M. van der Mullen, and D.C. Schram, to be published (1996).
- [23] G.J. Meeusen, E.A. Ershov-Pavlov, R.F.G. Meulenbroeks, M.C.M. van de Sanden, and D.C. Schram, *J. Appl. Phys.* **71** (9), 4156 (1992).

Influence of Molecular Processes on the Hydrogen Atomic System in an Expanding Argon-Hydrogen Plasma

R.F.G. Meulenbroeks R.A.H. Engeln C. Box I. de Bari
M.C.M. van de Sanden J.A.M. van der Mullen D.C. Schram

*Eindhoven University of Technology, Department of Physics,
P.O. Box 513, 5600 MB Eindhoven, The Netherlands*

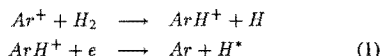
Abstract. An expanding thermal arc plasma in argon-hydrogen is investigated by means of emission spectroscopy. The hydrogen can be added to the argon flow before it enters the thermal arc plasma source or it can be flushed directly into the vacuum expansion vessel (1-20 vol.% H₂). The atomic state distribution function for hydrogen, measured at a downstream distance of 20 mm, turns out to be very different in the two cases. For injection in the arc, three particle recombination is a primary source of hydrogen excitation, whereas measurements with hydrogen injected into the vessel clearly point to a molecular channel (dissociative recombination of formed ArH⁺) populating atomic hydrogen levels.

I. INTRODUCTION

Expanding thermal arc plasmas are used in a variety of applications such as plasma deposition and etching and particle sources [1]-[4]. The fundamental study of this type of plasma has concentrated on pure argon plasmas and argon-hydrogen mixtures [5]-[8]. The plasma expands out of a cascaded arc through a conically shaped nozzle into a low-pressure background. The initially supersonic expansion ends in a stationary shock after 40-70 mm, which is followed by a subsonic relaxation region.

As was reported before [7, 8], hydrogen molecules play a major role in the very fast ionization loss that has been measured using Thomson scattering on an expanding argon-hydrogen plasma. Atomic processes cannot account for this anomalous loss of ions. It has been made plausible [8] that at least an important fraction of these hydrogen molecules must originate from the stainless steel vessel walls. The fact, that the volume of the vessel (about 300 litres) causes the residence time of particles to be fairly large (around 1 second) may induce a recirculation pattern inside the vessel. This flow could well be responsible for the transport of the formed molecules back into the plasma [7].

The following set of reactions is responsible for the fast ionization loss:



At temperatures in the expansion (around 0.2 eV), the competing charge exchange reaction (the creation of H₂⁺) is of little importance [9]. If the formed ArH⁺ ion carries little rovibrational energy, the excited hydrogen atom is formed in the *p*=2 state. If important rovibrational excitation is present (the potential well of the molecular ion has a depth of about 4 eV [10]), hydrogen states *p*=3 or higher may be formed, which can be readily observed by simple emission spectroscopy. The origin of the high rovibrational excitation of ArH⁺ will be discussed later.

II. EXPERIMENT

The expanding plasma experiment has been described before [5] and will only be summarized here. The thermal plasma source (a cascaded arc) is operated at the same settings as used in [7, 8]: arc current: 45 A, arc voltage 100-140 V (depending on hydrogen seed fraction), background pressure 40 Pa, and total gas flow 3.5 standard liters per minute (SLM). The hydrogen seed fractions are 1,2,3,4,5,7,10, and 20 vol.% H₂; hydrogen is added to the flow before it enters the cascaded arc or injected directly into the vessel. These two conditions will be referred to as "arc seeding" and "vessel injection", respectively.

The optical emission spectroscopy (OES) experiment has been described in [7]. It contains a fairly standard mirror-scanned optical system. A few modifications have been implemented: a different monochromator (Bentham M300) with a Hamamatsu R1617 photomultiplier tube is used. The slit widths are chosen to obtain a resolution of 0.16 nm. Furthermore, an extra mirror was added to make possible the use of an external ribbon lamp for calibration of the last part of the optical system (including the last two lenses, the monochromator, and the photomultiplier, Fig. 1). The calibration procedure is the following. At the beginning of a measuring period of about 4 weeks a calibration using a tungsten ribbon lamp, placed inside the vacuum vessel (at the plasma position), is performed. Immediately after that calibration (covering the entire light path) a calibration using the external ribbon lamp is made, covering the last part of the optical system. This is done by turning the step motor driven rotating mirror (RM in Fig. 1) in order to focus the external ribbon lamp on the pinhole (Fig. 1). Every two or three days, this latter calibration is repeated, and the calibration with the ribbon lamp in the vessel is repeated at the end of the measuring period. The differences between the calibrations appear to be quite small (typically 3%).

This calibration procedure makes possible a very accurate determination of absolute level densities of atomic states. The main source of error for the hydrogen states is the plasma

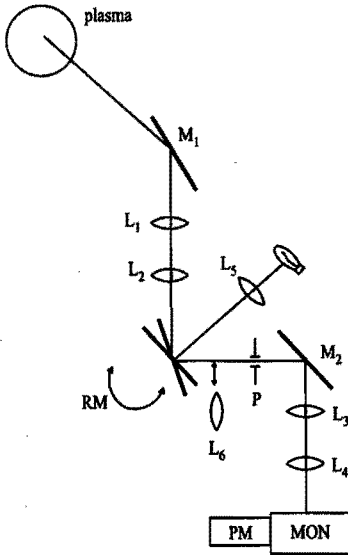


Figure 1: The emission spectroscopy experiment. The plasma radiation is focused on the entrance slit of the monochromator (MON) by a system of lenses (L_1 , $f = 750$ mm, L_2 , $f = 500$ mm, L_3 , $f = 200$ mm, L_4 , $f = 150$ mm) and mirrors (M_1 , M_2). P designates a 0.5 mm diameter pinhole and PM the photomultiplier tube. Photon counting electronics are used to record the incoming radiation. A rotating mirror (RM) is used to make lateral scans of the plasma. To use the external ribbon lamp (RL), the rotating mirror has to be turned, and the ribbon is focused on the pinhole by lenses L_5 ($f = 200$ mm) and L_6 ($f = 150$ mm). The latter can be (reproduceably) inserted in the optical system when a calibration using the external ribbon lamp is required.

reproducibility (10-15%). In the case of argon, the inaccuracies in the transition probabilities (around 25-50%) become dominant [7, 11].

All lateral scans are performed at a downstream axial distance of $z=20$ mm. The expansion axis is labeled z , with the origin at the expansion nozzle. The lateral scans are converted into radial profiles by means of Abel inversion, yielding radial profiles of the absolute level density per statistical weight. Measurements are performed on the Balmer series of hydrogen (data can be found in [11] or [7]), as well as on several argon lines (also given in [7]). The latter was mainly done to check the calibration: in our recombining plasma jet, the population factors b_p (an indication of the departure from Saha-equilibrium [7, 12]) should tend to unity for highly excited levels. For a pure argon expanding plasma, one can use the measured values of T_e and n_e (Thomson scattering, [5, 7]) to calculate the b_p factors. In this case, a very satisfactory approach to unity is observed for levels near the continuum,

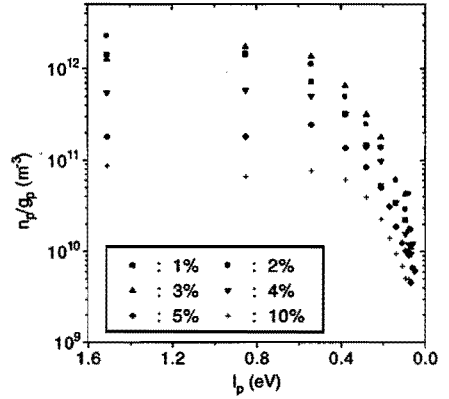


Figure 2: The Boltzmann plots n_p/g_p vs. I_p for the arc seeding case at a downstream distance of 20 mm, for different hydrogen seed fractions. The hydrogen is admitted to the flow before it enters the arc.

where a Saha-equilibrium is expected (compare [7]). This constitutes a reliable check of the calibration of the OES system, as the Thomson scattering data are known to be very accurate (compare [5]).

III. RESULTS

The results will be discussed in two parts. For the sake of clarity, we shall first discuss the measurements where hydrogen is added to the flow before it enters the arc (arc seeding), after which we shall turn to the second set of measurements, where the hydrogen is injected in the vacuum vessel.

A. Arc seeding

Typical n_p/g_p vs. I_p (absolute level densities per statistical weight vs. the ionization energy of the level concerned) plots are given in Fig. 2. The character is clearly recombining. Sometimes a slight inversion is observed. Strong inversions can be observed in similar plasmas (e.g., Ref. [13], where a similar set up with a magnetic field is used).

To calculate the population factors b_p , we need the hydrogen ion concentration. For arc seeding, the ratio of argon to hydrogen ions can be calculated with the method described in Refs. [14] and [7] using highly excited hydrogen and argon levels. The n_e and T_e values needed for the calculation are taken from Ref. [8]. The H^+/Ar^+ concentration ratios are similar to those reported in [7]: around 1:70 for a 2 vol.% seed fraction, increasing to 1:4 for 3 vol.%. For measurements with higher seed fractions (above 4 vol.%), the ratio cannot be determined, because the argon emission disappears. This is a result from the arc ionization changing from argon to hydrogen. The lines used for the H^+/Ar^+ ratio calculation are hydrogen 377.1 and 388.9 nm, and argon 531.8 and 506.0 nm (see [7, 11]), as these

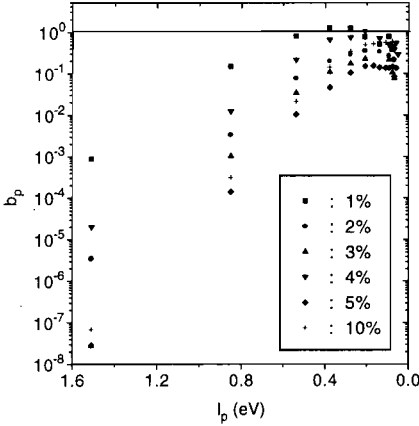


Figure 3: The population factors b_p vs. I_p for the arc seeding case at a downstream distance of 20 mm.

levels should be well within the region of Saha equilibrium.

Fig. 3, then, gives the b_p vs. I_p plots, for arc seed fractions of 1-10 vol.%. The absolute b_p values cannot be considered very accurate for higher seed fractions, where the ion concentration ratios are unknown. The ‘‘bulge’’ in b_p that was reported before [7] around level $p=5-7$ is not observed in all cases. It should be noted, that the deviation from equilibrium (e.g., by comparing the b_p values for $p=3$) becomes larger for higher seed fractions: this is consistent with the observed decrease in n_e , as reported in Ref. [8]. Clearly, the electron impact processes lose importance for higher seed fractions, causing the lower part of the excitation system to become more and more radiation dominated.

We can try to explain the observed hydrogen population densities by considering only three particle recombination of H^+ . To do so, we have to determine, which part of the total deexcitation (three particle recombination) flow passes a certain level, say $p=3$. At ambient conditions (n_e around $2.5 \times 10^{19} \text{m}^{-3}$ and T_e around 1500 K), the hydrogen system is dominated by radiative deexcitation below level $p=4$. Above that level, collisional deexcitation is dominant, resulting in mainly stepwise deexcitation in that part of the system [12]. Radiative deexcitation being dominant in the lower part of the excitation system, a comparison of the radiative transition probabilities [11] starting from $p=4$ shows, that about one-third of the recombination flow should pass $p=3$.

The rate constant for three particle recombination is taken from Van de Sanden [15]: $K_{3p} = 3.3 \times 10^{-21} T_e^{-4.5} \text{m}^6 \text{s}^{-1}$. As stated above, we assume the depopulation of $p=3$ to be due to radiation: the collisional deexcitation process can be shown to be slower by a factor of about 10. Thus, the total $p=3$ density $n_{p=3}$ can be calculated:

$$n_{H,p=3} A_{3,downward} \approx \frac{1}{3} n_e^2 n_{H^+} + K_{3p}, \quad (2)$$

with $A_{3,downward}$ the total radiative destruction of the level

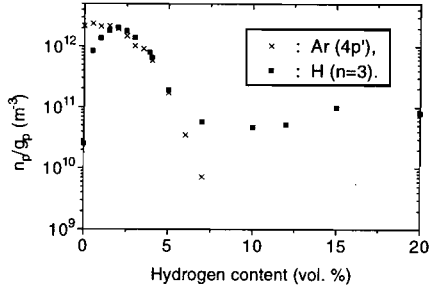


Figure 4: The hydrogen $p=3$ and argon $4p'$ level densities per statistical weight vs. the hydrogen arc seed fraction for the arc seeding case. The argon n_p/g_p values have been divided by 20 to make clear the difference in behaviour.

(10^8s^{-1}). For $n_e = 3.4 \times 10^{19} \text{m}^{-3}$, $T_e = 1500 \text{K}$, and an $n_{H^+} : n_{Ar^+}$ ratio of 1:70, this results in $n_3/g_3 \approx 2 \times 10^{12} \text{m}^{-3}$. This estimate is in agreement with the observed $2.5 \times 10^{12} \text{m}^{-3}$ for a 2% arc seed fraction. No additional processes need to be considered to explain the hydrogen level population at the center of the plasma jet. At the edges, some extra input may be necessary to explain the observed population of hydrogen levels, as the electron density profile is more narrow than the hydrogen $p=3$ density profile, while the electron temperature profile is relatively flat. This means, that three particle recombination can no longer fully account for the observed emission at the edges of the plasma jet.

An interesting feature is observed when measurements are performed at H_α and argon 696.5 nm ($4p'$) for increasing hydrogen seed fractions: see Fig. 4. For argon, a steady decrease is observed, caused by the arc ionization changing from argon to hydrogen. H_α shows a behaviour similar to that reported in [8]. The H_α radiation (above 7 vol.%) can probably be attributed to three particle recombination, as no argon ions are left [8]. An extra input, however, could be formed by dissociative recombination of H_2^+ ions formed by charge exchange between H^+ and rovibrationally excited H_2 molecules [4]. To end in $p=3$, the participating H_2 molecule should carry considerable rovibrational excitation (3-4 eV). For lower seed fractions, where Ar^+ is the most abundant ion, reactions (1) probably are dominant, as the H_2 molecule does not need to carry that much rovibrational excitation to make a creation of a $p=3$ state possible.

If we assume, for the arc seeding case, three particle recombination to be dominant, the strong increase in H_α for low seed fractions should be caused by more and more hydrogen entering the arc. The decrease above 2 vol.% must then be caused by the arc becoming less efficient, as indicated by Thomson scattering measurements [8].

B. Vessel injection

In the case of vessel injection, the hydrogen is injected far away from the expansion nozzle in the vessel itself. The flows are kept the same as in the arc seeding case. It is useful to

point to the main differences between arc seeding and vessel injection.

(a) When hydrogen is injected into to vacuum vessel, we can be sure that our plasma source remains unaffected: the cascaded arc will produce a pure argon plasma, which constitutes a well-known source of argon ions [5, 15]. Measurements have learned, that the arc plasma source changes when hydrogen is mixed to the argon flow before it enters the arc: a lower electron density is measured when H_2 is injected in the arc [8].

(b) A possible difference concerns the rovibrational population of the hydrogen molecules inside the vessel. When hydrogen is injected in the vessel at 300 K, only the $v=0$ vibrational state is populated. As the plasma itself has a temperature of only 0.2 eV, any significant rovibrational excitation (e.g., 2 eV or more) should come from wall-association [16]. This process could bring about a "second generation" of hydrogen molecules formed by association of hydrogen atoms [originating from reactions (1)] at the vessel walls. When hydrogen is injected in the arc, some rovibrational excitation may originate from molecules surviving the arc (where the temperatures are around 1 eV). It is, however, more probable that excited hydrogen molecules are formed at the vessel walls, as has been concluded before [1, 7, 8].

(c) For the OES work, the main difference lies in the population mechanism of the hydrogen excited levels. As was shown above, three particle recombination can fully account for the observed $p=3$ population for the arc seeding case. The fact that the population factors b_p approach unity for low I_p also points in this direction. When hydrogen is injected in the vessel, only one channel of hydrogen excited level population is still possible: dissociative recombination of rovibrationally excited ArH^+ ions ending in H excited states. It should be pointed out that no H^+ or excited H can be formed by electron impact in view of an extremely small Boltzmann exponent at ambient temperatures of 0.2 eV. In the following it will be shown, that a relatively small amount of rovibrationally excited molecular ions suffices to account for the observed hydrogen Balmer radiation in the vessel injection case.

Fig. 5 gives the n_p/g_p vs. I_p plots for the vessel injection case. The distribution is clearly different from the arc seeding case: only the lower three to five levels are observed. Since these levels are not expected to be in Saha equilibrium with the continuum, a calculation of ion concentration ratios (as discussed in Sec. III A) is probably not possible. Also, b_p factors can not be calculated. Furthermore, the H^+ concentration must be very low, since a significant hydrogen ion concentration should bring about emission of higher excited states, populated by three particle recombination.

Before turning to a more quantitative explanation of these results, we must exclude one specific excitation mechanism for $p=3$: dissociative recombination of (low excited) ArH^+ ending in $p=2$ and subsequent collisional excitation to $p=3$. We can get an estimate of the rate constant $K_{2,3}$ for this excitation process by applying a hard-sphere approximation [12]:

$$K_{n,n+1} \approx 4\pi a_0^2 p^4 v_{th} \frac{g_{n+1}}{g_n} \exp\left(\frac{-\Delta E_{n,n+1}}{kT_e}\right), \quad (3)$$

with a_0 Bohr's radius, p the principal quantum number, g_n the statistical weight of level p , v_{th} the electron thermal speed,

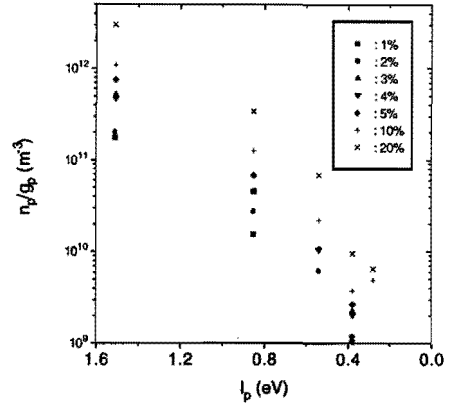


Figure 5: The Boltzmann plots (n_p/g_p vs. I_p) for different hydrogen seed fractions, when hydrogen is injected into the vessel. Note the very pronounced difference with Fig. 2, due to different excitation mechanisms in the two cases.

$\Delta E_{n,n+1}$ the energy gap between levels p and $n+1$, and k Boltzmann's constant. For the ambient conditions ($n_e = 5.2 \times 10^{19} m^{-3}$, $T_e = 2000$ K), Eq. (3) yields $K_{2,3} \approx 3.3 \times 10^{-17} m^3 s^{-1}$. If the population of level $p=3$ is governed by a Corona-like balance of electron excitation from $p=2$ and radiative destruction, we can write:

$$n_{H,p=3} A_{3,downward} = n_{H,p=2} n_e K_{2,3}, \quad (4)$$

which for a 2 vol. would lead to a total $p=2$ density of $2.1 \times 10^{17} m^{-3}$. If these $p=2$ states are produced by dissociative recombination of ArH^+ , the following balance should hold (the plasma is optically thin for hydrogen radiation in the case of low hydrogen concentrations):

$$n_{H,p=2} A_{2,1} = n_{Ar^+} n_{H_2} K_1, \quad (5)$$

where the rate constant K_1 for the formation of ArH^+ is $1.1 \times 10^{-15} m^3 s^{-1}$ [17] at ambient temperatures. The transition probability $A_{2,1} = 4.7 \times 10^8 s^{-1}$. The second dissociative recombination step of reactions (1) is known to be faster by a factor of about 100, depending on conditions. As the first step thus limits the production of ArH^+ ions, we have to use K_1 in the above balance. Eq. (5) leads to a H_2 density of about $1.7 \times 10^{21} m^{-3}$. This value is unrealistic, as the total neutral density at $z=20$ mm is around $9 \times 10^{20} m^{-3}$ [8].

For the vessel injection case, we can thus safely exclude the following population mechanisms for $p=3$ and higher: (a) three particle recombination (which would require a significant H^+ density), (b) electron excitation (the Boltzmann exponent is extremely small), and (c) dissociative recombination of ArH^+ ending on $p=2$ and subsequent collisional excitation to $p=3$ (which would require an unrealistic H_2 density).

In our view, only one mechanism remains: dissociative recombination of rovibrationally excited ArH^+ . We can es-

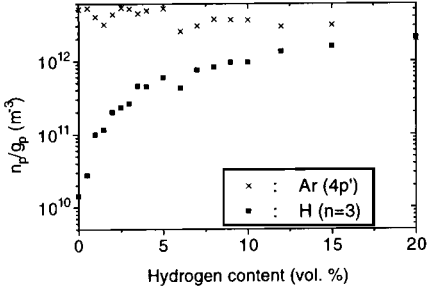


Figure 6: The hydrogen $p=3$ and argon $4p'$ level densities per statistical weight vs. the hydrogen admixture: hydrogen is injected in the vessel. The argon $4p'$ densities have been divided by a factor 8 to make possible a comparison of the behaviour of the two excited states.

timate the amount of hydrogen needed to accomplish the observed hydrogen excited level populations. We neglect for the moment the question whether a rovibrationally excited hydrogen molecule that participates in reaction (1) actually produces a rovibrationally excited ArH^+ ion. We shall come back to this later. A balance analogous to Eq. (5) can be written for $p=3$:

$$n_{H,p=3} A_{3,downward} = n_{Ar} + n_{H_2^v,J} K_1. \quad (6)$$

In this balance the electron density is known: $n_e = 5.2 \times 10^{19} \text{m}^{-3}$; this equals the argon ion density in the vessel injection case. Inserting the known values in Eq. (6) yields a density of rovibrationally excited molecules (with enough internal energy to make possible the excitation of the ArH^+ ion and, thus, of the formed H atom) of $n_{H_2^v,J} = 6.3 \times 10^{15} \text{m}^{-3}$ for a 2 vol.% injection in the vessel. If we assume the maximum total H_2 density in the plasma to be equal to 2% of the total neutral density ($9 \times 10^{20} \text{m}^{-3}$), the H_2 density would amount up to $1.8 \times 10^{19} \text{m}^{-3}$. If any rovibrational excitation is supplied by wall association, the number of excited hydrogen molecules appears to be reasonable.

Support for this production mechanism for $p=3$ states can also be deduced from Fig. 6, which shows the behaviour of H $p=3$ and argon $4p'$ densities for different vessel seed fractions. Eq. (6) predicts the $p=3$ density to be proportional to the H_2^v,J density (for a constant Ar^+ density). Fig. 6 shows, that the $p=3$ population is proportional to the total H_2 density. That the Ar^+ density must be more or less constant is indicated by the fact, that the argon $4p'$ level density decreases only by a factor of 2-3 (the argon population is dominated by three particle recombination). A logarithmic representation is chosen for Fig. 6 (even though it obscures the mentioned proportionality) to clearly represent the lower $p=3$ data.

To illustrate the effect, that population of $p=3$ alone is not sufficient to explain the measurements, fig. 7 gives the n_p/g_p values for a 2 vol.% vessel injection. The drawn line represents a Boltzmann line with the electron temperature. Electron collisions are clearly not energetic enough to explain the pop-

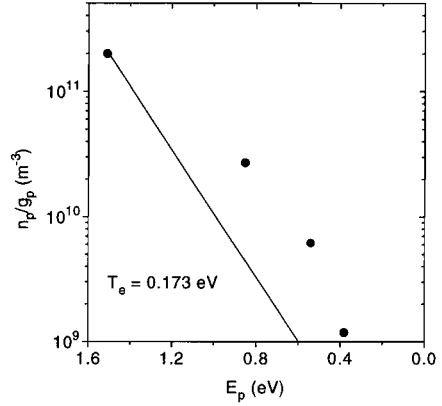


Figure 7: A Boltzmann plot for 2 vol.% hydrogen injection in the vessel. To indicate the possible Boltzmann equilibrium starting from level $p=3$, a line designating the (Thomson scattering) value of T_e has been drawn.

ulation of higher excited levels, as the latter are consequently above the Boltzmann line. Thus, some extra input at these higher levels (up to $p=5$) has to be made plausible. In the following, we shall show that this is indeed possible if the H_2 molecules that participate in reaction (1) carry considerable rovibrational excitation.

Thus we return to the question, whether a rovibrationally excited hydrogen molecule actually produces a rovibrationally excited ArH^+ ion. Following Gislason *et al* [18], a simple argument can be constructed. As the first reaction in Eq. (1) is a classic spectator stripping reaction, it can be thought to be instantaneous. The transferral of internal energy from $\text{H}_2(v,J)$ to $\text{ArH}^+(v',J')$ then depends on the amount of vibrational energy that is potential energy at the instant of reaction. This leads to the following estimate for the internal energy of the formed ArH^+ :

$$E_{int}(\text{ArH}^+) \approx \frac{1}{2}E + \frac{3}{4}E_{int}(\text{H}_2) - \Delta H_0^0, \quad (7)$$

where E represents the relative kinetic energy of the reactants, $E_{int}(X)$ is the internal energy of species X, and ΔH_0^0 is the reaction enthalpy (equal to -1.53 eV). It is assumed that half of the vibrational energy is kinetic at the instant of reaction.

If we represent Eq. (7) in a figure, Fig. 8 is obtained. It shows the relation between the internal energy of the H_2 molecule and the internal energy of the ArH^+ molecular ion. If a (wall-associated) H_2 molecule carries a large amount of rovibrational excitation, highly excited levels can be formed in the dissociative recombination of ArH^+ . This mechanism can explain the observed population of excited states.

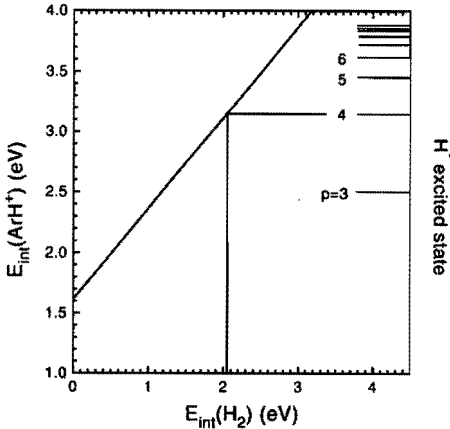


Figure 8: The relation between the internal energies (E_{int}) of H_2 and ArH^+ during the first reaction of Eq. (1). The H^* excited levels that can (energetically) be reached during subsequent dissociative recombination of ArH^+ are indicated. For example: to reach $p=4$, the H_2 molecule has to be rovibrationally excited by about 2 eV. The assumption is that half of the vibrational energy is kinetic at the instant of reaction.

IV. CONCLUSIONS

The investigation of the argon-hydrogen plasma jet by OES and Thomson scattering leads to the following conclusions:

When hydrogen is mixed to the flow before it enters the cascaded arc, the hydrogen emission in the expanding plasma can be explained by three particle recombination at the center of the plasma jet at $z=20$ mm. If there is any input from dissociative recombination, it must be at least an order of magnitude less important at the center. It may, however, be of importance at the plasma periphery. The importance of three particle recombination at the plasma center is confirmed by comparing the $p=3$ densities for the arc seeding and vessel injection cases: at a 2 vol.% seed fraction, the latter are lower by a factor of ten. Higher seed fractions cannot be easily compared, as the arc efficiency is going down for the arc seeding case. A possible extra input for higher seed fractions could be formed by dissociative recombination of H_2^+ ions.

The population factors b_p approach unity for low I_p , pointing to some kind of Saha-equilibrium close to the continuum (arc seeding case). The "bulge" in the hydrogen b_p 's does not occur for all seed fractions and depends critically on the determination of n_e and the Ar^+/H^+ ratio.

For the arc seeding case it is clear, that the arc ionization changes from Ar^+ to H^+ , as all argon emission disappears for higher seed fractions. The efficiency of the arc seems to decrease as well, as indicated by the H_α intensity behaviour for different seed fractions.

When hydrogen is injected in the vessel, only one possible excitation mechanism remains: dissociative recombination of rovibrationally excited ArH^+ , ending on $p=3$ or even higher.

A Boltzmann equilibrium from this level upwards cannot fully account for the population of the higher excited levels ($p=4-6$). An extra input therefore has to be assumed at these levels. This requires the ArH^+ to carry considerable rovibrational excitation. In a simple argument, this excitation could be produced by associative charge exchange with rovibrationally excited H_2 molecules, produced at the vessel walls.

ACKNOWLEDGMENT

The authors would like to thank H.M.M. de Jong and M.J.F. van de Sande for their skillful technical assistance and M.N.A. Beurskens for the Thomson scattering measurements. This work is supported by the Netherlands Technology Foundation (STW). The work of M.C.M. van de Sanden is supported by the Royal Netherlands Academy of Arts and Sciences (KNAW).

References

- [1] R.F.G. Meulenbroeks, D.C. Schram, L.J.M. Jaegers, and M.C.M. van de Sanden, *Phys. Rev. Lett.* **69** (9), 1379 (1992).
- [2] A.J.M. Buuron, G.J. Meeusen, J.J. Beulens, M.C.M. van de Sanden, and D.C. Schram, *J. Nucl. Mat.* **200**, 430 (1993).
- [3] A.T.M. Wilbers, G.J. Meeusen, M. Haverlag, G.M.W. Kroesen, and D.C. Schram, *Thin Solid Films* **204**, 59 (1991).
- [4] M.J. de Graaf, R. Severens, R.P. Dahiya, M.C.M. van de Sanden, and D.C. Schram, *Phys. Rev. E* **48**, 2098 (1993).
- [5] M.C.M. van de Sanden, J.M. de Regt, G.M. Janssen, J.A.M. van der Mullen, D.C. Schram, and B. van der Sijde, *Rev. Scient. Instrum.* **63**, 3369 (1992).
- [6] R.F.G. Meulenbroeks, P.A.A. van der Heyden, M.C.M. van de Sanden, and D.C. Schram, *J. Appl. Phys.* **75**, 2775 (1994).
- [7] R.F.G. Meulenbroeks, A.J. van Beek, A.J.G. van Helvoort, M.C.M. van de Sanden, and D.C. Schram, *Phys. Rev. E* **49** (5), 4397 (1994).
- [8] R.F.G. Meulenbroeks, R.A.H. Engeln, M.N.A. Beurskens, R.M.J. Paffen, M.C.M. van de Sanden, J.A.M. van der Mullen, and D.C. Schram, *Argon-hydrogen expanding plasma jet: model and experiments*, accepted for publication in *Plasma Sources Sci. Technol.* (1995).
- [9] E.A. Gislason and G. Parlant, *J. Chem. Phys.* **94**, 6598 (1991).
- [10] D.M. Hirst, M.F. Guest, and A.P. Rendell, *Mol. Phys.* **77**, 279 (1992).
- [11] W.L. Wiese, M.W. Smith, and B.M. Miles, *Atomic Transition Probabilities* National Bureau of Standards monograph NSRDS-NBS22, Washington D.C. (1969).

- [12] J.A.M. van der Mullen, *Phys. Rep.* **191**, 109 (1991).
- [13] H. Akatsuka and M. Suzuki, *Phys. Rev. E* **49**, 1534 (1994).
- [14] G.J. Meeusen, E.A. Ershov-Pavlov, R.F.G. Meulenbroeks, M.C.M. van de Sanden, and D.C. Schram, *J. Appl. Phys.* **71**, 4156 (1992).
- [15] M.C.M. van de Sanden, J.M. de Regt, and D.C. Schram, *Phys. Rev. E* **47**, 2792 (1993).
- [16] B. Jackson and M. Persson, *J. Chem. Phys.* **96**, 2378 (1992).
- [17] K.M. Ervin and P.B. Armentrout, *J. Chem. Phys.* **83**, 166 (1985).
- [18] Eric A. Gislason, private communication (1994), K. Dong, E.A. Gislason, and M. Sizun, *Chem. Phys.* **179**, 143 (1994).

Depolarization Rayleigh Scattering as a Means of Molecular Concentration Determination in Plasmas

R.F.G. Meulenbroeks D.C. Schram L.J.M. Jaegers
M.C.M. van de Sanden

*Dept. of Physics, Eindhoven University of Technology
P.O.Box 513, 5600 MB Eindhoven, The Netherlands*

Abstract. The difference in polarization for Rayleigh scattered radiation on spherically and non-spherically symmetric scattering objects has been used to obtain molecular species concentrations in plasmas of simple composition. Using a Rayleigh scattering diagnostic, the depolarized component of the scattered signal, proportional to the density of molecules in the plasma, was measured. This new method has been used to locally determine molecular species densities in pure nitrogen and pure hydrogen expanding plasmas. The results were used to obtain the dissociation degree of an expanding hydrogen plasma.

The fundamental study of hydrogen kinetics in plasmas is of vital importance for the realization of hydrogen negative ion (H^-) or hydrogen neutral (H^0) sources. The latter are important for surface studies and surface modification, whereas H^- sources are crucial links in neutral beam injectors for fusion plasmas. In the process of negative ion production (and destruction) in hydrogen plasmas, the H_2 molecular density, the hydrogen neutral density, as well as the shape of the electron energy distribution function are important parameters [1, 2, 3]. Furthermore, hydrogen plays a pertinent role in plasma deposition, as it is commonly added as an etching agent in order to improve the quality of the deposit. In order to understand the deposition mechanism, knowledge of the hydrogen kinetics is essential as well.

In the search for enhancement of particle source strength (and, thus, deposition rates), expanding thermal plasmas have proven to be successful [4, 5, 6]. In this method, a cascaded arc produces an atomized and partially ionized particle beam which expands into a low-pressure background. Expanding cascaded arc plasmas in hydrogen are used successfully as H^0 neutral sources and may be serve for volume production of H^- negative ions as well.

As the cascaded arc produces a hot (12 000 K), thermal plasma, it can be considered as producing only atoms and atomic ions, e.g. H and H^+ in the hydrogen case. In hydrogen, the study of the expansion out of the cascaded arc is severely hindered by anomalous recombination. This recombination, in which residual hydrogen molecules play a pertinent role, results in a low electron density and, consequently, little light emission. Also other expanding molecular plasmas (e.g., nitrogen) show this recombination, although to a lesser extent.

The mechanism responsible for this fast recombination in the first few centimeters of the expansion is charge exchange between atomic ions (H^+) and molecules (vibrationally excited H_2) and subsequent dissociative recombination of the formed molecular ion (H_2^+) [7]. The molecules necessary for this process are not produced in significant amounts by the arc and, thus, must be formed by association, most likely at the

steel vessel walls. Together with a strong recirculation flow in the vessel, this wall association process will provide a reentry flow of (vibrationally excited) hydrogen molecules into the expansion.

Because of the little light emission, traditional plasma diagnostics, such as optical emission spectroscopy, cannot be used on this type of plasmas. Furthermore, quantitative information on this anomalous recombination requires quantitative knowledge of the abundance of molecules in their electronic ground states, i.e. not readily observable by passive means. So, a *spatially resolved*, active molecular concentration measurement is essential for research on expanding hydrogen or nitrogen plasmas, and would be extremely useful in other kinds of plasma particle sources (and plasma etching and deposition research) as well.

A well-known active diagnostic such as Rayleigh scattering makes no distinction between atoms and molecules, except in polarization characteristics. The new method introduced here makes use of this fact to obtain molecular species densities in these relatively "dark" hydrogen and nitrogen plasmas.

Electromagnetic radiation can scatter off free electrons in a plasma in a process called Thomson scattering [8, 9]. For scattering off bound electrons, the elastic process is the well-known Rayleigh scattering ($\Delta h\nu = 0$ for the scattered radiation), whereas the inelastic version ($\Delta h\nu \neq 0$) is known as Raman scattering.

If polarized incident radiation is scattered off free electrons, the 90° scattered Thomson signal either remains polarized (if the polarization vector of the incident radiation is perpendicular to the plane through the incident wave vector and the line of sight to the observer) or is absent (if the polarization vector lies in this plane). This is a consequence of the specific scattering geometry (e.g. [10]).

In the case of Rayleigh scattering, the situation is somewhat more complicated. In a simple classical approach of scattering [11], one can show that the 90° Rayleigh scattered radiation is fully polarized only if the scattering objects are spherically symmetric, e.g., in the case of ground state atoms. In the case

of non-spherically symmetric molecules a small component of the scattered radiation is depolarized. According to this classical approach, the ratio of the depolarized (say, horizontal) and polarized (vertical) scattering components I_h/I_v for vertically plane polarized incident radiation and a medium of linear molecules is given by:

$$\rho \equiv \frac{I_h}{I_v} = \frac{3\gamma^2}{45\alpha^2 + 4\gamma^2}, \quad (1)$$

where $\alpha = \frac{1}{3} \times (\alpha_{\parallel} + 2\alpha_{\perp})$ is the average dipole polarizability (α_{\parallel} and α_{\perp} are the components of the polarizability tensor along the internuclear axis and perpendicular to it), and $\gamma = (\alpha_{\parallel} - \alpha_{\perp})$ is the polarizability anisotropy. The components of the polarizability tensor are all frequency dependent [12].

In the quantum mechanical treatment, Eq. (1) must be modified to include the effect of Raman scattering. The Raman peaks are very weak in intensity compared to the Rayleigh peak, but they are strongly depolarized. If only the central (Rayleigh) peak is considered, the depolarization ratio for this peak (ρ_{Rayl}) in the quantum mechanical treatment is 4 times smaller than the one calculated from Eq. (1) [12]. This, however, is an approximation, and it limits the accuracy of the method described here: this ρ_{Rayl} slightly depends on the rovibrational state of the scattering molecules. It can be shown, that the total averaged ρ_{Rayl} changes about 10% for a temperature change (and, hence, a rovibrational redistribution) from 300 K to 1400 K in the case of hydrogen. Theoretical values for the α 's [12, 13, 14] can be inserted to obtain the Rayleigh peak depolarization ratios for 532 nm radiation and a temperature of 300 K: $\rho_{Rayl,H_2} = 2.3 \times 10^{-3}$, $\rho_{Rayl,N_2} = 2.69 \times 10^{-3}$. In the following, we will consider only the Rayleigh peak depolarization.

In the case of Rayleigh scattering on a plasma, depolarization may also be due to the presence of excited atomic states. In the cases discussed here, however, we may totally neglect this influence, as the number of excited states is very small compared to the number of molecules and ground state atoms (typically smaller by a factor of $10^6 - 10^{10}$).

Figure 1 shows the expanding cascaded arc plasma: a wall stabilized, continuously operated cascaded arc produces a hot, thermal plasma (diam: 4 mm) at subatmospheric pressure ($\pm 0.6-0.2$ bar). This plasma is allowed to expand into a heavily pumped, low pressure (p_{back} around 1-1000 Pa) background through a conically shaped nozzle, creating a supersonically expanding plasma jet. This plasma source is described in detail elsewhere [4, 6].

The plasma conditions for the hydrogen measurements will be referred to as *condition 1*: $I_{arc} = 37$ A, $V_{arc} = 208$ V, H_2 flow = 3.0 SLM, $p_{back} = 715$ Pa. For the nitrogen case, *condition 2*: $I_{arc} = 45$ A, $V_{arc} = 160$ V, N_2 flow = 3.5 SLM, $p_{back} = 170$ Pa.

The combined Thomson-Rayleigh set up is sketched in figure 2 and consists of a high-power frequency-doubled Nd:YAG laser (wavelength 532 nm) with the beam imaged onto the plasma by a lens and two mirrors. The laser dump is placed far outside the vessel to reduce the stray light. The 90° scattered radiation is imaged onto a polychromator entrance slit. The signal passes an image intensifier and is sampled by a photo

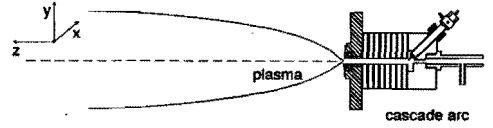


Figure 1: The expanding cascaded arc experiment. A thermal plasma at atmospheric pressure is created in a cascaded arc, consisting of three cathodes, a number of electrically isolated copper plates, and an anode plate. All these parts are water cooled. The plasma expands into a low pressure region, creating a supersonically expanding plasma jet.

diode array. The polarizer is placed in front of the polychromator entrance slit. The apparatus has been used very successfully in determining electron temperatures, electron densities, and neutral densities, locally and with high accuracy [8].

Measuring a plasma depolarization signal is cumbersome, since the signal is very weak. Three things must be carefully calibrated: (a) the stray light from the laser radiation; (b) the fact that the polarizer is non-ideal and will thus show a ("parasitic") signal even if it is perpendicular to the polarization of a plane polarized incident beam; and (c) the true depolarization signal for a known amount of gas in the vessel at room temperature.

(a) The vessel stray light is taken into account by measuring, without plasma, at a very low ($\ll 1$ Pa) pressure. This vessel stray light measurement is subtracted from the subsequent Rayleigh measurement. Actually, the stray light level is very low, and this makes possible the detection of the weak depolarization signal.

(b) The parasitic depolarization signal was measured by performing Rayleigh scattering measurements on pure argon gas in the vessel. Argon produces no depolarization by itself, so all "depolarization" measured is due to the polarizer itself. To be able to correct for this effect, the polarized and depolarized signals were measured for different argon pressures: the ratio $I_h/I_v \equiv \rho_{parasitic}$ turned out to be constant and equal to $(6.0 \pm 0.6) \times 10^{-4}$. Each depolarization measurement will therefore consist of a measurement of the vertical and horizontal signals. The amount of parasitic depolarization can then be calculated from the vertical signal and $\rho_{parasitic}$.

(c) The calibration was performed by measuring the polarized (sample time 240 s) and depolarized (sample time 1800 s) scattering components, for known amounts of hydrogen or nitrogen in the vessel at room temperature. For a pressure of 1300 Pa, hydrogen gave a "clean" depolarized signal of 1500 counts, whereas nitrogen gave 3134 counts. The errors in these numbers, resulting from Poisson noise and the subtraction of the parasitic depolarization signal, are around 15%. The measured values of the ρ 's, then, are: $\rho_{Rayl,H_2} = (2.2 \pm 0.3) \times 10^{-3}$, $\rho_{Rayl,N_2} = (2.7 \pm 0.3) \times 10^{-3}$, in good agreement with the theoretical values. At room temperature, the particle densities in the calibration are $3.1 \times 10^{23} m^{-3}$. This

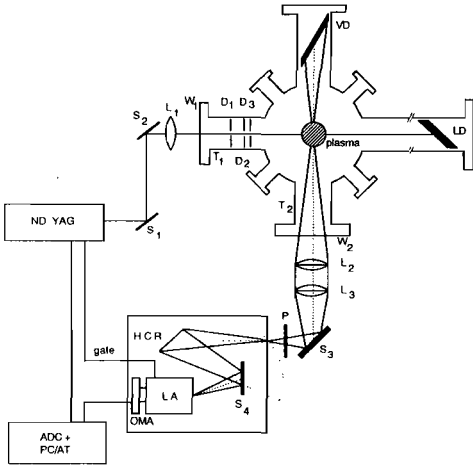


Figure 2: The Thomson-Rayleigh scattering set up. Frequency-doubled Nd:YAG radiation is focused into the plasma by a system of two dichroic mirrors (S_1 and S_2) and a lens (L_1). The stray light level is reduced by placing the laser dump (LD) far away (i.e., 2 meters), and by installing several diaphragms D_1 - D_3 . The scattered radiation is transmitted through an optical system consisting of lenses (L_2 and L_3) and a mirror (S_3). The dispersive element is a hollow concave grating (HCR), after which detection takes place by an image intensified optical multi channel analyzer (OMA). The gating of the light amplifier (LA) as well as the data processing is handled by a personal computer. The polarizer (P) is placed in front of the entrance slit of the polarychromator.

yields the calibration factors to obtain molecular densities in the plasma, provided the ρ_{Rayl} 's do not change too much due to the higher temperature in the plasma.

The measurements were carried out locally (detection volume $\approx 0.25\text{mm}^3$) at different distances from the expansion nozzle: at $z = 15$ mm for condition 1, and at $z = 20$ mm and $z = 150$ mm for condition 2. Due to the dissociation and the higher temperature in the plasma (and the resulting low molecular density at the same pressure), depolarization signals are weaker than in the calibration: (160 ± 50) counts for 1800 s measuring time for condition 1. With the calibration as described under (c), the hydrogen molecular density was calculated to be $(3 \pm 1) \times 10^{22}\text{m}^{-3}$. An additional result can be obtained if we assume pressure equilibrium at this position and calculate the total plasma density with the gas temperature equal to the rotational temperature, measured in a similar experiment [15]: $T_{rot} \approx 1400$ K. The total density is, then, equal to about $5.2 \times 10^{22}\text{m}^{-3}$, resulting in a $[H]/[H_2]$ concentration ratio for the plasma at this point of 0.7 ± 0.3 . This is an essential result, as a plasma of this type is used as a H^0

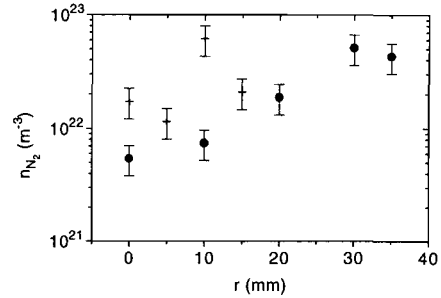


Figure 3: Results of molecular concentration measurements on an expanding nitrogen plasma jet. Radial scans (r : distance from the center of the plasma jet) were made for two axial positions: $z = 20$ mm (+), and $z = 150$ mm (•).

particle source.

The results for the nitrogen plasma (condition 2) are given in figure 3. In this case, a radial scan was performed at both $z = 20$ mm and $z = 150$ mm (axial and radial scans can be made easily in this experiment, by moving the plasma and keeping the diagnostics fixed). The number density of molecules clearly increases at the edges of the plasma.

We conclude:

The difference in polarization characteristics of Rayleigh scattering on atoms and molecules can be used to determine the concentration of the molecules in plasmas (or gases) containing only one depolarizing molecular component, such as the plasmas mentioned, where molecules other than H_2 and N_2 are not present in significant amounts.

Every high quality Thomson-Rayleigh diagnostic with an effective stray light reduction can be adapted for this kind of measurement by simple insertion of a polarizer and proper calibration.

The accuracy of the method is limited by the fact, that the temperature influence on ρ_{Rayl} is neglected, and by the weakness of the effect, which even with long sampling times results in noisy signals. The detection limit is around 10^{21}m^{-3} . Eventually, turning the polarization vector of the incident laser radiation by 90° to make it lie in the plane of incident radiation and line of sight will reduce the noise level because in this case only the depolarized radiation is observed.

The measurements clearly indicate, that, in the hydrogen case, the density of molecules close to the expansion nozzle is unexpectedly high. This fact can only be explained in terms of wall association in combination with a recirculation flow, as was indicated above. In the case of nitrogen, a similar process may occur, as the number density of molecules increases to the edges of the plasma. In both cases, this information is essential to understand the fast ionization loss in the expansion.

This new application of a widely known phenomenon, de-

polarization of Rayleigh scattered radiation, can give spatially resolved information about the density of ground state molecules, information which is difficult to obtain by other means. This knowledge can be essential for research on particle sources and plasma etching or deposition.

We would like to thank A.J.G. van Helvoort, M.J.F. van de Sande, A.B.M. Hüsken, and H.M.M. de Jong for their help and skillful technical assistance during the measurements.

References

- [1] M. Bacal and G.W. Hamilton, *Phys. Rev. Lett.* **42** (23), 1538 (1979).
- [2] J.R. Hiskes and A.M. Karo, *J. Appl. Phys.* **56**, 1927 (1984).
- [3] M.B. Hopkins and K.N. Mellon, *Phys. Rev. Lett.* **67** (4), 449 (1991).
- [4] P.K. Bachmann, J.J. Beulens, G.M.W. Kroesen, H. Lydtin, D.C. Schram, and D.U. Wiechert, *Surf. Mod. Techn.* **III**, 69 (1989).
- [5] J.J. Beulens, A.J.M. Buuron, L.A. Bisschops, A.B.M. Hüsken, G.M.W. Kroesen, G.J. Meeusen, C.J. Timmermans, A.T.M. Wilbers, and D.C. Schram, *J. Phys. (Paris) Colloq.* **51**, C5-361 (1990).
- [6] A.T.M. Wilbers, G.J. Meeusen, M. Haverlag, G.M.W. Kroesen, and D.C. Schram, *Thin Solid Films* **204**, 59 (1991).
- [7] M.J. de Graaf, R.P. Dahiya, F.J. de Hoog, M.J.F. van de Sande, and D.C. Schram, *J. Phys. (Paris) Colloq.* **51**, C5-387 (1990).
- [8] M.C.M. van de Sanden, J.M. de Regt, G.M. Janssen, J.A.M. van der Mullen, B. van der Sijde, and D.C. Schram, accepted for publication in *Rev. Scient. Instrum.* (1992).
- [9] J. Sheffield, *Plasma Scattering of Electromagnetic Radiation* Academic Press, New York (1975).
- [10] E. Hecht and A. Zajac, *Optics*, Addison-Wesley Massachusetts (1974).
- [11] R.L. Rowell and G.M. Aval, and J.J. Barrett, *J. Chem. Phys.* **54** (5), 1960 (1971).
- [12] A.L.Ford and J.C. Browne, *Phys. Rev. A* **7** (2), 418 (1973).
- [13] J. Rychlewski, *Mol. Phys.* **41** (4), 833 (1980).
- [14] U. Hohm and K. Kerl, *Mol. Phys.* **69** (5), 803 (1990).
- [15] M.J. de Graaf, D.K. Otorbaev, M.C.M. van de Sanden, and D.C. Schram, *to be published* (1992).

CARS on Expanding Thermal Arc Plasmas

R.F.G. Meulenbroeks

R.A.H. Engeln

J.A.M. van der Mullen

D.C. Schram

Eindhoven University of Technology, Department of Physics,

P.O. Box 513, 5600 MB Eindhoven, The Netherlands

Abstract. The expanding plasma emanating from a thermal arc plasma source that can be used for deposition of thin films is studied using laser spectroscopic techniques. The argon-hydrogen plasma is characterized by very fast recombination, that cannot be explained by atomic processes. To explore this phenomenon, that has been related to wall-association of hydrogen atoms and recirculation, CARS (coherent anti-Stokes Raman scattering) is performed on (argon-)hydrogen plasmas. The periphery of the plasma appears to be rich in hydrogen molecules, in accordance with the recirculation model. No highly rovibrationally excited states are detected in the periphery, in spite of the spectrometer's very good sensitivity (0.1 Pa H₂ at 300 K). For the plasma, rotational and vibrational temperatures as well as absolute H₂ densities are measured. A simple model for the observed (non-Boltzmann) rotational populations is developed.

I. INTRODUCTION

Expanding thermal arc plasmas are used in a variety of applications, which include the deposition of diamond, diamond-like carbon, amorphous hydrogenated carbon, and amorphous hydrogenated silicon thin films [1]. When the thermal arc is operated either on pure hydrogen or on an argon-hydrogen mixture, it can be used as a particle source for hydrogen radicals or hydrogen positive and negative ions [2, 3]. Fundamental research on expanding plasmas focuses on the study of argon-hydrogen mixtures. The principle parameters that have to be determined are particle densities (electrons, neutrals and ions) and temperatures. To this end, active and passive spectroscopic techniques are employed. The results are interpreted by comparison with numerical models.

In this paper we will summarize some of the properties of the argon-hydrogen expanding thermal arc plasma and describe in more detail the measurement of rovibrationally excited H₂ molecules by CARS spectroscopy in and around the expanding plasma jet.

II. EXPERIMENT AND DIAGNOSTICS

The expanding thermal arc plasma has been described elsewhere [4, 5] and we will only give a brief description here. A subatmospheric (0.2-0.6 bar) plasma from a thermal arc (at high electron density) expands into a vacuum vessel, creating a plasma jet. The expansion direction defines the z -axis, with the origin at the expansion nozzle. Hydrogen can be added to the argon plasma in two ways: either by burning the arc on an argon-hydrogen mixture ("arc injection"), or by burning the arc on pure argon, and flushing hydrogen directly into the vessel ("vessel injection"). Basic plasma conditions are: arc current $I_{arc} = 45$ A, arc voltage $V_{arc} = 50-100$ V, total flow = 3.5 SLM (standard liters per minute), and background pressure $p_{back} = 40-133$ Pa. The thermal arc is moveable within a vacuum vessel without significantly changing the plasma. This greatly facilitates the axial and radial scanning of the plasma

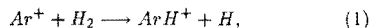
without moving the diagnostics.

Three diagnostics are applied to the plasma jet:

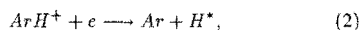
- *Optical Emission Spectroscopy (OES).* Passive spectroscopy in order to determine the excited level populations of hydrogen and argon. The set up is a fairly standard, calibrated, mirror-scanning system, described in detail in [5].
- *Thomson-Rayleigh scattering.* A frequency doubled Nd:YAG laser is used for this diagnostic. Photons are scattered off free and bound electrons in the plasma and detection of the scattered (Doppler-shifted) radiation gives direct, local, and accurate information about electron and neutral densities and electron temperatures. The diagnostic has been described elsewhere [4], a few important results will be discussed below.
- *Coherent Anti-Stokes Raman Scattering (CARS)* In order to detect rovibrationally excited H₂, a CARS diagnostic has been realized; it will be described below.

In order to get an impression of the processes that are important in the expanding jet it is appropriate to discuss some of the basic properties (cf. [5, 6, 7]). The main characteristic of the argon-hydrogen jet is its anomalously fast recombination - as compared to the purely atomic argon case. As can be seen in Fig. 1, the electron density decreases by an order of magnitude, even for tiny admixtures of H₂.

This enormous ionization loss has been attributed to a combination of wall-association and recirculation inside the vacuum vessel. In this process, hydrogen atoms associate to molecules at the vessel walls and are transported towards the plasma beam again by recirculation. For low hydrogen seed fractions, where the dominant ion is argon, the following reactions can occur:



followed by:



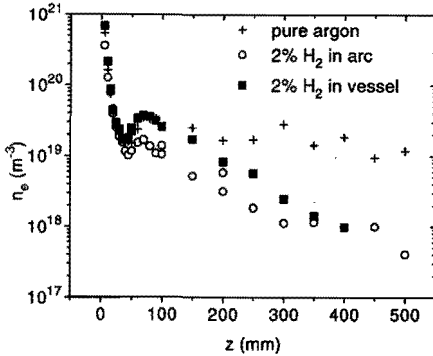


Figure 1: Electron density vs. axial position (z) profiles of different expanding jets: pure argon, arc injection, and vessel injection.

during which excited H atoms are formed. In the case of "arc injection", the H_2 molecules necessary for these reactions do not all originate from the arc (where a high degree of dissociation is assumed) but from the stainless steel vessel walls. A quasi one-dimensional model [7] solving mass, momentum, and energy balances for the plasma particles confirms the existence of an external H_2 input into the jet. The model predicts that this reentry flow penetrates the plasma around the shock position (i.e., around $z=40-70$ mm in Fig. 1).

Absolute emission spectroscopy on the argon and hydrogen atomic systems shows that all the argon emission disappears for seed fractions above 7 vol.%. As argon emission is due only to three particle recombination (low T_e , around 0.2 eV), this means that the arc does not produce any argon ions for these seed fractions. The dominant ion therefore probably is H^+ for seed fractions above 7 vol.% [3, 5, 7].

Fig. 1 actually represents the close investigation of the recirculation effect by a set of Thomson scattering experiments: a comparison is made between a pure argon jet, a 2% hydrogen-in-argon jet and a pure argon jet with 2 vol.% hydrogen flushed directly into the vacuum vessel. The pure argon and "vessel injection" cases can be seen to clearly coincide up to $z=100$, i.e., the deviation starts after the shock region. The hydrogen-argon "arc injection" case shows a similar behaviour, but has lower densities right from the start. The decrease after $z=100$ is remarkably similar for the "arc injection" and "vessel injection" cases. Eventually, a calculation shows that equal amounts of hydrogen are needed to explain the ionization loss after $z=100$. The ionization loss after the shock is thus thought to be totally determined by the background gas and the molecules present there.

In order to scrutinize this phenomenon of very fast recombination through a molecular channel, a CARS diagnostic has been realized for the state-selective detection of hydrogen molecules.

III. CARS SPECTROSCOPY

A. Theory

The CARS process and signal generation has been described in a number of articles (e.g., [8]-[11]) and we shall only give a brief account here. CARS is a coherent analog of Raman scattering with the advantage, that the signal is created as a coherent beam, thus greatly enhancing the sensitivity. This is the main reason why CARS was chosen as a diagnostic for our low pressure hydrogen-containing plasma. CARS has been chosen in stead of other methods, such as Resonance Enhanced Multi Photon Ionization (REMPI) or VUV absorption, because its relatively easy *in situ* applicability in our case.

The CARS signal (at frequency $\omega_3 = 2\omega_1 - \omega_2$) is generated through the third order non-linear susceptibility $\chi^{(3)}$ of the probed molecule. The anti-Stokes power (P_3) depends on the power of the pump (P_1 at ω_1) and Stokes (P_2 at ω_2) lasers as follows:

$$P_3 = K |\chi^{(3)}|^2 P_1^2 P_2, \quad (3)$$

where K is a proportionality constant. The $\chi^{(3)}$ consists of a resonant and a non-resonant part: $\chi^{(3)} = \chi_{NR}^{(3)} + \chi_{res}^{(3)}$. The resonant part is greatly enhanced when a Raman resonance is probed, i.e., when $\omega_1 - \omega_2 = \omega_{v,J}$, where $\omega_{v,J}$ is the frequency of a particular Raman transition. The resonant third-order susceptibility $\chi_{res}^{(3)}$ associated with a certain isolated Q branch transition can be written as:

$$\chi_{res}^{(3)} = K' N [\rho_{v,J} - \rho_{v+1,J}] (v+1) \frac{d\sigma}{d\Omega} h(\omega_1 - \omega_2). \quad (4)$$

In this last equation, K' is a proportionality constant, N is the total number of molecules, ρ stands for the probability of occupation of a certain rovibrational state, $\frac{d\sigma}{d\Omega}$ is the (0-1) spontaneous Raman scattering cross section, and $(v+1)$ reflects the growth of this cross section with increasing vibrational quantum number. The form function $h(\omega_1 - \omega_2)$ reflects the line shape. In our Doppler-limited regime, this function can be written as [12]:

$$h(\omega_1 - \omega_2) = \frac{1}{u\sqrt{\pi}} \times \int_{-\infty}^{+\infty} \frac{e^{-(v/u)^2}}{\omega_{v,J} - \omega_1 + \omega_2 - i\gamma_{v,J} + (\omega_1 - \omega_2)v/c} dv, \quad (5)$$

where $\omega_{v,J}$ is the frequency of the transition considered and $\gamma_{v,J}$ its width at half maximum (FWHM), u is the root mean square velocity, $u = \sqrt{2kT/m}$, v is the molecule's velocity, and c is the speed of light. In practice $\gamma_{v,J} = 0$ can be taken in our case, where pressures are well below 500 Pa. In this case the line width and shape is determined by the Doppler effect (0.09-0.15 cm^{-1} FWHM, at temperatures ranging from 500-2000 K). The dye linewidth is around 0.07 cm^{-1} , the pump laser can be considered monochromatic (0.005 cm^{-1}). In our case of well-separated lines (because of the large molecular constants of H_2), we do not have to worry about interfering lines: as the surface of a line can be very well determined, the spectral line shape does not have to be considered. Doppler

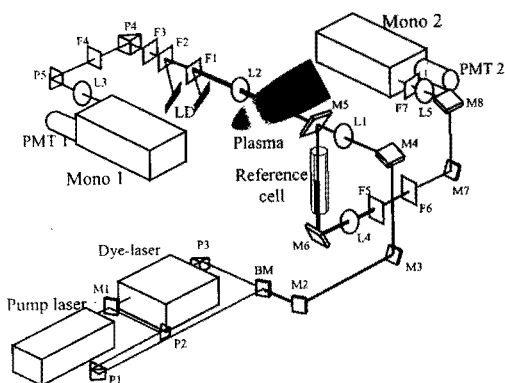


Figure 2: The CARS spectrometer. Nd:YAG frequency doubled radiation is used for the pump beams and to pump the dye laser arrangement: a dichroic beam combiner (BM) is used to make the red beam coincide with one of the green beams. A system of mirrors (M_2 - M_8) takes the beams up to the experiment. M_5 is a flat quartz plate used to split off 10% of the laser energy, which is led through the reference cell. P_1 - P_5 are suprasil prisms, L_1 - L_5 are suprasil lenses. (L_1 , L_2 , and L_4 : $f=1$ m). The CARS signal is filtered from the green beam by a set of filters (F_1 - F_3 and F_5 - F_6). F_4 represents an eventual neutral density filter. LD designate laser dumps, PMT designates a photomultiplier tube.

broadening, however, does have an effect as it decreases the peak height of a line, which impedes the measurement of very faint lines.

With an appropriate calibration on hydrogen gas, absolute values of $N[\rho_{v,J} - \rho_{v+1,J}]$ can be obtained using the above description. If a number of transitions is monitored, absolute values of the population densities of individual rovibrational states can thus be calculated. We shall return to this later when we describe the measurements procedure.

B. The CARS spectrometer

The experiment is depicted in Figs. 2 and 3. An injection seeded Nd:YAG laser (Quanta Ray GCR230, 300mJ/pulse @ 532 nm, 50 Hz, single longitudinal mode) is used for the ω_1 beam (bandwidth 0.005 cm^{-1}); it also pumps a Quanta Ray PDL3 dye laser (bandwidth around 0.07 cm^{-1}). The dye liquid is a mixture of DCM and LDS698 (Exciton) solved in methyl alcohol in a mass ratio of 3:1; it delivers conversion in the region of 660-700 nm.

Eventually, the used laser output powers are around 10-20 mJ/pulse for the green and around 0.5 mJ for the red. The ω_1 and ω_2 beams are in a crossed beam arrangement (BOX-CARS), and the detection volume has dimensions of about 20x0.18 mm. A small part (10%) of the beams is split off after the CARS lens ($f=1$ m) by a ($\lambda/20$) flat quartz plate and led through a reference cell (1 m length) containing 7 bars of

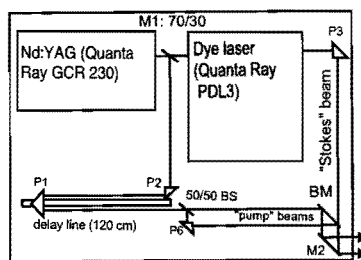


Figure 3: The CARS laser table. The Quanta Ray lasers are positioned on a Plato optical table, supported by concrete blocks. This figure shows in some detail the delay line (to correct for the delay in the dye laser), the BOX-CARS beam splitter (P_6), and the beam combiner (BM) which aligns the red and green beams.

argon. The non-resonant CARS signal created here is used as a reference to cancel out shot-to-shot variations in beam overlap and laser power, as well as variations in the dye laser output at different wavelengths. Extreme care has been taken to make the reference and main branches as identical as possible, especially up to the position of CARS signal generation. The correct pressure dependence (intensity proportional to the square of the pressure) has been verified in the reference cell and vacuum vessel.

After collimation by a second lens the blue anti-Stokes signals are separated from the green pump beam by filtering. Both main and reference CARS signals are guided through identical 1 m Czerny-Turner monochromators (Hilger-Engis Monospek 1000) for separation of signal from residual green light. This filtering is very effective: no signal is obtained if either the green or the red beam is dumped before the CARS lens (L_1). Signals are detected using fast photomultiplier tubes (Hamamatsu R1355, cooled to -25°C), using a tapered bleeder resistor network in order to insure good pulse linearity. When the CARS signal is very strong (e.g. in the case of a $v=0$, $J=1$ line), a set of calibrated neutral density (ND) filters is used to attenuate the signal. A fast, multi-channel, gated ADC (LeCroy 2249A) simultaneously integrates the main and reference PM tube outputs during a 150 ns time interval, gated by the Q-switch synchronization signal generated by the Nd:YAG laser unit.

The stepping of the dye laser and the monochromators, as well as the processing and storage of the ADC outputs is controlled by a 486 PC. A measurement is performed by scanning the dye laser in steps of 0.015 cm^{-1} over the different H_2 Q branch resonances, taking 50 or 100 measurements at each point. Both monochromators are set to the correct position for detection of the generated anti-Stokes signal. The main signal is immediately (pulse-by-pulse) divided by the reference signal and stored for further processing. The program automatically skips the intervals between Raman resonances, since these are relatively far apart in hydrogen.

For a better grasp of what is passing inside the vacuum vessel (which is not easily accessible in our case), a CCD camera

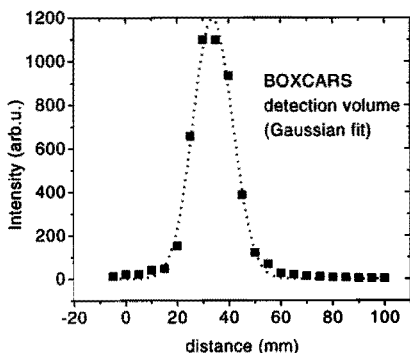


Figure 4: A measurement of spatial resolution in the reference branch by probing the non-resonant CARS signal generated in a 2 mm thick quartz plate at different positions.

system is installed on which an attenuated second reflection (after lens L_1) of pump and dye lasers is focused. With appropriate filtering a black-and-white picture can be obtained that is representative of the situation in the main CARS generation volume, showing the beam overlap. This greatly facilitates the alignment of the set up and makes possible a check of the alignment while measuring.

C. Tests and measurement procedures

Before turning to measurements, the spectrometer has been carefully tested and calibrated, focusing on aspects such as linearity (of the detection system, especially the PM tubes and the ADC), spatial resolution, saturation effects, and detection limits.

The linearity of the detection system is checked using calibrated ND filters and proves to be excellent (within a few %).

Spatial resolution is measured in the reference branch. After removal of the argon cell a 2 mm quartz plate on a mounting is placed in the focal point of the laser beams. The signal now detected in the reference branch is due mainly to non-resonant CARS generated in the quartz. By moving the thin quartz plate through the detection volume, a measurement of the detection volume is basically performed. The result is shown in Fig. 4. With a beam separation of 35 mm at the CARS lens (leading to an angle between the BOXCARS beams of 1°), a spatial resolution of approximately 20-30 mm is achieved in the longitudinal direction.

In the plane perpendicular to the laser beams the resolution is determined by the waist of the focus, around $180 \mu\text{m}$.

The phenomenon of saturation in CARS is particularly important as it limits the laser powers that can be applied without significantly changing the population distribution in the plasma. This phenomenon has been studied extensively by Péalat *et al* [13]. The process that causes redistribution among the probed states is stimulated Raman scattering (SRS, [8]). To estimate the importance of this effect one has to measure the power dependence of the signal strength in order to check

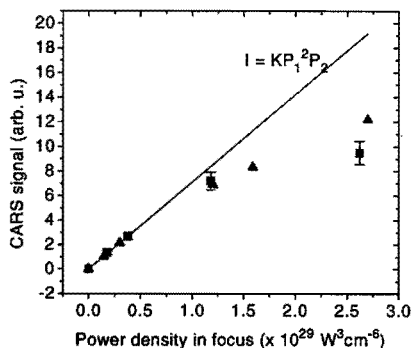


Figure 5: Power dependence measurement of the $\nu=0$, $J=1$ Q line. The triangles represent a model fit, where scaling has been performed by adjusting the focal waist diameter. The ideal behaviour ($I = KP_1^2 P_2$) is observed for low powers.

the validity of Eq. (3). This has been done using beam splitters in the first part of the green beam (i.e., just after the 70/30 beam splitter in Fig. 3). Measuring the power dependence is very cumbersome, as the removal of a beam splitter makes a realignment necessary. Nevertheless, the results are reproducible and Fig. 5 shows the surface of the measured $\nu=0$, $J=1$ peak (designating the transition by the lower level) vs. $P_1^2 P_2$. Although we are able to measure only a few points, the saturation behaviour is very clear for the higher laser powers.

Using a computer code by M. Péalat *et al.* at ONERA a simulation has been performed for the saturation behaviour. The procedure is completely analogous to the one described for N_2 in [13] and will not be fully discussed here. Using molecular data for H_2 and dye and pump powers in the vessel, a fit could be made to the points in Fig. 5 (i.e., for $\nu=0$, $J=1$), assuming a nine-mode dye laser ($\approx 0.07 \text{ cm}^{-1}$). Of course, the actual power density in the vessel is not known, because the actual beam waist can only be accurately calculated for the case of a perfect Gaussian laser beam. In the present case this is not possible, as the PDL3 dye laser delivers no Gaussian profile, whereas the injection seeded Nd:YAG laser has a reasonably Gaussian profile (>90% far field). The procedure therefore relies on adjusting the laser power densities, varying the value of the beam waist, to fit the model calculations to the experimental values. With a (reasonable) beam waist of around $180 \mu\text{m}$ a good fit has been obtained, shown in Fig. 5. In principle, this makes possible the correction of saturated data (as the dependence of the saturation on the ν quantum number is known [13]), but in practice we prefer to stay in the unsaturated region with pump and dye powers. However, some uncertainty is always present as it is very difficult to check on saturation behaviour of higher excited levels. We shall neglect the effects of saturation in the following.

In order to test the response of the entire system, so-called "argon-argon" measurements are performed before and after each measurement session. Here, the vessel is filled with 60 mbars of argon and a measurement of the non-resonant CARS

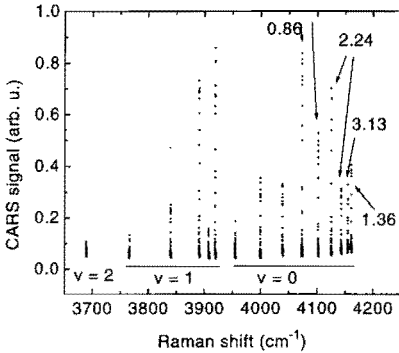


Figure 6: A typical measured CARS spectrum in a full H_2 plasma. ($z=150\text{mm}$). The values nd of the attenuating ND filters are indicated (the attenuation equals 10^{nd}).

signal on argon performed scanning the entire H_2 ($v=0$ - $v=4$) range, i.e., Raman shifts in the range 4162 - 3000 cm^{-1} . Since reference and main branches should show the same behaviour now, their ratio should remain constant - all uncertainties concerning beam overlap, dye laser output etc. should be symmetrical. This has been checked to be the case within 10% for every measurement.

A calibration has to be performed in order to obtain absolute values for the densities. Room temperature H_2 at a pressure of 70 Pa in the vessel is used for calibration: four levels are used, even though one would in principle suffice. Calibrations are also performed before and after each measurement session.

IV. CARS RESULTS

A. Measurement and processing

A typical measurement is shown in Fig. 6. It shows the distinct Raman resonances for $v=0$, $v=1$, and $v=2$ levels. In full H_2 , measurements could be taken up to $v=2$, $J=5$. The values of the attenuating ND filters are indicated.

Processing takes place by determining the surface of each line and correlating these surfaces to those in the H_2 calibration, using Eqns. (3) and (4). Corrections are made for the (v, J) dependence of the Raman cross section using data from Long [15] and others [16, 17]. In H_2 , we can use the isolated line approximation. In this manner, absolute density differences are obtained that have to be converted to densities using certain assumptions. In our case, we assumed the density of the level above the one that can just be measured to be negligible, so we assume for $v=2$ levels: $n(v=2, J) - n(v=3, J) \approx n(v=2, J)$. The error is probably not larger than a few percent under our conditions. For lower levels we follow Eqn. (4):

$$n(v=i, J) = n_{\text{measured}}(v=i, J) + n(v=i+1, J). \quad (6)$$

In the end, absolute densities can be obtained with a total accuracy of 10%. The detection limit of the system is around

$0.1\text{ Pa } H_2$ (300 K); during the measurements, densities per statistical weight as low as $2 \cdot 10^{17}\text{ m}^{-3}$ have been measured for $v=2$. Boltzmann plots of these measurements will be shown later on.

B. Results for argon-hydrogen mixtures

The first aim of the CARS measurements is to scrutinize the phenomenon of very fast recombination. Therefore CARS has been performed on 10 and 50 vol. % H_2 in Ar mixtures (vessel and arc injection, $I_{\text{arc}}=55\text{ A}$, total flow 3.5 SLM , background pressure 133 Pa). In all cases the view is confirmed that the background gas contains lots of relatively cold ($T_{\text{rot}}=400\text{ K}$, $T_{\text{vib}}=1100\text{ K}$) hydrogen molecules. In fact, the relative partial hydrogen pressure in the periphery of the plasma appears to be equal to the seed fraction: a x vol. % seed fraction results in a partial hydrogen pressure that is equal to x % of the total background pressure. This holds for both vessel and arc injection. No highly excited vibrational states were detected in the periphery of the plasma, within the detection limits. Other H_2 in Ar measurements are presented in detail in a separate paper [18].

Figures 7 and 8 give the results for the 50 vol.% H_2 in argon plasma. In these plots, the rotational temperatures are taken to be the temperatures in the $v=1$ state, as the $v=0$ population suffers from some contributions by the cold background gas. This is the case only for a 133 Pa background pressure, as the beam diameter in this case is of the same order as the spatial resolution along the laser beams (i.e., a few cm). Therefore, the radial dependencies should only be viewed upon as an indication. For the same reason, the vibrational temperatures are calculated using the $J=5$ levels of $v=0$ and $v=1$ (we can only measure these vibrational states in this plasma), as comparing the $J=1$ levels (for example) would lead to an underestimation of T_{vib} . This is caused by the relatively large amount of $(v=0, J=1)$ states in the cold background which are in the detection volume. The densities are taken to be the sum of all measured states, making appropriate corrections for states that can not be measured. The poor spatial resolution makes the construction of a pressure plot is not very useful: the measured density includes both hot and cold parts, but if the temperature of the hot part (i.e., the $v=1$ data) is assigned to the total density, the calculated pressures in the plasma jet would be too high.

However, the partial pressure in the periphery (where there are no special demands on spatial resolution) appears to be equal to 50% of the background pressure (i.e., $69\text{ Pa} \pm 10\%$), which is equal to the seed fraction of H_2 in Ar. Note, that this is not a trivial result as the arc plasma is characterized by a high dissociation degree.

In the following, the background pressures are lower ($\leq 40\text{ Pa}$), and in these cases the spatial resolution along the laser beams appears to be adequate, at least for distances from the nozzle larger than 20 mm or so.

C: Results for pure hydrogen plasmas

CARS measurements have also been performed on plasmas in pure hydrogen, both with and without a magnetic field to confine the plasma. The plasma conditions are: no magnetic

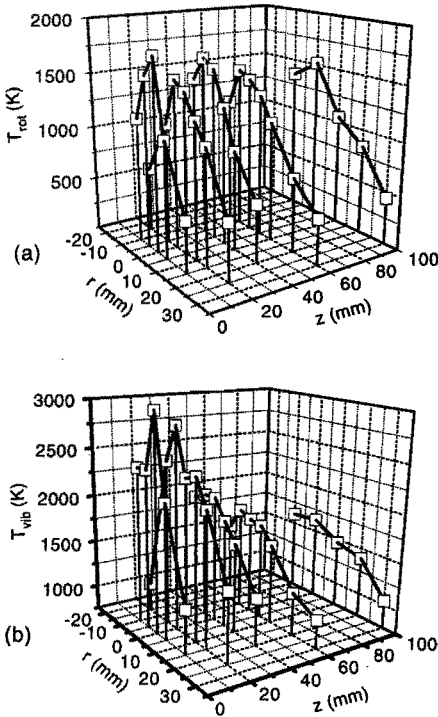


Figure 7: CARS measurements on a 50 vol.% H_2 in Ar plasma (arc injection). (a): rotational temperatures in the $v=1$ state; (b) vibrational temperatures calculated using the $J=5$ states.

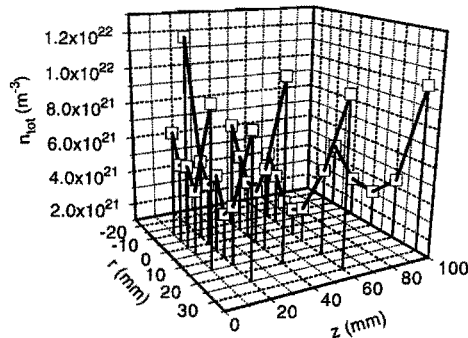
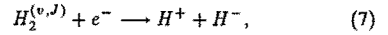


Figure 8: CARS density measurements on a 50% H_2 in Ar plasma.

field: $I_{arc} = 37.5$ A, flow: 3.5 SLM, $p_{back} = 40$ Pa; with magnetic field: $I_{arc} = 37.5$ A, flow: 2 SLM, $p_{back} = 20$ Pa, B -field: 1 kG. The B -field can be considered homogeneous over the entire length of the plasma. In the latter case the electrons are magnetized, whereas the ions are not. The magnetized plasma has been studied in view of the possible high density of negative ions there [19]. As negative ions may be formed by the well-known dissociative attachment reaction:



where highly excited H_2 is necessary [21] to make the reaction efficient, studying the $H_2^{(v,J)}$ population is essential.

The results are shown in Fig. 9 for the non-magnetized plasma, and in Fig. 10 for the magnetized case. Shown are typical Boltzmann plots for the $v=0$ to $v=2$ states, and axial dependencies for the major parameters, T_{rot} , T_{vib} , p and n_{tot} . T_{rot} has been taken from the $v=1$ data. The rotational temperatures are equal for $v=0$, $v=1$, and $v=2$, as can be seen from the Boltzmann plot in Fig. 9 (b), at $z = 150$ mm. T_{vib} has been calculated using the $J=3$ or (whenever possible) the $J=5$ states.

It may be useful to ponder a little on the spatial resolution and the reasons we have to believe that it is sufficient in these lower pressure cases (i.e., the reason why we can believe the $v=0$ rotational distributions to be virtually undisturbed by the periphery gas). In the argon-hydrogen measurements under (B), the $v=0$, $J=0-3$ levels always show a rotational temperature that is unrealistically low: around 400 K, in clear disagreement with T_{rot} in $v=1$ (Fig. 7). The T_{rot} of 400 K corresponds to the temperature measured in the peripheral gas. So in this case, the spatial resolution along the laser beams is inadequate: some cold background gas is measured along with the hot plasma. In the lower pressure case, however, the $v=0$, $J=0-5$ T_{rot} 's are in good agreement with the $v=1$ and $v=2$ data, at least for downstream distances larger than 20 mm. Therefore, we assume the rotational distributions in Figs. 9 and 10 to be "real", and that they contain no artefacts.

Considering Figs. 9 and 10, it is worth noting that, even per statistical weight, the population in a high rotational level of $v=0$ can be as large as the population in a lower rotational level in $v=1$ at the same (total) energy. With this advantage of a larger statistical weight, more energy can be carried by rotations than by vibrations in our plasma. This is an important observation. It distinguishes these expanding plasmas from many other plasma sources, where the rotational temperature is usually very low compared to the vibrational temperature (e.g., [12]). In the latter cases, research therefore often focuses on the *em* vibrational population distribution. The measurements in this section can serve as an example for a situation where the rotational population is very important. In this respect our situation is somewhat similar to that encountered in combustion research [20].

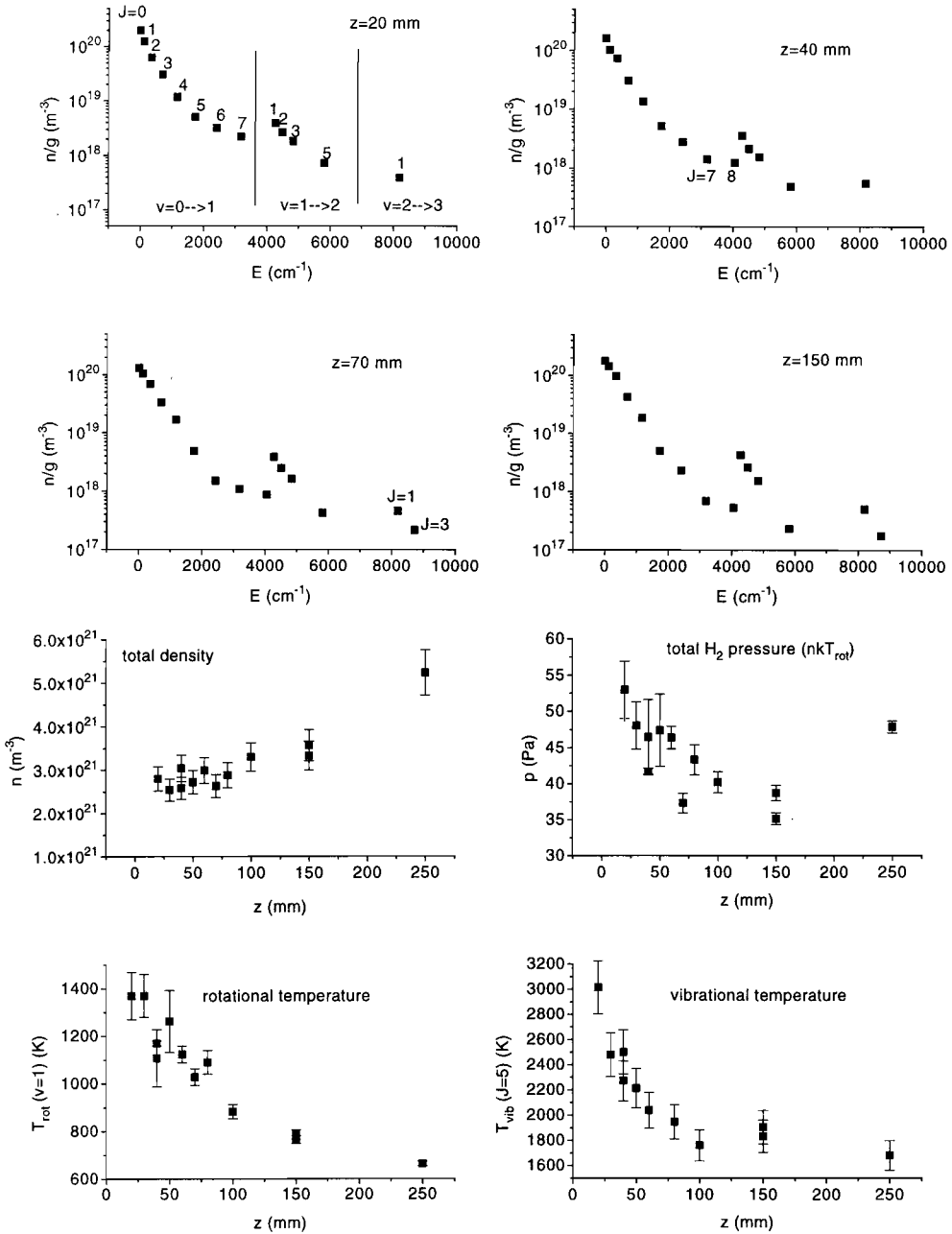


Figure 9: CARS results for a full hydrogen plasma: Boltzmann plots for different axial positions, and axial dependencies of T_{rot} , T_{vib} , pressure p , and total density n . The axial position is denoted by z , E is the energy, and n/g represents the density per statistical weight.

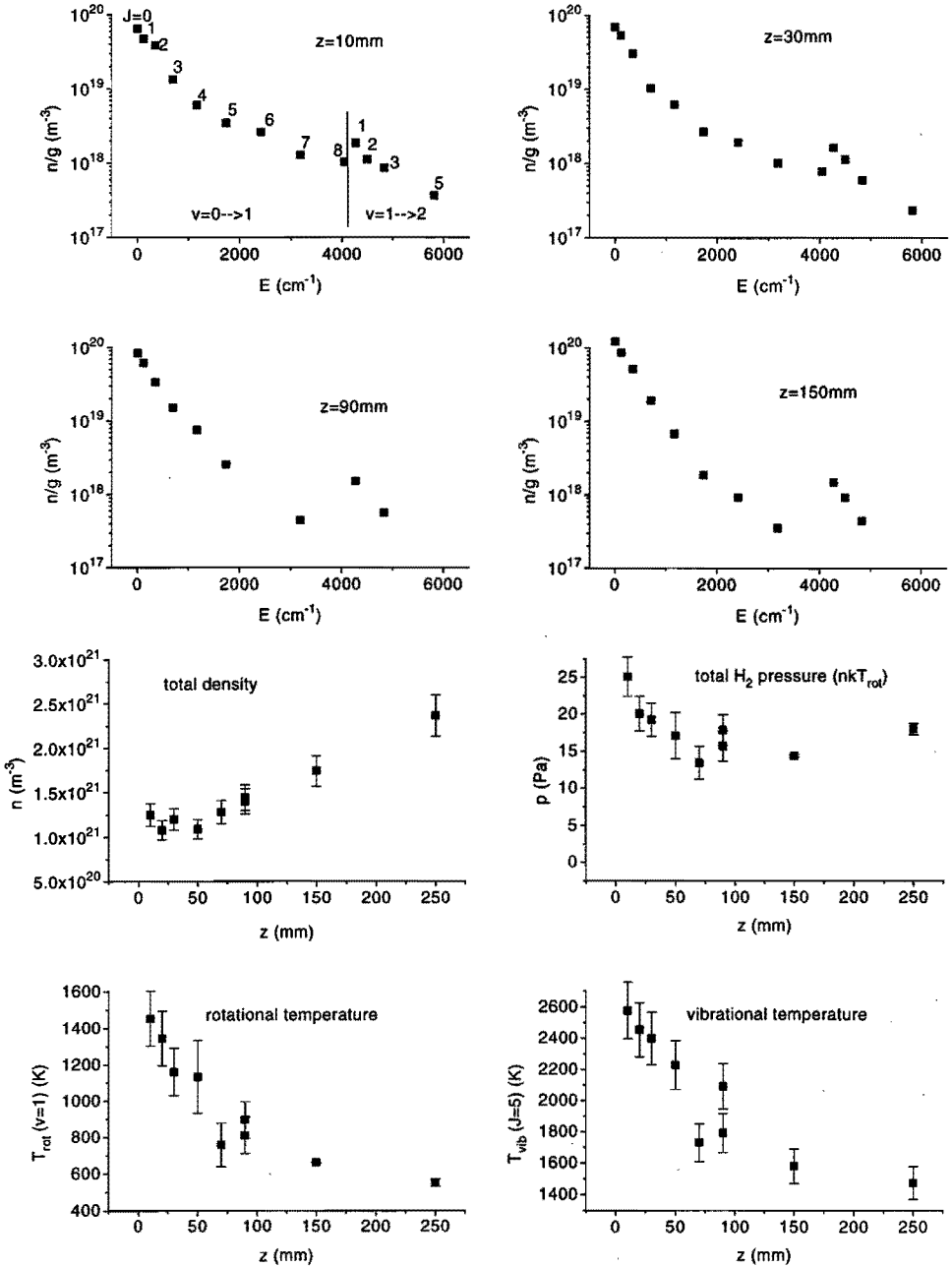


Figure 10: CARS results for the magnetized hydrogen plasma beam.

It follows from the pressure plots in Figs. 9 and 10, that the dissociation degree in the plasma jet must be minimum, as the measured H_2 pressures account for the total background pressure. Note, that high pressures are measured near the nozzle. This could be an artefact: we can expect to measure some background gas there (the beam diameter is still small) and still ascribe a high ($v=1$) rotational temperature to the total measured H_2 density at these positions. This would lead to an overestimation of the pressure.

The fact, that the measured dissociation degree in the plasma is so low is very surprising, as power input measurements show, that the arc must have a dissociation degree of around 70% for an arc current of 37.5 A [22]. This has been more or less confirmed by depolarization Rayleigh scattering measurements very close to the arc [2]. A further indication follows from the analysis of the rotational populations, measured by CARS, in the following section. It is our opinion, that only an effective wall association process in combination with a recirculation flow can explain these results [5, 7, 18].

Furthermore, no great dissimilarities are obvious from a comparison between Fig. 9 and Fig. 10. Indeed, the hydrogen molecular population hardly seems to be influenced by the fact, that a totally different *plasma* is present in the magnetized case. Especially the absence of highly excited vibrational states in the magnetized case makes less probable the occurrence of mechanism (7) as a main H^- production channel. If H^- is present in large amounts, a different mechanism might be necessary. The formation through Rydberg or highly (electronically) excited H_2 , as proposed by Garscadden *et al* in [23] might be considered.

V. ROTATIONAL RELAXATION MODEL

An attempt has been made to explain the non-Boltzmann rotational distributions in Fig. 9 by considering hot H_2 gas (i.e., the 30% that is not dissociated) flowing out of the arc, relaxing to an infinitely large, cool H_2 background. During the relaxation by rotational-translational inelastic collisions (R-T collisions), higher states relax more slowly. The rate for a given $\Delta J=L$ can be expressed in the rate for relaxation for $L \rightarrow 0$, as has been established by DePristo *et al.* [24]:

$$k(J_i \rightarrow J_f) = g_{J_f} \exp\left(\frac{E_{J_i} - E_{J_f}}{kT_{gas}}\right) \times \sum_L \begin{pmatrix} J_i & L & J_f \\ 0 & 0 & 0 \end{pmatrix}^2 g_L |A_L^{J_i}|^2 k(L \rightarrow 0), \quad (8)$$

where J_i and J_f are the initial and final J values, $J_i > J_f$ is the largest of the two. The exponential follows from microreversibility, the $3j$ symbol expresses the recoupling of J_i with L to form J_f , g denotes the statistical weight, and $A_L^{J_i}$ denotes an "adiabaticity" factor, defined by:

$$A_L^{J_i} = \frac{1 + \tau_L^2/6}{1 + \tau_{J_i}^2/6}, \quad (9)$$

where $\tau_J = 2\pi T_c/T_J$, with T_c the collision time and T_J the characteristic time of rotation for a given J . The adiabaticity

factor accounts for the effectivity of momentum exchange for given collision and rotation times. It is close to 1 for our conditions.

The above gives the framework for a very simple model to explain the rotational distributions. For a flux of 3.5 SLM (i.e., $1.4 \cdot 10^{21} s^{-1}$), a 70% dissociation degree, an estimated velocity of $5 \cdot 10^3 m/s$ (see below), and a beam diameter at $z=20$ mm of 15 mm, we obtain a concentration of approximately $5 \cdot 10^{20} m^{-3}$ at $z=20$ mm. The total H_2 density at that position (measured by CARS, Fig. 9) is around $2.8 \cdot 10^{21} m^{-3}$. In the model we use a hot density of $5 \cdot 10^{20} m^{-3}$, and a cold H_2 density of $2.3 \cdot 10^{21} m^{-3}$. A set of simple differential equations is constructed for the first 14 levels in the $v=0$ manifold. The system looks as follows:

$$\begin{aligned} u \frac{dn_0}{dz} &= N(n_2 k_{2,0} - n_0 k_{0,2}) \\ u \frac{dn_1}{dz} &= N(n_3 k_{3,0} - n_1 k_{1,3}) \\ u \frac{dn_i}{dz} &= N(n_{i+2} k_{i+2,i} + n_{i-2} k_{i-2,i}) \\ &\quad - n_i [k_{i,i+2} + k_{i,i-2}] \\ &\quad (2 \leq i \leq 12) \\ u \frac{dn_{13}}{dz} &= N(n_{11} k_{11,13} - n_{13} k_{13,11}) \\ u \frac{dn_{14}}{dz} &= N(n_{12} k_{12,14} - n_{14} k_{14,12}), \end{aligned} \quad (10)$$

where $k_{i,j}$ denotes a rate (calculated using (8)), N is the density of collision partners (i.e., the cold H_2), and n_i are the densities for each rotational level. We only consider $\Delta J=2$ collisions, because of nuclear spin conservation for H_2 (ortho and para H_2 conservation). Larger (even) ΔJ steps are neglected [25]. The speed of the jet is represented by u , which has been cast in the following (assumed) form:

$$u(z) = u_0 \cdot \exp(-z/l), \quad (11)$$

where u_0 is the speed at the origin (the nozzle), taken to be $7 \cdot 10^3 m/s$ (calculated using pressure and flow data from a similar experiment) and l is a characteristic length, taken to be 70 mm. The expanding jet mixes with the background gas (at 600 K) with velocity $u(z)$, and both the thermal energy and the translational energy are taken into consideration in the calculation of the rate constant $k(2 \rightarrow 0)$ at a certain energy. The cross sections for $2 \rightarrow 0$ at temperatures in the range 500-4000 K are calculated using data from Green [26]. A second order polynomial fit delivers for this temperature range:

$$k_{2 \rightarrow 0}(T) = -1.55 \cdot 10^{-18} + 2.65 \cdot 10^{-21} T + 5.5 \cdot 10^{-25} T^2, \quad (12)$$

where T is the collision energy in K.

The system is solved using MAPLE [27] with a Boltzmann distribution at 3000 K (which seems to be a reasonable value for hot molecules leaving the arc) as a $z = 0$ boundary condition.

Fig. 11 shows the results for the model, together with the measurements in a pure hydrogen plasma (no magnetic field) at two different positions. In using *one* model population to describe the populations at two positions, we implicitly

assume, that the increase in area of the primary beam (hot population) is balanced by a decrease in velocity, because the hot and cold model populations remain the same. The total H_2 density at the two z positions is about equal (Fig. 9). In spite of the many assumptions, the model appears to describe the measurements very well. Because CARS "sees" both the hot and cold populations, the temperature in the lower part of the rotational manifold seems rather low, whereas the tail is hot. As the tail slowly relaxes, the total distribution becomes more and more Boltzmann-like.

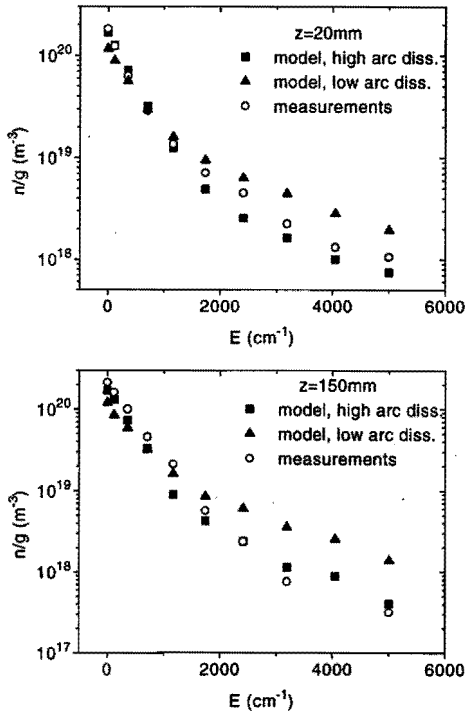


Figure 11: The results of the quasi one-dimensional model compared to the rotational distributions in $v=0$, at two axial positions. The squares denote the model with a 70% dissociation degree in the arc, the triangles denote the model with a low dissociation degree (10%) in the arc. The latter has been added to emphasize the fact, that a substantial dissociation degree inside the cascaded arc has to be assumed in order to explain the measurements. The plasma is a freely expanding pure hydrogen jet (cf. Fig. 9).

The dissociation degree of 70% inside the arc is a necessary condition to obtain a good agreement. To illustrate this a few runs with the program have been performed using a very low dissociation degree (10%) in the arc. In this case the majority of the arc output flux consists of molecules with a temperature of 3000 K, relaxing to a background gas at 600 K (just as in the above). Using the same speed profile and the same

expressions for the rate constants, results are obtained that deviate significantly from the experimental findings (Fig. 11). Apparently, the large amount of hot molecules does not relax quickly enough in this case. This is a further indication that the arc does dissociate to a large extent, even though the model is probably not accurate enough to distinguish between, e.g., a 70 or 80% arc dissociation degree.

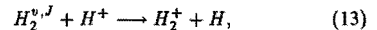
VI. CONCLUSIONS

The expanding argon-hydrogen plasma jet is characterized by an anomalously fast recombination that can only be explained by molecular channels involving hydrogen molecules. This is clearly indicated by the Thomson scattering measurements. CARS measurements show that large amounts of hydrogen molecules are indeed present in the periphery of the plasma, even though they appear to be rather cool. The partial H_2 pressure in the periphery of the jet equals the seed fraction of H_2 , whether it be injected in the arc or in the vessel. A recirculation pattern in the vacuum vessel is thought to be responsible for the transport of (wall-associated) molecules into the plasma.

The measurements on pure hydrogen confirm the older depolarisation Rayleigh scattering [2] and active probe [28] measurements, as all show a marginal dissociation degree in the vessel (i.e., the hydrogen pressure is equal to the background pressure within the experimental errors). An exact comparison between the two methods is difficult, as depolarization Rayleigh scattering is a crossed-beam experiment with a very high spatial resolution, whereas CARS has a poorer resolution along the laser beams. Furthermore, the former method can only be applied at higher pressures. The low dissociation degree in the vessel, in combination with the *high* dissociation degree in the arc must be caused by a wall association process being dominant.

The axial dependencies of T_{rot} and T_{vib} show no stationary shock front, which is so evident in pure argon and deluted Ar- H_2 mixtures [4, 5].

In the expanding pure hydrogen plasma only states up to $v=2$ can be detected. De Graaf *et al* [3] assume a total $v=4$ density of about $10^{19}m^{-3}$ in order to explain the anomalous recombination in a very similar pure hydrogen expanding plasma. The highly excited molecules were thought to originate from the vessel walls [29]. The hot molecules are necessary to make the reaction:



exothermic (the energy deficit is around 2 eV). The formed H_2^+ can either react with H_2 in order to form H_3^+ or with an electron in a very fast dissociative recombination reaction. The formed H_3^+ can also dissociatively recombine, so either process will lead to a very effective ionization loss once the H_2^+ is formed.

The CARS measurements in this paper, however, clearly show the absence of large amounts of highly excited molecules around the plasma (where a T_{vib} of about 1100 K is observed). At the measured T_{vib} 's in the plasma, a $v=4$ density for the free expanding pure hydrogen jet can be estimated to be around $5 \cdot 10^{16}m^{-3}$ for axial positions between $z=40$ and 150 mm. This discrepancy of more than two orders of magnitude is

not well understood, but a different mechanism may have to be found in order to explain the observed ionization loss. Examples could be the expansion speed of the H^+ leaving the arc (translational energy), a pronounced importance of highly excited *rotational* states (e.g., a plateau in the rotational population below the detectivity of the CARS set up), or a combination of the mentioned possibilities of energy input (translational, rotational, and vibrational energy).

A similar problem arises for the supposedly H^- rich magnetized hydrogen plasma: in this case even higher excitation is necessary to make reaction (7) effective. But again only low T_{vib}^+ 's are observed (Fig. 10), which lead to estimated $v=4$ densities of a few times $10^{16}m^{-3}$. A strong plateau in the *rotational* population (just below the detection limit of the CARS set up) could be of influence here. If the presence of high densities of negative ions can be verified, however, it is clear that the standard "dissociative attachment involving vibrationally excited molecules"- explanation cannot account for the production of these negative ions.

The simple rate-model of a two-population H_2 gas seems to be able to describe the observed rotational distributions rather well for the freely expanding hydrogen jet. In this view, hot arc H_2 at 3000 K (representing the 30% fraction that is not dissociated) expands into the vessel and relaxes to cold (600 K) hydrogen gas. The latter is supposed to constitute an infinite reservoir of cool gas. The model shows that the assumption of a high dissociation degree in the arc is necessary in order to explain the rotational state distribution.

ACKNOWLEDGMENT

This work is supported by the Netherlands Technology Foundation (STW). The skillful technical assistance of H.M.M. de Jong, A.B.M. Hüsken, and M.J.F. van de Sande is gratefully acknowledged. Marco Box, Paulo Freire, Marc Beurskens and Leon Jacobs are thanked for their help during the measurements. The people at ONERA Palaiseau (notably Jean-Pierre Taran, Michel Péalat, and Michel Lefebvre) have made a significant contribution through the many helpful discussions about the practical and theoretical aspects of CARS. The useful discussions with prof. J. Uhlenbusch, P. Jauernik, and S. Hädrig of Düsseldorf University, as well as with Richard van de Sanden (Eindhoven Univ.) and Nader Sadeghi (Grenoble Univ.) are gratefully acknowledged.

References

- [1] See for example A.J.M. Buuron, G.J. Meeusen, J.J. Beulens, M.C.M. van de Sanden, and D.C. Schram, *J. Nucl. Mater.* **200**, 430 (1993); R.J. Severens, G.J.H. Brussaard, M.C.M. van de Sanden, and D.C. Schram, *Appl. Phys. Lett.* **67** (4), 491 (1995).
- [2] R.F.G. Meulenbroeks, D.C. Schram, L.J.M. Jaegers, and M.C.M. van de Sanden, *Phys. Rev. Lett.* **69** (9), 1379 (1992) (chapter 6).
- [3] M.J. de Graaf, R. Severens, R.P. Dahiya, M.C.M. van de Sanden, and D.C. Schram, *Phys. Rev. E* **48** (3), 2098 (1993).
- [4] M.C.M. van de Sanden, J.M. de Regt, G.M. Janssen, J.A.M. van der Mullen, B. van der Sijde, and D.C. Schram, *Rev. Sci. Instrum.* **63**, 3369 (1992).
- [5] R.F.G. Meulenbroeks, A.J. van Beek, A.J.G. van Helvoort, M.C.M. van de Sanden, and D.C. Schram, *Phys. Rev. E* **49** (5), 4397 (1994) (chapter 3).
- [6] R.F.G. Meulenbroeks, R.A.H. Engeln, M.C.M. van de Sanden, J.A.M. van der Mullen, and D.C. Schram, *Proceedings International Symposium on Plasma Chemistry 1995* (1995).
- [7] R.F.G. Meulenbroeks, R.A.H. Engeln, M.N.A. Beurskens, R.M.J. Paffen, M.C.M. van de Sanden, J.A.M. van der Mullen, and D.C. Schram, *Plasma Sources Sci. Technol.* **4**, 74 (1995) (chapter 4).
- [8] A.J. Druet and J.-P. E. Taran, *Prog. Quant. Electron.* **7**, 1 (1981).
- [9] J.-P. E. Taran, *CARS spectroscopy*, in *Applied Laser Spectroscopy*, Ed. W. Demtröder and M. Inguscio, Plenum Press, New York (1990).
- [10] V. Kornas, V. Schulz-von der Gathen, T. Bornemann, H.F. Döbele, and G. Prosz, *Plasma Chem. Plasma Processing* **11**, 171 (1991).
- [11] T. Doerk, J. Ehibeck, P. Jauernik, J. Stáncó, J. Uhlenbusch, and T. Wotika, *J. Phys. D: Appl. Phys.* **26**, 1015 (1993).
- [12] M. Péalat, J.-P.E. Taran, and J. Taillet, *J. Appl. Phys.* **52** (4), 2687 (1981).
- [13] M. Péalat, M. Lefebvre, and J.-P.E. Taran, *Phys. Rev.* **38** (4), 1948 (1988). See also: R.P. Lucht and R.L. Farrow, *J. Opt. Soc. Am. B* **6**, 2313 (1989).
- [14] M. Péalat, M. Lefebvre, B. Scherrer, and J.-P. E. Taran, *private communication* (1995).
- [15] D.A. Long, *Raman Spectroscopy*, Mc.Graw-Hill, London (1977).
- [16] J. Rychlewski, *Mol. Phys.* **41** (4), 833 (1980).
- [17] K. Chen, M. Chuang, C.M. Penney, and W.F. Banholzer, *J. Appl. Phys.* **71** (3), 1485 (1992).
- [18] R.F.G. Meulenbroeks, D.C. Schram, M.C.M. van de Sanden, and J.A.M. van der Mullen, *to be published* (1995) (chapter 8).
- [19] M.C.M. van de Sanden, Z. Qing, D.K. Otorbaev, M.J. de Graaf, J.C.A. Wevers, and D.C. Schram, *Proceed. 5th Europ. Workshop on the Prod. and Appl. of Light Neg. Ions*, 41 (Dublin, 1993).

- [20] See for example: D.A. Greenhalgh, *Quantitative CARS Spectroscopy*, in *Advances in Non-Linear Spectroscopy*, R.J.H. Clark and R.E. Hester, eds. Wiley New York (1988); *Combusting Flow Diagnostics*, D.F.G. Durão, M.V. Heitor, J.H. Whitelaw, and P.O. Witze, eds. NATO ASI Series, Kluwer Academic Amsterdam (1992).
- [21] M. Bacal, A.M. Bruneteau, W.H. Graham, G.W. Hamilton, and M. Nachman, *J. Appl. Phys.* **52** (3), 1247 (1981).
- [22] M.J. de Graaf, Z. Qing, H.W.A. Tolido, M.C.M. van de Sanden, and D.C. Schram, *J. High Temp. Chem. Process.*, suppl. to no. 3, 11 (1992).
- [23] Alan Garscadden and Rajesh Nagpal, *Plasma Sources Sci. Technol.* **4**, 268 (1995).
- [24] A.E. DePristo, S.D. Augustin, R. Ramaswamy, and H. Rabitz, *J. Chem. Phys.* **71**, 580 (1979); J. Derouard and N. Sadeghi, *Chem. Phys.* **88**, 171 (1988).
- [25] D.L. Thompson, *J. Chem. Phys.* **75** (4), 1829 (1981).
- [26] S. Green, *J. Chem. Phys.* **62** (6), 2271 (1975).
- [27] MAPLE is a registered trademark of 766884 Ontario inc. Waterloo Maple Software.
- [28] D.K. Otorbaev, M.J. de Graaf, M.C.M. van de Sanden, and D.C. Schram, *Contrib. Plasma Phys.* **35** (3), 195 (1995).
- [29] B. Jackson and M. Persson, *J. Chem. Phys.* **96**, 2378 (1992).

Wall Association and Recirculation in Expanding Thermal Arc Plasmas

R.F.G. Meulenbroeks D.C. Schram M.C.M. van de Sanden
J.A.M. van der Mullen

*Eindhoven University of Technology, Department of Physics,
P.O.Box 513 5600 MB Eindhoven, The Netherlands*

Abstract. In recent years, extremely rapid recombination as well as other effects in expanding thermal arc plasmas have been attributed to wall association of radicals (mainly H) and recirculation in the expansion vessel. Coherent anti-Stokes Raman scattering (CARS) measurements on H₂ and HD when the arc burns on a mixture of H₂ and D₂ show conclusive new evidence for this view.

Models and experiments in the field of plasma chemistry generally focus on the description of radical kinetics and radical detection. Because of the very complex plasma kinetics (literally hundreds of reactions may be involved), global understanding is difficult to attain [1]. In this letter we want to specifically address the formation of stable molecules, which appears to dominate the plasma we have studied and may play an essential role in many other types of plasma as well. The simple view resulting from this consideration may rapidly lead to clear understanding of the plasma chemistry in many cases.

Plasma deposition and etching techniques are becoming ever more important tools for the manufacturing of small structures in semiconductor materials, as well as for the coating of materials with thin films (e.g., amorphous hydrogenated carbon and silicon, diamond, graphite) [2]. Plasma sources are also used for the creation of useful particles, such as H⁻ ions, H⁺ ions, or H radicals [3]. Different types of plasma generators are used (RF, microwave, DC) for the creation of deposition precursors or (etching) radicals, but a common factor is a fairly large (5-100 liters) vacuum vessel, usually made out of stainless steel. The question now is to what extent the composition of the source plasma is representative for the composition in the vacuum treatment vessel. The *residence time* of a particle in the vessel can attain appreciable values, seconds or more. This implies the principal possibility of many wall reactions, with a pronounced influence on the radical (and stable molecule) populations in the treatment region.

In this study, a DC wall stabilized thermal arc plasma source is used for the deposition of thin films [4] and as a hydrogen particle source [5]. The thermal, subatmospheric plasma is allowed to expand into a low-pressure vessel (volume around 100 liters), creating an expanding plasma jet. Monomers (C₂H₂, CH₄, SiH₄) are injected in the jet and deposition takes place on a downstream substrate. The arc is usually operated in pure argon or in a mixture of argon and hydrogen. In the case of a particle source, the carrier gas is pure hydrogen. In all these cases, residence times are around 0.3-2 seconds, and a recirculation flow is present in the vessel. These characteristics favor a major role for wall processes, leading to the formation of stable molecules from radicals (e.g., H₂ from H). The plasma is recombining and afterglow-like, with low electron temperatures (T_e around 0.2 eV) and low electron densities (n_e around 10^{16} m^{-3} when H₂ is used in considerable amounts

[e.g., 10 vol.% H₂ in argon]). These T_e and n_e values rule out a major importance for electron kinetics. This makes the expanding jet an ideal object for the study of wall reactions, as the plasma emerging from the arc mainly consists of radicals and molecules.

The actual research on the above mentioned wall phenomena is performed with a plasma jet experiment which has been described in detail in [6]. As the wall association process creates a population of stable molecules around the plasma jet itself, i.e., in the "dark" periphery, active (laser) plasma diagnostics have to be employed in order to obtain the required data. As this study focuses on argon-hydrogen and pure hydrogen plasmas, a high-sensitivity CARS spectroscopy experiment has been realized to perform density and temperature measurements on rovibrationally excited H₂ (and HD, when the arc operates on a H₂/D₂ mixture). The aim is to prove that the measured amounts of stable molecules around (and in) the plasma can only be explained by assuming that wall association and recirculation are dominant processes.

The CARS spectrometer is a scanning BOXCARS experiment, using a reference branch in order to cancel out experimental peculiarities such as a specific dye response spectrum. The experiment will be described in detail in a forthcoming paper [7]; CARS specifics can be found in review articles (e.g., [8]). At this moment it suffices to note that the set up is very sensitive, capable of state-selective detection of H₂ at very low pressures (a spectrum can be taken at 0.1 Pa H₂ at 300 K). A 3:1 mixture of Exciton DCM and Exciton LDS698 dyes has been used to cover the H₂ and HD spectral regions, in a Raman shift range of 4165-3000 cm⁻¹. Absolute total density calibration to an accuracy of $\pm 10\%$ is possible. Using the appropriate correction factors for the Raman cross sections [9], absolute HD state densities can also be determined. Effects of saturation in the CARS spectrum ([10]) have been shown to be negligible for our laser powers [7]. Spatial resolution is obtained by crossing the beams (BOXCARS): the detection volume has a length of ≈ 2 cm and a diameter of $\approx 180 \mu\text{m}$.

It is useful to take a look at the general characteristics of the argon-hydrogen plasma by considering some Thomson scattering results, presented in Fig. 1. The n_e values have been measured on the axis of the expanding jet and show the behaviour of an argon plasma with small amounts of hydrogen added. A very pronounced influence is observed, even for very

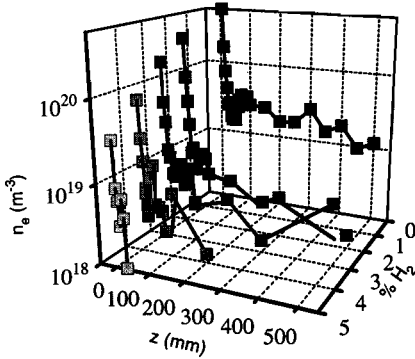


Figure 1: Thomson scattering data for the electron density vs. axial position for pure argon and different hydrogen-argon admixtures. The axial position z increases with increasing downstream distance from the nozzle. The impact of small additions of H_2 to the flow is clearly visible.

low hydrogen seed fractions. The hydrogen is admixed to the argon flow before it enters the arc. The plasma conditions are the following: arc current $I_{arc}=45$ A, voltage $V_{arc}=50$ V, total flow 3.5 standard liters per minute (SLM), vessel background pressure $p_{back}=40$ Pa.

The hydrogen admixtures are in % by volume. The anomalously fast recombination has been attributed to the formation of ArH^+ molecular ions from Ar^+ and H_2 . This strongly points to wall association, as H_2 molecules are very unlikely to survive the 1 eV environment of the plasma inside the arc, especially at lower seed fractions. In this view, only Ar^+ , H^+ , Ar , H , and e^- leave the arc, forcing the wall to be considered as the major source for H_2 molecules needed to explain the fast recombination [11, 12].

The measurements that have been performed are the following: (1) CARS measurements on 10 vol.% H_2 in argon mixtures. The hydrogen is added to the flow before it enters the arc (arc injection), but in a second experiment it is flushed directly into the vessel, the arc operating on pure argon (vessel injection); (2) CARS measurements on H_2 and HD when the arc burns on a 50/50 mixture of H_2 and D_2 ; (3) ditto with the arc burning on H_2 , while D_2 is flushed into the vessel; (4) ditto with the arc burning on D_2 , with H_2 flushed into the vessel.

1. *CARS on Ar- H_2 mixtures.* In order to prove the existence of similar populations of H_2 around the plasma for arc and vessel injection, CARS measurements are carried out under the following conditions: $I_{arc}=45$ A, flow=3.5 SLM, $p_{back}=140$ Pa, 10 vol.% H_2 in Ar. The results for the H_2 partial pressures (taken as the product of total density of all measured states, the rotational temperature, and Boltzmann constant) are depicted in Fig. 2. The radial scan is made by moving the plasma inside the vessel, as this can be done without significantly changing the plasma [6].

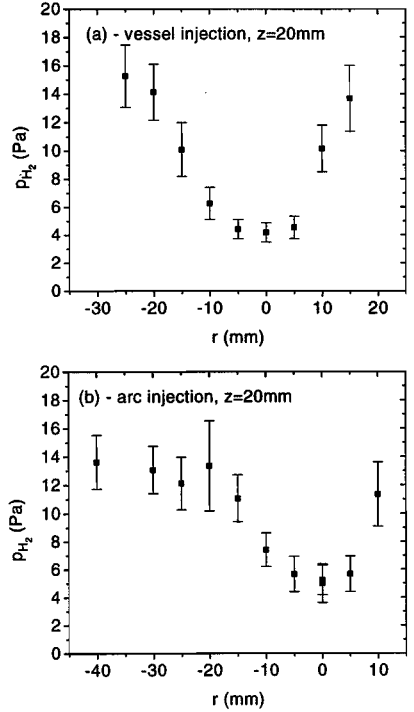


Figure 2: Radial profiles at a downstream distance of 20 mm for the H_2 partial pressure in a 10 vol.% H_2 in Ar mixture. Graphs are shown both for vessel (a) and arc (b) injection. Partial pressures are calculated using $p = nkT_{rot}$, where n is the sum of all measured state densities. The background pressure is 140 Pa.

The plots clearly show that in both cases (vessel and arc injection) the partial pressure of H_2 in the periphery of the jet equals 10% of p_{back} , within the measurement accuracy. As we have to assume an almost complete dissociation of H_2 in the arc at these seed fractions, this means that the measured H_2 in the arc injection case must have been formed at the vessel walls, as it can be easily shown that volume association of H_2 is negligible in our case [13].

2. *CARS on H_2 - D_2 mixtures.* In this case the conditions are the following: $I_{arc}=37.5$ A, $V_{arc}=100$ V, flow: 3.5 SLM (50% H_2 and 50% D_2 by volume, both injected in the arc), $p_{back}=40$ Pa. Measurements on H_2 and HD concentrations and temperatures are performed both in the plasma (at axial position $z=70$ mm (z denotes the distance from the onset of the expansion), and a radial position $r=0$) and in the periphery (at $z=20$ mm, $r=20$ mm). In the latter case the laser beams are clearly over the plasma jet. For the axis of the jet, at an axial position of $z=70$ mm, rotational Boltzmann plots for both H_2 and HD are given in Fig. 3. A summary of the results is given in table 1, clearly pointing to a total mixing in the formation

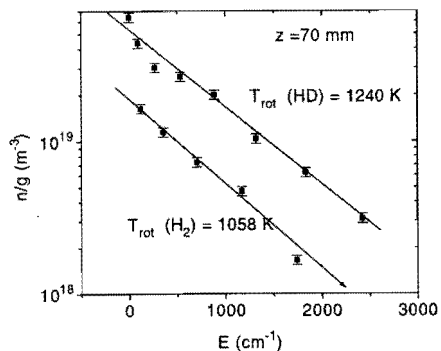
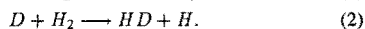
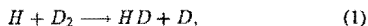


Figure 3: Boltzmann plots constructed from the H_2 and HD measurements in the plasma (i.e., at $z=70$ mm and $r=0$).

of products, as $H_2:HD:rest = 1:2:1$ in partial pressures (and densities as well, as the temperatures are very similar). We think it safe to assume, that the "rest" will consist mainly of D_2 . At this moment, D_2 is outside the measurement range, as it would require different experimental conditions (dyes, dichroics).

A discussion of these measurements necessarily starts with an evaluation of the dissociation degree inside the cascaded arc. This dissociation degree has been measured by power input measurements on pure H_2 arcs and has been determined to be around 70% (of the input flow) for an arc current of 37.5 A [14]. The fact that we observe (also in pure hydrogen, [7, 15]) a low dissociation degree inside the vessel (maximum 10%), a vessel (i.e., wall) association process must be considered. Assuming that, in the above case, 70% of the particles leaving the arc are H and D radicals, the walls must be saturated with H and D; subsequent association and desorption of molecules should lead to the observed $H_2:HD:D_2$ ratio of 1:2:1. The 30 vol.% of molecules leaving the arc are most probably of the same constitution, as perfect mixing is to be expected there. The final mixture in the vessel corresponds exactly with the measurement results.

A point of concern are volume reactions of the type:



These reactions have been studied extensively [16] and show a significant threshold behaviour at low temperatures (Fig. 4). It is clear, that at the temperatures inside the vessel (400-1200 K, [7] and table 1), these reactions can be neglected. In the arc, however, at high densities and temperatures, these reactions can play a dominant role, (as rates may approach higher values: the threshold behaviour is no longer important at 1 eV temperatures) leading to total mixing of the part of the molecules that is not dissociated.

3. and 4. H_2 and HD CARS on other H_2-D_2 mixtures. In this last set of measurements, the arc is operated on either full H_2 or D_2 (37.5 A, 2 SLM), while the other constituent is flushed directly in the vessel (1 SLM, $p_{back} = 40$ Pa). So

Table 1: The CARS results for HD and H_2 . Experimental errors are around 7-10% for T_{rot} and n . The resultant error for the pressure should be around 14-20%. The experimental conditions are: $p_{back} = 40$ Pa, $I_{arc} = 37.5$ A. Flows: H_2-D_2 arc: 1.75 SLM H_2 and 1.75 SLM D_2 ;

		H_2-D_2 arc	H_2-D_2 arc
		periphery	plasma
		($z=20$ mm)	($z=70$ mm)
		($r=20$ mm)	($r=0$ mm)
HD	T_{rot} (K)	398 K	1240 K
HD	n (m^{-3})	4.1×10^{21}	9.5×10^{20}
HD	nkT (Pa)	22.2	16.3
H_2	T_{rot} (K)	383 K	1058 K
H_2	n (m^{-3})	2.1×10^{21}	5.1×10^{20}
H_2	nkT (Pa)	10.9	7.5

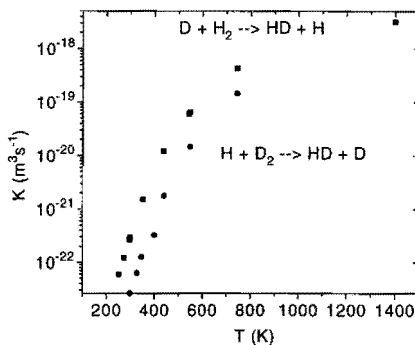


Figure 4: The rates for atom-molecule volume reactions vs. temperature, according to ref. [16].

here we encounter the situation where only H (D) radicals leave the arc (representing a 70% dissociation degree in the arc), whereas D_2 (H_2) is injected in molecular form. Table 2 shows the remarkable results: the HD density is very low (partial pressure 1.2 Pa) in the case of a D_2 arc, and the HD signal even drops to the detection limit in the case of a H_2 arc. Following the reasoning under 2., this means that there is no full dissociation of the vessel-injected molecules. No total mixing can thus occur at the vessel walls. Some conversion to HD is observed, however, so some dissociation must occur in the volume. This leads to the conclusion that reactions (1-2) are responsible for dissociation of a small part of the vessel-injected molecules. Note, that dissociation processes through these volume reactions leads to HD production as well. Volume processes can also play a minor role when H_2 and D_2 are injected in the arc, but evidently they cannot account for total mixing: this can only be the case when most of the molecules are dissociated (in the arc) when they enter

Table 2: The results of the HD and H₂ CARS measurements. The arc is burning on either H₂ or D₂, the other constituent (D₂ or H₂, resp.) is flushed into the vessel. Conditions are: $p_{\text{back}} = 40$ Pa, $I_{\text{arc}} = 37.5$ A. Flows: H₂ arc: 2 SLM H₂ in arc, 1 SLM D₂ in vessel; D₂ arc: 2 SLM D₂ in arc, 1 SLM H₂ in vessel.

		H ₂ arc	D ₂ arc
		periphery ($z=r=20$ mm)	periphery ($z=r=20$ mm)
HD	T_{rot} (K)	≈ 375 K	375 K
HD	n (m ⁻³)	$\approx 3 \times 10^{19}$	2.4×10^{20}
HD	nkT (Pa)	≈ 0.15	1.2
H ₂	T_{rot} (K)	373 K	343 K
H ₂	n (m ⁻³)	4.0×10^{21}	3.1×10^{21}
H ₂	nkT (Pa)	20.7	14.5

the vessel. The rates given in Fig. 4 confirm the marginal importance of volume reactions.

The asymmetry between the H₂ and D₂ arc cases can then be attributed to three effects: (a) the arc is slightly more efficient when operated on D₂ (more D radicals); (b) at lower temperatures, the rate for reaction (1) can be as many as 8 times slower than that for reaction (2) ([16] and Fig. 4); (c) wall adsorption may be more efficient for H than for D radicals.

The above measurements can be used to formulate a rough model of the expanding arc plasma with a dominant role for recirculation. We start by looking at the residence time in the 300 liter vessel, which is around 2 s for the given flows and pressures (40 Pa, 3.5 SLM). The transit time of a particle in the beam (at an estimated speed of 3000 m/s) is around 0.3 ms and a comparison of the volumes of the beam and the periphery leads to an estimated recirculation time of 25 ms. From these values, the number of recirculations per residence time follows to be 80, so each particle can "see" the wall very often. This would lead to a complete association at the wall even at values for the association coefficient (the probability of a H₂ molecule leaving after a collision of H with the H-saturated wall collision) as low as 0.05. In this picture, the radicals leaving the arc are completely recycled in the form of stable molecules: the composition of the plasma is therefore determined mainly by the recirculation and the wall association. This view explains the measurements under (1) and (2). The measurements with the H₂ (D₂) arc point to incomplete dissociation, leading to a marginal HD population. It may be worth noting, that only the very good sensitivity of the CARS experiment makes the asymmetry detectable.

The essential importance of this view lies in the fact, that the composition of plasmas of this type can be entirely determined by recycled stable monomers. Furthermore, dissociation of all basic molecules (in this case, H₂ and D₂) is necessary to obtain total mixing: volume processes are not fast enough, as is indicated by the measurements under (3) and (4). Careful measurements using advanced diagnostics can therefore lead

to a better global understanding of plasma chemistry in general and of deposition and etching plasmas and plasma sources in particular.

ACKNOWLEDGMENT

The authors gratefully acknowledge the assistance of H.M.M. de Jong, M.J.F. van de sande, A.B.M. Hüsken, M.N.A. Beurskens, C. Box, and especially R.A.H. Engeln for technical assistance and help during the measurements and the construction of the CARS set up. This work is supported by the Netherlands Technology Foundation (STW). The work of one of us (M.C.M. vd S.) is supported by the Royal Netherlands Academy of Arts and Sciences (KNAW).

References

- [1] See for example: M.J. Kushner, *J. Appl. Phys.* **63**, 2532 (1988).
- [2] See for example: *Diamond and Diamond-like Films and Coatings*, ed. R.E. Clausing *et al.*, Plenum New York (1991); W. Luft and Y.S. Tsuo, *Hydrogenated Amorphous Silicon Alloy Deposition Processes*, Marcel Dekker, New York (1993).
- [3] M. Bacal, G.W. Hamilton, *Phys. Rev. Lett.* **42** (23), 1538 (1979).
- [4] A.J.M. Bauron, G.J. Meeusen, J.J. Beulens, M.C.M. van der Sanden, and D.C. Schram, *J. Nucl. Mater.* **200**, 430 (1993).
- [5] R.F.G. Meulenbroeks, D.C. Schram, L.J.M. Jaegers, and M.C.M. van de Sanden, *Phys. Rev. Lett.* **69** (9), 1379 (1992); M.J. de Graaf, R. Severens, R.P. Dahiya, M.C.M. van de Sanden, and D.C. Schram, *Phys. Rev. E* **48** (3), 2098 (1993).
- [6] M.C.M. van de Sanden, J.M. de Regt, G.M. Janssen, J.A.M. van der Mullen, D.C. Schram, and B. van der Sijde, *Rev. Sci. Instrum.* **63** (6), 3369 (1992).
- [7] R.F.G. Meulenbroeks, R.A.H. Engeln, J.A.M. van der Mullen, and D.C. Schram, *to be published* (1995).
- [8] S. Druet and J.P. Taran, *Progr. Quantum Electr.* **7**, 1 (1981).
- [9] J. Ryszlewski, *Mol. Phys.* **41** (4), 833 (1980).
- [10] M. Pealat, M. Lefebvre, and J.P. Taran, *Phys. Rev.* **38** (4), 1948 (1988).
- [11] R.F.G. Meulenbroeks, A.J. van Beek, A.J.G. van Helvoort, M.C.M. van de Sanden, and D.C. Schram, *Phys. Rev. E* **49** (5), 4397 (1994).
- [12] R.F.G. Meulenbroeks, R.A.H. Engeln, M.N.A. Beurskens, R.M.J. Paffen, M.C.M. van de Sanden, J.A.M. van der Mullen, and D.C. Schram, *Plasma Sources Sci. Technol.* **4**, 74 (1995).

- [13] J.E. Bennett, D.R. Blackmore, *Proc. Roy. Soc. A* **305**, 553 (1968).
- [14] M.J. de Graaf, Z. Qing, H.W.A. Tolido, M.C.M. van de Sanden, and D.C. Schram, *J. High Temp. Chem. Process.*, suppl. to no. **3**, 11 (1992).
- [15] D.K.Otorbaev, M.J. de Graaf, M.C.M. van de Sanden, and D.C. Schram, *Contrib. Plasma Phys.* **35** (3), 195 (1995).
- [16] M.B. Bowers, B.H. Choi, and K.T. Tang, *Chem. Phys. Lett.* **136** (2), 145 (1987) and references herein.

General Conclusions

R.F.G. Meulenbroeks

*Eindhoven University of Technology, Department of Physics,
P.O. Box 513, 5600 MB Eindhoven, The Netherlands*

Having presented the main body of the thesis material in the form of complete journal articles, each with its own conclusion section, it is appropriate to summarize the main findings here. The aim of this section, then, is to scrutinize the conclusions of the (argon)-hydrogen work, as some of the earlier conclusions have to be re-evaluated. The results of the CARS measurements, for example, more or less refuted the older "vibrational-excitation-through-wall-association"-theory. The following aims to put the contents of mainly chapters 3-6 into a more recent perspective. As chapters 1 and 2 form a somewhat separate section, their conclusions are only endorsed here.

THE HISTORY OF RECIRCULATION

A. Anomalous recombination

The notion that "something's wrong" with expanding argon-hydrogen plasmas stems from some six years back, when comparisons were made between expanding plasmas in pure argon and argon-hydrogen mixtures. One of the most simple (and reliable) observations concerns the light emission: a pure argon jet is characterized by a bright white-red emission over a length of almost a meter, whereas addition of only a few percent of hydrogen to the flow (i.e., in the arc) causes the light emission to drop dramatically: only a faint red glow remains in the first few centimeters of the expansion. A freely expanding pure hydrogen plasma emits virtually no visible radiation at all. As the light emission of these recombining plasmas is governed by ion-electron (three-particle, stepwise) recombination reactions [1] and other processes involving charged particles, an observation of "light going out" basically points to a very rapid ionization loss. At least partly this ion loss proceeds through non-visible channels as, e.g., dissociative recombination of ArH^+ ending in a $p=2$ state of H. It is this ionization loss that has been measured using Thomson scattering in Figs. 4 of chapters 3 and 4. It has been noted and analyzed in a similar experiment by De Graaf *et al.* [2, 3].

From the beginning it was clear, that this "anomalous" recombination can not be attributed to any known atomic process. Three particle recombination should have comparable rates for H^+ and Ar^+ , as the upper part of the Ar^* system, where three particle recombination initially produces excited states, is essentially hydrogen-like. The argon jet clearly shows three particle recombination to be unable to account for a major ionization loss. Therefore, in the (argon)-hydrogen case, molecular channels have to be considered, and the only molecule present in sufficient abundance is H_2 . The reaction between Ar^+ and H_2 is known to be very fast (rate coefficient around $10^{-15}\text{m}^3\text{s}^{-1}$) so relatively small amounts of H_2 can

explain the observations. Combined with the necessary supposition, that small seed fractions of H_2 will probably be totally dissociated in the 1 eV environment of the arc this leads to the conclusion that wall association must be an important process. Volume association, a three particle process following $\text{H} + \text{H} + \text{H}(\text{H}_2) \rightarrow \text{H}_2 + \text{H}(\text{H}_2)$, is too slow.

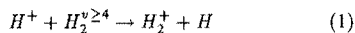
B. Dissociation degree

Around the same time observations on pure hydrogen plasmas had shown that the expanding plasma in pure hydrogen was not quite living up to the expectations, as the *dissociation degree* in the vessel turned out to be rather low: around 10 % of the particles in the vessel are H radicals. This number has been established using techniques as active actinometry [4, 5] and depolarization Rayleigh scattering (chapter 6), both rather cumbersome methods. These results are in clear contradiction with measurements on the power consumption of the arc, which point to an arc dissociation degree of 70-100%, depending on conditions ([4, 6], and section V of chapter 7). This also clearly hints at an important association process in the vessel - and again, the wall is a prime subject as a third body for association.

C. Wall association and vibrational excitation

The above considerations led to a gradual acceptance of wall association as a prime process in molecular expanding plasmas. Wall association of hydrogen radicals into H_2 molecules, however, is known to produce vibrationally hot molecules, as the association process releases about 2 eV of energy. Calculations and observations show that this energy can be stored in vibrational excitation [7, 8]. As volume vibrational relaxation is a slow process [9], these molecules should be able to carry this excess energy to the plasma jet in a recirculation flow.

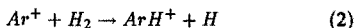
This reentry flow of vibrationally very hot molecules proved to be a kind of "*deus ex machina*". Only when the participating H_2 molecules are vibrationally hot can the reaction



become exothermic. The resulting high rate (rate coefficient around $2.5 \cdot 10^{-15}\text{m}^3\text{s}^{-1}$, see also chapter 3) can explain the very fast recombination in pure hydrogen plasmas. De Graaf *et al.* calculated a H_2 $v=4$ (corresponding to 2 eV of internal energy) population of around 10^{19}m^{-3} to explain the observed ionization loss [3].

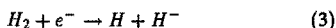
In chapters 3 to 5 of this thesis, the same wall excitation process is used to explain certain peculiarities in the H^* emission.

The reaction



is exothermic for ground state H_2 by its nature (owing to the higher ionization potential of Ar in comparison with H), but subsequent dissociative recombination into Ar and H^* can in principle only populate $p=2$ levels, whereas $p=3-6$ are observed even when cold H_2 is flushed into the vessel (chapter 5). So here, the ionization loss in argon-hydrogen plasmas can be well explained by cold H_2 , but the emission data forces one to consider some kind of extra energy input during dissociative recombination of ArH^+ . In view of the above, the assumption that rovibrational energy in the H_2 molecule is transferred to the resulting ArH^+ ion (reaction (2)) seems reasonable, and further analysis shows that this makes possible the population of higher excited states (chapter 5). This same process has been assumed to cause the "bulges" in the hydrogen b_p plots (Fig. 11 of chapter 3). The rovibrationally excited molecules were assumed to be formed at the vessel walls both in the case of arc and vessel injection. In this view, vessel injection leads to radical formation in reaction (2) and these radicals induce a "second generation" of wall-associated H_2 .

This rovibrational excitation "*deus ex machina*" also proved to be needed, when indications came that expanding plasmas in pure hydrogen with a magnetic field might hold large quantities of H^- negative ions [10]. The well-known dissociative attachment reaction:



can only reach appreciable rates when the participating H_2 molecule carries significant vibrational excitation (i.e., $v \geq 6$ or so). So again, wall association in combination with recirculation has been assumed to account for these "hot" molecules.

D. CARS results: answers, more questions

The alleged prime influence of rovibrationally excited H_2 in so many processes -also in deposition plasmas!- made the validation or falsification of the above views essential. Therefore, the $\text{H}_2^{v,f}$ had to be measured absolutely, accurately, *in situ* and with a high sensitivity. These very high experimental demands led us to prefer the CARS option to Raman scattering (too insensitive), REMPI (not applicable *in situ*), and VUV absorption spectroscopy (cumbersome, difficult to apply *in situ* in our specific case). The realized set up has been extensively described in chapter 7. It proves to be state-of-the-art in sensitivity.

In view of the above, the CARS measurements are very surprising indeed. The peripheral H_2 appears to be present in large amounts, but its temperature is surprisingly low: around 400 and 1100 K for the rotational and vibrational temperatures, respectively. At these temperatures, high densities of highly excited H_2 are not to be expected. This appears to be the case for plasmas in argon-hydrogen, pure hydrogen, and pure hydrogen with B-field (chapter 7). Also in the plasma jet, low densities of $v \geq 2$ are measured. In the following, the impact of these results will be examined.

- a. *Anomalous recombination.* First of all, the recombination in the case of argon-hydrogen is not influenced,

as reaction (2) is always exothermic by about 1.5 eV. So, relatively cold molecules can account for the observed ionization loss. In this case the CARS results support the former conclusions regarding wall association as a means of creating a large H_2 population around the plasma, as has been concluded in chapters 7 and 8. Of particular importance is the observation that the partial pressure of H_2 in the periphery equals the seed fraction, whether the H_2 is initially dissociated (when fed through the arc) or not. The importance of wall association has been established in this way. This point will be addressed later on when dissociation degrees are discussed.

- b. In the case of *pure hydrogen*, however, a difficult situation arises. As reaction (1) relies on rovibrational excitation in order to be fast, the observed extremely fast recombination can still not be well understood, at least not through the measured vibrational populations. Possible escapes are *translational velocity* (of the H^+ ions leaving the arc) giving energy input, and processes taking place in the arc or in the nozzle. Any non-dissociated H_2 leaving the arc will be extremely hot! Furthermore, the rotational excitation of low vibrational states (just below the CARS sensitivity, so a continuation of the trend shown in Fig. 11 of chapter 7) could carry significant amounts of energy. Of course, a possible combination of these mechanisms should also be considered.
- c. For H^- production, an even larger discrepancy exists, effectively ruling out the occurrence of reaction (3) (with *vibrationally* excited molecules) as a candidate for negative ion production. This calls for an alternative H^- production scheme, possibly through considerable *rotational* population of H_2 or through highly excited electronic states of H_2 , as proposed by Garscadden *et al* [11] recently. That is, only if the presence of large amounts of negative ions can be confirmed.
- d. In some of the reasoning in chapters 3, 4 and 5 concerning the Ar and H emission, the presence of highly rovibrationally excited molecules is essential. For example, the emission from H^* states $p=4$ and higher when cold H_2 is injected into the argon jet from the outside (vessel injection) has been explained using excited "second generation" H_2 (chapter 5). However, one important difference exists between this case and the case under b.: the number densities of $v=4$ (and higher) states necessary to explain the recombination for a pure hydrogen plasma are within the detection limits of our CARS set up, whereas the number densities of excited H_2 considered in chapters 3, 4, and 5 are very low (around 10^{16}m^{-3}). This is well below the detection limit of any CARS set up. However, as has been mentioned in chapter 5, these densities cannot be fully explained by a Boltzmann distribution with T_{vib} around 1000-2000 K. Again, other energy input mechanisms may have to be considered: the kinetic energy of the reacting particles (notably Ar^+ from the arc), or rotational excitation.
- e. In the HD- H_2 data and the experiments on pure H_2 plasmas, the CARS measurements show their power: the dis-

sociation degree has been determined to be low (around 10%, the margins or error in the CARS data). Combined with the data on the high dissociation degree inside the arc, this is the most definite proof for the importance of wall association to date. The HD-H₂ results in chapter 8 are very important because they show a new species (HD) formed in the plasma. Using the arc dissociation data once more, the observed large amounts of HD can only be explained by wall association.

E. Present view

Combining all the data available at this moment, the following view of the cascaded arc expanding plasma can be formulated.

Starting from the data on a high dissociation degree of H₂ when fed through the arc, the assumption is made that particles leaving the arc are mainly Ar, Ar⁺, H, H⁺, and e⁻ in the argon-hydrogen case, and mainly H, H⁺, e⁻, some 30% of (hot) H₂, and small amounts of H₂⁺ in the pure hydrogen case. The H atoms cover the stainless steel vessel walls because the relatively long (2 s) residence time in the large vessel makes them "see" the wall often. Association (possibly including rovibrational excitation) takes place at the wall; the resulting molecules can, however, be deactivated at the walls as well [12]! Vibrational deactivation through wall collisions can be very effective (only one or a few collisions are needed), thus causing a low (rotational/vibrational) temperature of the molecules when they arrive near the plasma. These cool molecules cause the fast recombination observed in argon-hydrogen plasmas.

So the plasma is surrounded by a reservoir of cool H₂ which mixes with the plasma (mean free paths being of the order of a few mm) and may eventually heat up a little. Most of the observed higher excited states (see chapter 7), however, originate from hot molecules that survived the arc (in the pure hydrogen case). These hot molecules relax to the cool background gas. As CARS observes both the hot and the cool population, curved non-Boltzmann rotational distributions arise, as has been demonstrated by the simple model in chapter 7. The model also shows that the arc itself must dissociate to a large extent.

References

- [1] M.C.M. van de Sanden, J.M. de Regt, and D.C. Schram, *Phys. Rev. E* **47** (4), 2792 (1993).
- [2] M.J. de Graaf, R.P. Dahiya, J.L. Jeauberteau, F.J. de Hoog, M.J.F. van de Sande, and D.C. Schram, *J. Phys. (Paris)*, Colloq. **51**, C5-387 (1990).
- [3] M.J. de Graaf, R. Severens, R.P. Dahiya, M.C.M. van de Sanden, and D.C. Schram, *Phys. Rev. E* **48** (3), 2098 (1993).
- [4] M.J. de Graaf, Ph.D. Thesis Eindhoven University of Technology (1994).
- [5] D.K. Otorbaev, M.J. de Graaf, M.C.M. van de Sanden, and D.C. Schram, *Contrib. Plasma Phys.* **35** (3), 195 (1995).
- [6] M.J. de Graaf, Z. Qing, H.W.A. Tolido, M.C.M. van de Sanden, and D.C. Schram, *J. Phys. High Temp. Chem. Process.*, suppl. to no. **3**, 11 (1992).
- [7] B. Jackson and M. Persson, *J. Chem. Phys.* **96**, 2378 (1992).
- [8] See for example: D.K. Otorbaev, M.C.M. van de Sanden, and D.C. Schram, *Plasma Sources Sci. Technol.* **4**, 293 (1995), and references therein.
- [9] J.H. Kiefer and R.W. Lutz, *J. Chem. Phys.* **44** (2), 668 (1966); M. Cacciatore, M. Capitelli, and G.D. Billing, *Chem. Phys. Lett.* **157** (4), 305 (1989).
- [10] M.C.M. van de Sanden, Z. Qing, D.K. Otorbaev, M.J. de Graaf, J.C.A. Wevers, and D.C. Schram, *Proceed. 5th European Workshop on the Production and Application of Light Negative Ions*, 41, Dublin (1993).
- [11] A. Garscadden and R. Nagpal, *Plasma Sources Sci. Technol.* **4**, 268 (1995).
- [12] M. Cacciatore, *private communication* (1995).

Molecular Processes in Expanding Plasmas

A laser spectroscopic study

SUMMARY

Fundamental research on expanding thermal arc plasmas is of essential importance in view of the applications of this type of plasma, such as deposition of amorphous hydrogenated silicon and carbon thin films. Pure hydrogen plasmas and mixtures in argon and hydrogen have special applications as particle sources (e.g., H neutral atoms, H⁺ and H⁻ ions). This thesis aims to gain a better understanding of the processes that dominate these plasmas.

In order to obtain the necessary experimental data, a number of diagnostics has been developed and applied. The combination of several diagnostics with numerical models proves to be especially powerful to describe the expanding plasma. The diagnostics that have been applied are the following: *optical emission spectroscopy* to determine the absolute population densities of argon and (atomic) hydrogen excited states, *Fabry-Pérot interferometry* for argon neutral line shape analysis, and *Thomson and Rayleigh scattering* for the accurate determination of the electron and neutral densities and the electron temperature. Furthermore, a new laser diagnostic has been developed: *depolarization Rayleigh scattering*. In this method, the depolarization of Rayleigh scattered photons in the case of non-spherically symmetric scattering objects is used to determine the density of molecules in plasmas of simple composition (e.g., a full-hydrogen expanding plasma, with only H₂ molecules as a depolarizing component).

Finally, a complicated laser diagnostic technique has been developed, constructed, and applied in order to determine the absolute population densities of rovibrational states of the H₂ molecule: *coherent anti-Stokes Raman scattering (CARS)*. Rovibrationally excited H₂ molecules in the ground electronic state are thought to play a dominant role in a number of processes, including the observed very fast recombination when H₂ is added to an argon plasma and the formation of H⁻ negative ions. The H₂ molecules are, however, very difficult to measure state-selectively, especially *in situ* and at low pressures (around 50 Pa and lower), and CARS is the only feasible diagnostic in our situation. The realized CARS experiment has a high sensitivity: a spectrum can be taken in 0.1 Pa of H₂, provided the rotational temperature does not significantly exceed 300 K. The set up has also been used to investigate plasmas in H₂ and D₂ (measuring H₂ and HD), focusing on the production of HD molecules.

The combination of data from the different diagnostics with numerical modeling has led to a more thorough understanding of the processes that govern the argon-hydrogen plasma jet. Examples are the explanation of the mentioned

very fast recombination through a molecular channel involving H₂ molecules, insight in the wall-association of hydrogen atoms into molecules and subsequent reentry of the molecules in the plasma, and the observation and modeling of non-Boltzmann distributions in the rovibrational level manifold of H₂. The CARS work proves to be especially important, as it provides accurate quantitative information about the major constituent of expanding hydrogen plasmas, thus putting to the test many theories that have been developed and used for this type of plasma.

Ralph Meulenbroeks, October 1995

Moleculaire Processen in Expanderende Plasma's

Een studie met behulp van laser-spectroscopie

SAMENVATTING

Fundamenteel onderzoek aan plasma's, die uit een thermische boog expanderen, is van essentieel belang gezien de toepassingen van dit type plasma, zoals de depositie van amorfe, gehydrogeneerde koolstof- en siliciumlagen. Plasma's in puur waterstof en argon-waterstofmengsels kennen verder speciale toepassingen als deeltjesbronnen (bijvoorbeeld voor H neutrale radicalen, H^+ ionen en H^- negatieve ionen). Het doel van deze studie is het verkrijgen van meer inzicht in de processen, die van dominant belang zijn in dit type plasma.

Om de noodzakelijke experimentele data te verkrijgen zijn een aantal plasmadiagnostieken ontwikkeld en toegepast. De combinatie van deze verschillende meetmethoden met numerieke modellen blijkt zeer effectief te zijn om het expanderende plasma te beschrijven. De volgende diagnostieken zijn toegepast: *optische emissie spectroscopie* om de absolute bevolkingsdichtheden van de aangeslagen toestanden van neutraal argon en waterstof te meten, *Fabry-Pérot interferometrie* voor lijnformanalyse van lijnen van neutraal argon en *Thomson- en Rayleighverstrooiing* voor de nauwkeurige bepaling van elektronen- en neutralendichtheden en elektronentemperaturen. Verder is een volledig nieuwe lasermeetmethode ontwikkeld: *depolarisatie-Rayleighverstrooiing*. Hierbij wordt de depolarisatie van Rayleigh-verstrooid licht in het geval van niet-bolsymmetrische verstrooiingsobjecten gebruikt om dichtheden van moleculen te meten in plasma's met een eenvoudige samenstelling (bijv. expanderende plasma's in vol waterstof, met H_2 als enige depolariserende component).

Tenslotte is een gecompliceerde laser-meettechniek ontwikkeld, geconstrueerd en toegepast, teneinde de absolute bevolkingsdichtheden van individuele rovibrationele niveaus van het H_2 molecuul te bepalen: *coherente anti-Stokes Raman verstrooiing*, ofwel CARS. Al dan niet hoog (rovibrationeel) aangeslagen H_2 in de elektronische grondtoestand wordt geacht een dominante rol te spelen in een aantal belangrijke processen, zoals de zeer snelle recombinitie, die waargenomen wordt wanneer H_2 aan een puur argon plasma wordt toegevoegd, en de vorming van negatieve waterstofionen (H^-). De meting ervan is echter zeer moeilijk, met name *in situ* en bij lage druk (rond 50 Pa en lager). CARS is de enig mogelijke techniek in ons geval en de gerealiseerde opstelling heeft een zeer hoge gevoeligheid: een spectrum kan nog verkregen worden voor 0.1 Pa H_2 , mits de rotationele temperatuur niet te ver boven 300 K ligt. Met deze opstelling zijn ook metingen verricht (H_2 en HD) aan plasma's in H_2 en D_2 , waarbij de vorming van HD moleculen centraal staat.

De combinatie van de gegevens uit de verschillende meet-

methoden met numerieke modellen heeft geleid tot een diepgaander begrip van de processen die een expanderend argon-waterstofplasma beheersen. Voorbeelden zijn de verklaring van de genoemde buitengewoon snelle recombinitie via een moleculair kanaal (waarin H_2 een dominante rol speelt), inzicht in de wandassociatie van waterstofradicalen tot moleculen (en het opnieuw binnendringen van deze moleculen in het plasma) en de vorming van niet-Boltzmannse verdelingen in de rotationele bevolking van H_2 . Met name het CARS-werk blijkt zeer belangrijk, aangezien deze techniek nauwkeurige, kwantitatieve informatie levert over de grootste deeltjesfractie in waterstofplasma's. Hierdoor kunnen toegepaste modellen voor dit type plasma getest worden.

Ralph Meulenbroeks, oktober 1995

Dankwoord

Zoals duidelijk te zien aan de auteurslijsten en dankbetuigingen in de afzonderlijke artikelen, is ook dit proefschrift niet het werk van één persoon. Daarom wil ik hier een aantal mensen, die mij in de afgelopen jaren, zowel in als buiten de Kopzaal, terzijde hebben gestaan, met name noemen en bedanken.

Met tomeloze energie en nooit aflatend enthousiasme gaf Daan Schram als eerste promotor mede vorm aan dit werk - ondanks de onverwachte „visitaties” en de vrijdagmiddag-suggesties om (arbeidsintensieve) zaken in „het programma naar voren te schuiven” een eer om in jouw groep te mogen werken; een groep, die door jouw ruimdenkendheid een heel menselijk aanzicht heeft.

Joost van der Mullen wil ik bedanken voor zijn intensieve begeleiding, het zeer kritisch lezen van het manuscript en de hevige discussies (LIF versus CARS of toch maar allebei??) die uiteindelijk toch steeds weer duidelijkheid schepten. En we hebben er uiteindelijk toch een prachtig lasersysteem aan over gehouden...

Met bijzonder veel plezier kijk ik terug naar de tijd, dat Richard Engeln (van de torsies) als post-doc werkzaam was op de Kopzaal. Twee handen op één (CARS-) buik? Volgens mij wel. Jouw aanstekelijke lach, enthousiasme, houwjtjes-touwjtjes oplossingen en wijsheden-uit-grootmoeders-tijd hebben me heel veel gegeven. En niet alleen een fantastische CARS-opstelling, dus. Maar goed, zoals het klokje thuis tikt, tikt het nergens...

Twee mannen en één onwillige PC: en toch zo'n plezier, om met Richard van de Sanden vier jaar lang een kamer te delen! Begonnen als directe begeleider werd je steeds meer een zeer betrokken collega. Veel van jouw ideeën zijn verwoord in de voorgaande pagina's; de hevige discussies, hoge fluittonen en humor (how's Joepy?) zal ik niet licht vergeten. Nu kun je eindelijk de ruimte gaan innemen, die je toekomt...

Prof. Uhlenbusch, Frits de Hoog en Niek Lopes Cardozo wil ik bedanken voor het kritisch lezen van het proefschrift.

This is an appropriate place to thank once more the people that were so helpful during the conception and building of the CARS set up. I feel especially indebted to the ONERA-LAERTE group in Palaiseau, France. Jean-Pierre Taran, Michel Péalat, and Michel Lefebvre have been a great help over the years, from the first letter concerning H₂-CARS to the last detail on saturation. Thanks also to the University of Düsseldorf group, especially prof. J. Uhlenbusch, Paulus Jauernik (*The Pope*), and Sven Hädrig.

En dan de technici... Herman, hoewel lang van draad geweldig met alles wat met optiek te maken heeft; onze eigen Ries (mijn beste vriend? ...en zo zuiver ook!), die de meest krankzinnige uitvindingen wist te realiseren en natuurlijk Bertus, voor wie geen software- of hardware-zee te hoog ging. Voor Frans en alle mannen én vrouwen van Marius geldt eigenlijk iets soortgelijks: in de werkplaats bleek alles mogelijk, iedere keer opnieuw.

De niet geringe hoeveelheid werk, die in de loop der jaren

door een heel leger studenten is verzet moet hier natuurlijk ook een plaats krijgen. Zonder jullie was het dus écht niet gelukt! En dan heb ik het over de volgende mensen (in volgorde van opkomst): Paul van der Heijden, Arno van Helvoort, Luciën Jaegers, Angelo Griguoli, Annemarie van Beek, Martijn *Ace of Spades* Steenbakkers, Edgar van de Ven, Roger *wizzzz* Paffen, Marc *Smashin' Pumpkin* Beurskens (the quintessential student), Jan Snoeijer, Isa de Bari, Marco *BOX' CARS* Box, Paulo *uuuuuh, huh, huh...* Freire, Frank Umans en Leon Jacobs. Ontzettend bedankt, allemaal.

De ETP groep zorgde voor een zeer prettige promotie-omgeving, waar ik me dan ook uitstekend thuis voelde. Dank jullie wel, Mark, Sjaak, Arno, Ad, Zhou, Hans, John, Seth, Jeroen, Ger (hah hah), Dany, Bert, René, Bart, Ko, en Ton. Niet van ETP, maar wel belangrijk: Lambert Bisschops en Hans Freriks. Een speciaal woordje van dank voor de secretaresses, Jeanne, Rina en Marianne, die steeds voor gezelligheid én serieuze zaken klaarstonden.

Dank ook aan de volgende personen, die op verschillende manieren hebben bijgedragen: Henk-Jan en Leo (lay-out van de kaft), Ruth Gruijters voor de plaatjes, Dave Vender, Darryl Skinner en Sharon St. Onge (who checked on the English), Paul Graff - de druk bezette technicus van Spectra Physics, die heel wat afgetobt heeft op de Kopzaal -, Boudewijn Verhaar en Djoormat Otorbaev (for the many helpful discussions).

En dan is er een groot aantal vrienden, kennissen en anderen, die me in de persoonlijke sfeer erg gesteund hebben, vooral tijdens dat moeilijke laatste jaar. De lijst wordt zeker incompleet, maar ik begin er toch aan: Sharon St. Onge, Wim Straesser, Henk Guldemond en eigenlijk iedereen in en rond dat geweldige Concertgebouworkest, Agnostic Ömer (*Da Mad Turk - you're a real pal*), Har Har, Do It Up, Raven (*Live at the Inferno!*), Pantera (*Fuckin' Hostile!*), Mark de Graaf, Anna Basemans en „de donderdag-groep”, de mensen van het Kushi-instituut te Amsterdam (hi Deborah), Elly Nagelkerke, Erik Janse (*Fire! Fire!*), Lia de Meyer, Beavis&Butt-Head (*This is gonna be COOL...*), Jeanne v.d. Oever, Hetty Visser, Janna Albracht, (*et tu...*) Marion Lensen, Simone Keijzer, Wim Raaymakers& Carolien Loots, Sonja van Vonderen (of Bongers?), Nigel C.B. Durrant, Anita Meulendijks en Els Gielens.

En intens laatste woord van dank voor twee mensen, die gedurende mijn gehele promotietijd (en daarvoor...) zeer dichtbij me zijn geweest: Ingrid, vriendin en vertrouweling voor alle vreugde en pijn en natuurlijk Gijs, voor de ontmoetingen, voor de „*Kindertotenlieder*”, „*Nacht*” en andere prachtige muziek en voor een altijd warm hart. Bedankt.

Curriculum Vitae

21 augustus 1967	Geboren te Eersel.
juni 1985	Diploma Athaeneum B, Hertog Jan College, Valkenswaard.
juli 1989	Staatsexamen Muziektheorie.
april 1991	Doctoraal examen Technische Natuurkunde, Faculteit der Technische Natuurkunde, Technische Universiteit Eindhoven (met lof).
mei 1991 - juli 1992 juli 1993 - januari 1996	Assistent in Opleiding, Vakgroep Deeltjesfysica, Faculteit der Technische Natuurkunde, Technische Universiteit Eindhoven.
augustus 1992 - juni 1993	Contrabassist, Koninklijk Concertgebouworkest, Amsterdam.
juni 1994	Examen Uitvoerend Musicus (contrabas), Conservatorium voor Muziek, Maastricht (met onderscheiding).

STELLINGEN

behorende bij het proefschrift

MOLECULAR PROCESSES IN EXPANDING PLASMAS

A laser spectroscopic study

door

Ralph Meulenbroeks

23 januari 1996

1

De depolarisatie van Rayleigh-verstrooid licht kan gebruikt worden voor de bepaling van moleculaire dichtheden in plasma's en gassen.
Dit proefschrift.

2

Kennis van de invloed van rotationele excitatie op dissociatieve recombinitie is van essentieel belang voor het begrip van plasma- en astrofysische processen.

3

Uitgaande van een hoge dissociatiegraad van het thermische boogplasma is de conclusie, dat wandprocessen in het expansievat een essentiële rol spelen, onontkoombaar.
Dit proefschrift.

4

De zeer snelle recombinitie in een expanderende plasmabundel in puur waterstof kan niet berusten op de aanwezigheid van vibrationeel hoogaangeslagen waterstofmoleculen in het achtergrondgas.
De Graaf et al., Phys. Rev. E48, 2098 (1993); dit proefschrift.

5

Indien kan worden bevestigd, dat expanderende waterstofplasma's grote hoeveelheden atomaire negatieve ionen bevatten, zal een ander vormingsmechanisme dan de algemeen aanvaarde dissociatieve aanhechting, met vibrationeel hoogaangeslagen waterstofmoleculen, een rol moeten spelen.
Dit proefschrift.

6

De verklaring voor populatie-inversie in een expanderende plasmabundel, gegeven door Akatsuka en Suzuki, is gebaseerd op een onrealistisch lage electronentemperatuur.
Akatsuka en Suzuki, Phys. Rev. E49, 1534 (1994).

7

In de huidige politieke ontwikkelingen, op zowel kleine als grote schaal, weerspiegelt zich een zegetocht van het korte-termijndenken.

8

In zogenaamde arbeiderswoningen wordt, vanwege de relatief lage woonkosten, tegenwoordig een onevenredig groot percentage werklozen gehuisvest.

9

Vele ziektebeelden vinden zowel hun oorsprong als mogelijke genezing in het door de patiënt gevolgde eetpatroon.

Michio Kushi, „Makrobiotiek”.

10

In de hedendaagse „heavy metal”- en „death metal”-muziek geniet de Middeleeuwse lokrische kerktoonladder een ongekennde populariteit.

11

De stormachtige vooruitgang binnen de communicatie-technologie hoeft geenszins te leiden tot een verbetering van intermenselijke communicatie.

12

Het integer bedrijven van kunsten, ambachten en wetenschappen put uit éénzelfde inspiratiebron.

13

Wanneer de Liefde wenkt, dient zij gevolgd te worden.

Kahlil Gibran, „The Prophet”.
